Lidar profiling of ozone above the central San Joaquin Valley during the California Baseline Ozone Transport Study (CABOTS)

Final Report Contract No. 15RD012

Prepared for the California Air Resources Board and the California Environmental Protection Agency

Dr. Toshihiro Kuwayama

Cal/EPA California Air Resources Board
Research Division
1001 I Street
5th Floor
Sacramento, CA 95814
(916) 323-1506

Principal Investigators

Andrew O. Langford
NOAA Earth System Research Laboratory, Chemical Sciences Division

Boulder, CO 80305-3337, USA.
Phone: (303) 497-3115
Fax: (303) 497-5318
E-mail:andrew.o.langford@noaa.gov

Christoph J. Senff

Cooperative Institute for Research in Environmental Sciences,
University of Colorado, Boulder, CO, 80309, USA.
and

NOAA Earth System Research Laboratory, Chemical Sciences Division

Phone: (303) 497-6283
Fax: (303) 497-5318
E-mail:christoph.senff@noaa.gov

February 12, 2019

Contributing Researchers

Raul J. Alvarez, NOAA Earth System Research Laboratory, Chemical Sciences Division

Guillaume Kirgis, NOAA Earth System Research Laboratory, Chemical Sciences Division and CIRES, University of Colorado

Disclaimer

The statements and conclusions in this Report are those of the contractor and not necessarily those of the California Air Resources Board. The mention of commercial products, their source, or their use in connection with material reported herein is not to be construed as actual or implied endorsement of such products.

Acknowledgements

The analyses described here benefitted greatly from the unfunded model support provided by Dr. R. B. Pierce of NOAA/NESDIS (RAQMS), Mariusz Pagowski (RAP-Chem) of the NOAA ESRL Global Systems Division GSD, and Stéphanie Evan and Jerome Brioude (FLEXPART) of the Laboratoire de l'Atmosphere et des Cyclones (LACy), at the Université de La Réunion. We would also like to thank Ian Faloona and Dani Caputi of the University of California at Davis and Stephen Conley of Scientific Aviation, and Laura Iraci and Emma Yates of the NASA Ames AJAX Science team for making their aircraft measurements available for the intercomparisons shown in this report. We would like to thank Jin Xu and Eileen McCauley of CARB for their support and assistance in the planning and execution of the project and Cathy Burgdorf-Rasco of NOAA ESRL and CIRES for maintaining the CABOTS data site. The NOAA team is also grateful to Ann Weickmann, Scott Sandberg, and Richard Marchbanks for their assistance during the field campaign, and Tim Bonin and Alan Brewer for deriving the boundary layer heights from the NOAA Doppler lidar. The NOAA/ESRL lidar operations were also supported by the NOAA Climate Program Office, Atmospheric Chemistry, Carbon Cycle, and Climate (AC4) Program and the NASA-sponsored Tropospheric Ozone Lidar Network (TOLNet, http://www-air.larc.nasa.gov/missions/TOLNet/). The views, opinions, and findings contained in this report are those of the author(s) and should not be construed as an official National Oceanic and Atmospheric Administration or U.S. Government position, policy, or decision.

This Report was submitted in fulfillment of ARB contract no. 15RD012, “Lidar profiling of ozone above the central San Joaquin Valley during the California Baseline Ozone Transport Study (CABOTS)” by the NOAA ESRL Chemical Sciences Division under the sponsorship of the California Air Resources Board. Work was completed as of November 2018.

Contents

Definitions and Abbreviations

AGL	above ground level
AJAX	Alpha Jet Atmospheric eXperiment
AS	Asian
ASL	above sea level
BB	biomass burning
BBY	Bodega Bay
CABOTS	California Baseline Ozone Transport Study
CalNex	California Research at the Nexus of Air Quality and Climate Change
CARB	California Air Resources Board
CARES	Carbonaceous Aerosols and Radiative Effects Study
CCOS	Central California Ozone Study
CIMSS	Cooperative Institute for Meteorological Satellite Studies
CIRES	Cooperative Institute for Research in Environmental Sciences
CRO	Chews Ridge Observatory
CSD	Chemical Sciences Division
ESRL	Earth System Research Laboratory
FAST-LVOS	Fires, Asian, and Stratospheric Transport- Las Vegas Ozone Study
GFDL	Geophysical Fluid Dynamics Laboratory
GFS	Global Forecasting System
GMD	Global Monitoring Division
GSD	Global Systems Division
HRRR	High-Resolution Rapid Refresh
IOP	Intensive operating period
LIDAR	Light Detection and Ranging
LVOS	Las Vegas Ozone Study
MDA8	Daily maximum 8-h average
MLH	Mixed layer height
NARR	North American Regional Reanalysis
NCEP	National Centers for Environmental Prediction
NCOS	non-controllable ozone source
NESDIS	National Environmental Satellite, Data, and Information Service
NOAA	National Oceanic and Atmospheric Administration
NPS	National Park Service
RAP-Chem	Rapid Refresh with Chemistry
RAQMS	Realtime Air Quality Modeling System
NAAQS	National Ambient Air Quality Standard
ppbv	parts-per-billion-by-volume
SciAv	Scientific Aviation
SJSU	San Jose State University
SJV	San Joaquin Valley
SJVAPCD	San Joaquin Valley Air Pollution Control District
SJVAB	San Joaquin Valley Air Basin

SoCAB	South Coast Air Basin
ST	stratospheric
STT	stratosphere-to-troposphere transport
TOPAZ	Tunable Optical Profiler for Aerosols and oZone
UC	University of California
UTLS	upper troposphere/lower stratosphere
VMA	Visalia Municipal Airport
WRCC	Western Regional Climate Center

List of Figures

"moderate" and orange to "Unhealthy for Sensitive Groups" concentrations. The solid and dot-dash gray lines represent the major highways and railroads, respectively. Urban areas are outlined in light gray.

***Figure** 10. MDA8 O_3 measured by the TOPAZ in-situ monitor (VMA) and the nearby CARB, SJVAPCD, and Tachi-Yokut monitors shown in **Figure** 9 during the (a) first, and (b) second, CABOTS IOPs. The dashed and dotted horizontal black lines show the 2008 and 2015 NAAQS.*

***Figure** 11. Time series plots of the VMA in-situ (gray dots) and TOPAZ O_3 concentrations measured at 27.5 m (red line) during the (a) first, and (b) second CABOTS IOPs. The black and gray staircase lines represent the VMA and Hanford MDA8 O_3. The horizontal dashed and dotted lines show the 2008 NAAQS, and 2015 NAAQS/CARB 8-h standards, respectively.*

***Figure** 12. (a) Four-day time series comparing the O_3 mixing ratios measured by the 2B monitor in the TOPAZ truck (gray line) and retrieved by TOPAZ 800 m downrange and 27.5±5 m above the ground (filled black circles). The solid and dotted black lines show the 1-h measurements from the Visalia and Hanford monitors. (b) Scatter plot comparing the 27.5 m TOPAZ measurements to the interpolated 5 m in-situ measurements. The filled gray circles (dotted fit) show the entire CABOTS data set and the filled black circles (dashed fit) daytime measurements (0900 to 1800 PDT) and southeasterly (125 to 145°) winds greater than 2.5 m s^{-1}.*

***Figure** 13. Scatter plots comparing the 27.5 m TOPAZ measurements with the 1-h measurements from the regulatory monitors at (a) Visalia-N. Church Street, (b) Hanford, (c) Parlier, and (d) Porterville. The measurements in the upper box and x-axis label refer to the distance from the VMA and sampling height above ground, respectively. The Visalia monitor is operated by the California Resources Board. The remaining three are operated by CARB and the SJVAPCD. The TOPAZ measurements are interpolated to the 1-h time base of the regulatory measurements for the comparison.*

***Figure** 14. TOPAZ backscatter (27.5 m AGL) compared to the hourly $PM_{2.5}$ measurements from the (a) Visalia and (b) Hanford monitors. The closed and open symbols represent measurements made before and after the start of the Soberanes Fire on July 22, respectively. The linear regressions correspond to all the measurements.*

***Figure** 15. (top) Maps of the SJVAB showing the UC Davis/Scientific Aviation RLO (top) and EPA/BAAQMD (bottom) flight tracks coincident with the TOPAZ measurements. The filled black squares show regulatory surface monitors. The CABOTS sampling sites at CRO and VMA are marked by red triangles. The other abbreviations are the Fresno (FAT), Visalia (VIS), and Bakersfield (BFL) airport codes.*

***Figure** 16. RLO and EPA/BAAQMS flight tracks in the vicinity of TOPAZ. (a) RLO2 (June 2-4), (b) RLO4 (July 24-26), EPA1 (27-29 July), and (d) EPA2 (4-6 August). The red triangle marks the location of TOPAZ and the dashed black circles show the 5 km radius used for the profile*

***Figure** 48. Backscatter measurements from (a) May 28-31 and (b) June 28-31. The short-dash lines mark the approximate 800 and 600 hPa levels and the heavy solid black curve shows the boundary layer height inferred from the co-located RASS. The dashed boxes show the boundary layer, buffer zone, and free tropospheric layers used in **Figures** 50-53.*

***Figure** 49. Ozone measurements from (a) May 28-31 and (b) June 28-31. The short-dash lines mark the approximate 800 and 600 hPa levels and the heavy solid black curve shows the boundary layer height inferred from the co-located RASS. The dashed boxes show the boundary layer, buffer zone, and free tropospheric layers used in **Figures** 50-53.*

***Figure** 50. Ozone-backscatter relationship in the boundary layer (0.05 to 0.5 km) during the first (left) and second (right) IOP. The gray points show the measurements from the entire IOP and the colored points highlight the measurements from the days shown in **Figures** 48 and 49.*

Figure 51 shows that the post-Soberanes backscatter enhancement was much larger in the buffer zone (1-2 km) and more strongly correlated with ozone.

***Figure** 52. Same as **Figure** 51, but for the free tropospheric layer (4.0 to 5.0 km).*

***Figure** 53. Ozone-backscatter relationships in the buffer zone (1-2 km) on July 29 (red). The gray points show all the daytime measurements from the second IOP. The dashed lines in the lower panel show the buffer zone regression fits.*

***Figure** 54. Ozone (top) and backscatter (bottom) curtain plots from July 29 with the co-located SJVAPCD profiler wind measurements and boundary layer height superimposed. The dashed lines show the altitude range of the boundary layer (0.05 to 0.5 km AGL) and buffer layer (1-2 km AGL) covered by the data in **Figure** 53.*

List of Tables

Abstract

The NOAA Earth System Research Laboratory (ESRL) Tunable Optical Profiler for Aerosols and oZone (TOPAZ) mobile lidar was deployed to the Visalia Municipal Airport (VMA, 36.315°N, -119.392°E) in the late spring and summer of 2016 to probe the vertical distribution of ozone (O_3) and particulates above the San Joaquin Valley (SJV), and investigate the influence of O_3 transported aloft on surface concentrations in the SJV during the California Baseline Ozone Transport Study (CABOTS). The lidar was operated for an average of more than 10 hours per day during late spring (27 May to 18 June) and summer (18 July to 7 August) intensive operating periods (IOPs), acquiring a total of 440 hours of lidar data during the first (1654 8-min profiles over 22 days) and second (1686 8-min profiles over 21 days) IOPs. The lidar profiles were supplemented by *in-situ* O_3 and basic meteorological measurements at the VMA, and coordinated with aircraft measurements by the U. of California, Davis/Scientific Aviation and the NASA Ames AJAX project. In this report, we summarize the lidar observations and compare them with the surface and airborne measurements to assess their accuracy, and with the FLEXPART and NOAA ESRL GSD RAP-Chem models to estimate the influences of stratospheric intrusions, Asian pollution, and biomass burning on surface O_3 in the San Joaquin Valley.

Our analyses show that while elevated O_3 layers of apparent stratospheric or Asian origin appeared frequently in the middle troposphere (4-6 km) above the San Joaquin Valley during CABOTS, most of these layers passed over California without reaching the surface. In the few cases where O_3-rich lower stratospheric air and Asian pollution descended into the valley behind cold fronts, the descending free tropospheric air and co-mingled transport layers displaced much more polluted air at the surface leading to a net *decrease* in surface O_3 concentrations. The TOPAZ measurements also show that emissions from the Soberanes Fire near Big Sur led to O_3 enhancements of 10-20 ppbv or more in the San Joaquin Valley during late July and early August, directly contributing to the highest O_3 concentrations measured in 2016, and likely increasing the number of exceedance days in the San Joaquin Valley Air Basin by about 10%.

Executive Summary

The California Baseline Ozone Transport Study (CABOTS) was conducted in the late spring and summer of 2016 to study the impact of background ozone (O_3) on the surface concentrations in California, including the San Joaquin Valley (SJV), one of two "extreme" non-attainment areas in the U.S. The field campaign used several methods to characterize the distribution of O_3 aloft, and assess its impact on the surface concentrations. CABOTS included daily electrochemical cell (ECC) ozonesonde launches from Bodega Bay (BBY, 38.319°N, -123.075°E, 12 m above mean sea level, ASL) (6 May-17 August) and Half Moon Bay (HMB, 37.505°N, -122.483°E, 9 m ASL) (15 July-17 August) by the San Jose State University (SJSU), *in-situ* aircraft sampling of O_3 and other compounds above central California by the University of California at Davis (UC Davis)/Scientific Aviation and the NASA Alpha Jet Atmospheric eXperiment (AJAX), and O_3 and backscatter lidar measurements during the two intensive operating periods (IOP1: 27 May-18 June and IOP2: 18 July-7 August) by the truck-based NOAA Earth System Research Laboratory Chemical Sciences Division (NOAA ESRL CSD) Tunable Optical Profiler for Aerosols and oZone (TOPAZ) mobile lidar system at the Visalia Municipal Airport (VMA, 36.315°N, -119.392°E, 88 m ASL). Surface O_3 measurements were also made at the ozonesonde and lidar sites, and at the UC Davis monitoring station at the Chews Ridge Observatory (CRO, 36.306°N, -121.567°E, 1520 m ASL) located ≈195 km due west of Visalia in the Santa Lucia Mountains, as well as the extensive networks of regulatory surface monitors maintained by the California Air Resources Board, the San Joaquin Valley Air Pollution Control District (SJVAPCD), and the U.S. National Park Service (NPS).

In this report, we summarize the NOAA ESRL measurements of O_3 and particulate backscatter (ß) profiles above the SJV and compare the lidar profiles to *in-situ* measurements from nearby surface monitors and instruments flown aboard the UC Davis/Scientific Aviation Mooney and Alpha Jet research aircraft based at NASA's Ames Research Center. We then use the TOPAZ measurements in conjunction with model analyses from the NOAA ESRL Global Systems Division (GSD) RAP-Chem and FLEXPART models to investigate the impacts of long-range transport, stratospheric intrusions, and biomass burning on surface O_3 concentrations in the SJV during CABOTS.

Our analyses show that while elevated O_3 layers of apparent stratospheric or Asian origin appeared frequently in the middle troposphere (4-6 km) above the San Joaquin Valley during CABOTS, most of these layers passed over California without reaching the surface. In the few cases where O_3-rich lower stratospheric air and Asian pollution descended into the valley behind cold fronts, the descending free tropospheric air and co-mingled transport layers displaced much more polluted air at the surface leading to a net *decrease* in surface O_3 concentrations. The TOPAZ measurements also show that emissions from the Soberanes Fire near Big Sur led to O_3 enhancements of 10-20 ppbv or more in the San Joaquin Valley during late July and early August, directly contributing to the highest O_3 concentrations measured in 2016, and likely increasing the number of exceedance days in the San Joaquin Valley Air Basin by about 10% compared to other recent years.

1. Introduction

Ground-level ozone (O_3) is harmful to human and animal health [*U.S. Environmental Protection Agency*, 2014] and impairs plant growth and productivity [*Avnery et al.*, 2011a; b]. The U.S. Clean Air Act (CAA) accordingly designated O_3 a criteria pollutant, and established primary and secondary National Ambient Air Quality Standard (NAAQS) to protect human health and welfare, respectively. The CAA requires that these standards be reviewed periodically to consider the latest research findings and adjusted, if necessary, to ensure an "adequate margin of safety" for the public. The primary and secondary NAAQS for the maximum daily 8-h average (MDA8) O_3 mixing ratio were accordingly lowered from 75 to 70 parts-per-billion by volume (ppbv) in October 2015 following the most recent review [*U.S. Environmental Protection Agency*, 2015]. The new NAAQS is equivalent to the California Ambient Air Quality Standard (CAAQS) adopted in 2006 (https://www.arb.ca.gov/research/aaqs/caaqs/caaqs.htm).

Ozone is a secondary pollutant formed by photochemical reactions between nitrogen oxides (NOx) and volatile organic compounds (VOCs) emitted by natural and anthropogenic sources. Surface concentrations have declined across most of the U.S. over the last two decades as tighter emission controls have led to substantial reductions in anthropogenic NOx precursors [*Gaudel et al.*, 2018; *Jaffe et al.*, 2018]. The U.S. national average O_3 design value (ODV), i.e. the 3-yr average of the 4th highest MDA8 calculated from measurements made at 830 monitoring sites across the contiguous U.S., decreased from 78 parts-per-billion by volume (ppbv) in 2007 to 68 ppbv in 2016 (https://www.epa.gov/air-trends/ozone-trends#oznat). The declines have been smaller in the Southwestern U.S., however, and the 2014-2016 ODV in the San Joaquin Valley (SJV) of California remains well above the NAAQS at 94 ppbv, making the San Joaquin Valley Air Basin (SJVAB) one of only two "extreme" non-attainment areas in the U.S. (https://www.epa.gov/green-book) with the other being the nearby South Coast Air Basin (SoCAB). These persistent high O_3 concentrations adversely impact the health of the 4 million people living in the SJV as well as the $15 billion agricultural industry and iconic forests of the nearby Sequoia and Kings Canyon National Parks [*Panek et al.*, 2013].

Efforts to control surface O_3 are complicated by the fact that it also has significant background concentrations in the troposphere [*Jaffe et al.*, 2018]. This background consists largely of naturally-occurring O_3 transported downward from the stratosphere or produced by reactions of NOx and VOCs from non-anthropogenic sources such as lightning, wildfires, or soils and vegetation, but it also includes substantial contributions from upwind anthropogenic sources. Since O_3 is relatively long-lived in the free troposphere (≈1 month), the background concentrations measured at any given location can also include O_3 formed from anthropogenic precursors emitted thousands of kilometers away and even O_3 produced by local emissions that have circumnavigated the globe. Background O_3 exceeds 50 ppbv or 70% of the NAAQS in much of the Southwest during springtime [*Jaffe et al.*, 2018], greatly complicating efforts to reduce ambient concentrations by controlling the local NOx and VOC precursor emissions.

The O_3 problem in the San Joaquin Valley has been addressed by several major air quality studies over the years, including the San Joaquin Valley Air Quality Study (SJVAQS) in 1990

[*Lagarias and Sylte*, 1991] and the Central California Ozone Study (CCOS) in 2000 [*Reynolds et al.*, 2010]. The SJV was also a focus of the California Research at the Nexus of Air Quality and Climate Change (CalNex) field campaign in 2010 [*Brune et al.*, 2016; *Ryerson et al.*, 2013] and the northern SJV was also a focus of the coincident Carbonaceous Aerosols and Radiative Effects Study (CARES) [*Zaveri et al.*, 2012]. Although these and other studies (e.g. [*Beaver and Palazoglu*, 2009; *Dabdub et al.*, 1999; *Pusede and Cohen*, 2012]) have shown that local and regional photochemical production is the dominant source of the high surface O_3 in the SJV, it is well established that O_3 and other long-lived pollutants are also transported to the U.S. West Coast from East Asia [*Brown-Steiner and Hess*, 2011; *Cooper et al.*, 2010; *Goldstein et al.*, 2004; *Hudman et al.*, 2004; *Jacob et al.*, 1999; *Jaffe et al.*, 2003a; *Jaffe et al.*, 1999; *Lin et al.*, 2012b; *Verstraeten et al.*, 2015; *Zhang et al.*, 2008; *Zhang et al.*, 2009], and that O_3-rich lower stratospheric air sometimes descends to the surface during tropopause folding events [*Langford et al.*, 2012; *Langford et al.*, 2015a; *Lin et al.*, 2012a], and can bring entrained transported Asian pollution [*Cooper et al.*, 2004a; *Cooper et al.*, 2004b; *Lin et al.*, 2012b] or biomass burning plumes downward with them [*Brioude et al.*, 2007]. Quantifying the impacts of long-range transport from Asia and stratospheric intrusions on surface O_3 in the SJV were primary objectives of the 2016 California Baseline Ozone Transport Study (CABOTS) organized by the California Air Resources Board (CARB) (https://www.arb.ca.gov/research/cabots/cabots.htm).

In this report, we summarize the NOAA Earth System Research Laboratory Chemical Sciences Division (NOAA ESRL CSD) contributions to CABOTS through the measurement of O_3 and particulate backscatter (ß) profiles above the SJV using the Tunable Optical Profiler for Aerosols and oZone (TOPAZ) mobile lidar [*Alvarez et al.*, 2011]. We compare the lidar profiles to *in-situ* measurements from nearby surface monitors and instruments flown aboard the UC Davis/Scientific Aviation Mooney [*Trousdell et al.*, 2016] and Alpha Jet research aircraft based at NASA's Ames Research Center [*Hamill et al.*, 2016; *Yates et al.*, 2015]. We then use the TOPAZ measurements in conjunction with model analyses from the NOAA ESRL Global Systems Division (GSD) RAP-Chem and FLEXPART models to investigate the impacts of long-range transport, stratospheric intrusions, and biomass burning on surface O_3 concentrations in the SJV during CABOTS. Of these sources, our analysis suggests that the Soberanes Fire had the greatest impact on surface O_3 and aerosols in the central San Joaquin Valley during the CABOTS field campaign.

2. The California Baseline Ozone Transport Study (CABOTS)

The CABOTS field campaign used several methods to characterize the distribution of O_3 aloft and assess its impact on surface concentrations in the San Joaquin Valley. The primary CABOTS measurements (**Figure** 1) were electrochemical cell (ECC) ozonesondes [*Johnson et al.*, 2002] launched daily from Bodega Bay (BBY, 38.319°N, -123.075°E, 12 m above mean sea level, ASL) (6 May-17 August) and Half Moon Bay (HMB, 37.505°N, -122.483°E, 9 m ASL) (15 July-17 August) by the San Jose State University (SJSU), *in-situ* aircraft sampling of O_3 and other compounds above central California by the University of California at Davis (UC Davis)/Scientific Aviation [*Trousdell et al.*, 2016] and the NASA Alpha Jet Atmospheric eXperiment (AJAX) [*Yates*

et al., 2015], and O_3 and backscatter lidar measurements during the two intensive operating periods (IOP1: 27 May-18 June and IOP2: 18 July-7 August) by the truck-based NOAA ESRL TOPAZ lidar system at the Visalia Municipal Airport (VMA, 36.315°N, -119.392°E, 88 m ASL). Surface O_3 measurements were also made at the ozonesonde and lidar sites, and at the UC Davis monitoring station at the Chews Ridge Observatory (CRO, 36.306°N, -121.567°E, 1520 m ASL) located ≈195 km due west of Visalia in the Santa Lucia Mountains, as well as the extensive networks of regulatory surface monitors maintained by the California Air Resources Board, the San Joaquin Valley Air Pollution Control District (SJVAPCD), and the U.S. National Park Service (NPS).

3. The San Joaquin Valley

3.1 Geography

The San Joaquin Valley encompasses the southern two-thirds (≈65,000 km^2) of the 700 km long Central Valley of California. The 100 km wide valley is bounded by the Southern Coast Ranges with elevations of less than 1.3 km ASL to the west, the Sierra Nevada (<4 km ASL) to the east, and the San Emigdio and Tehachapi Mountains (<2.4 km ASL) to the south. The flat valley floor rises gradually from sea level in the Sacramento–San Joaquin River Delta drainage separating the SJV from the Sacramento Valley (SV) to the north, to ≈130 m ASL near Bakersfield to the south. The SJV is one of the most important agricultural areas in the U.S., but the rural population is relatively sparse with nearly half of the 4 million residents living in one of six cities (Stockton, Modesto, Fresno, Clovis, Visalia, and Bakersfield) located along California State Route 99 (CA-99) (**Figure** 2). Fresno, the fifth most populous city in California and the largest in the SJV, was home to nearly 15% of the total SJV population in 2016 with 522,000 residents (630,000 when combined with nearby Clovis). The SJVAB encompasses not only the valley floor, but also the adjacent western slope of the Sierra Nevada including the Sequoia and Kings Canyon National Parks.

3.2 Meteorology

The San Joaquin Valley has a Mediterranean climate well-suited for agricultural production. The winters are usually cool and moist, but the summers are hot and dry with less than 5% of the annual precipitation falling between May and August. The principal summer wind patterns (blue arrows in **Figure** 2) are thermally-driven mesoscale circulations dominated by the onshore flow through the San Francisco Bay and Carquinez Strait. This northerly inflow brings ozone and other pollutants from the San Francisco Bay area and Sacramento [*Fast et al.*, 2012] up the valley towards Bakersfield, but also flushes the valley with clean marine air, particularly at night when the inflow can strengthen into a low-level jet (LLJ). Some of this flow exits the valley through the Tehachapi Pass into the Mojave Desert, but most is blocked by the mountains and recirculated northward where it interacts with cross-valley drainage flows and the LLJ to form an early morning low-level counterclockwise circulation (small blue arrows in **Figure** 2) known as the Fresno eddy [*Bao et al.*, 2008; *Lin and Jao*, 1995] that fosters the buildup of ozone in the central SJV near Fresno [*Beaver and Palazoglu*, 2009].

The northerly inflow is modulated by diurnal valley flows and mountain-plains circulations that create up-valley/down-valley and upslope/downslope winds along the flanks of the Sierra Nevada and Coastal Ranges [*Bao et al.*, 2008; *Zhong et al.*, 2004]. The daytime upslope winds carry O_3 and other pollutants from the valley into the surrounding mountains [*Panek et al.*, 2013] and the return (compensation) flows [*Rampanelli et al.*, 2004; *Zardi and Whiteman*, 2013] from the mountains create persistent pollution layers between 1 and 2 km above the valley when the synoptic forcing is weak [*De Young et al.*, 2005; *Fast et al.*, 2012; *Gohm et al.*, 2009].

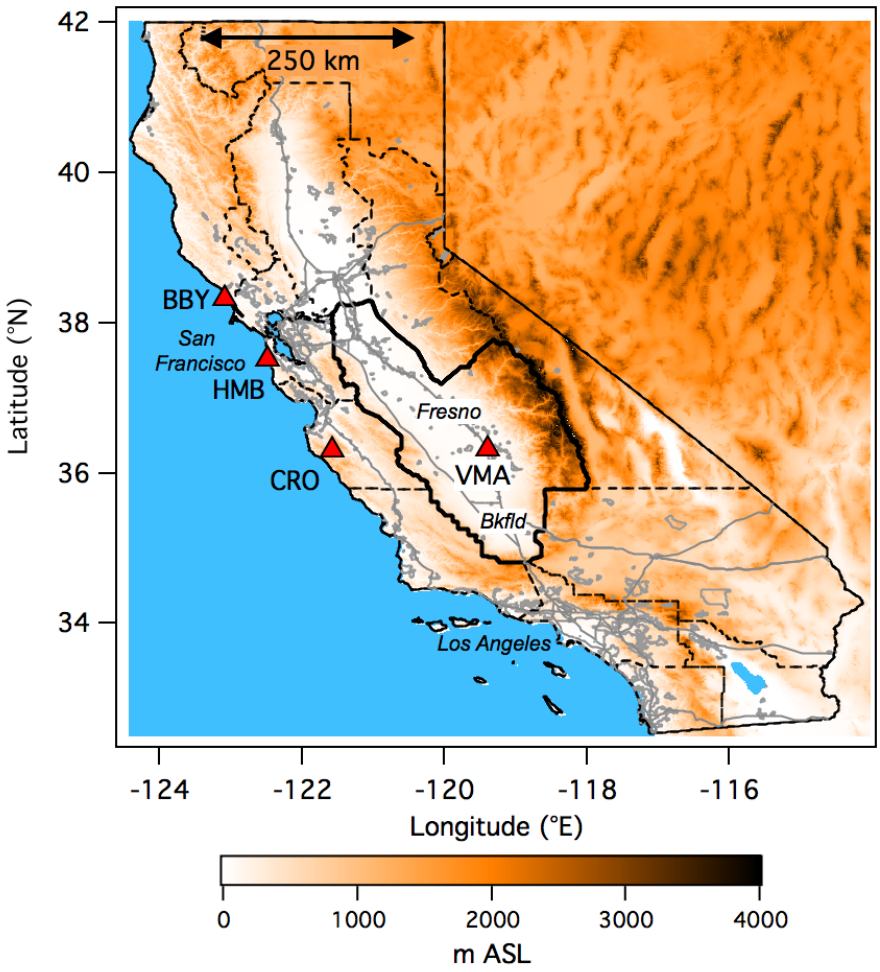

***Figure** 1. Topographic map of California showing the CABOTS measurement sites (red triangles) at Bodega Bay (BBY), Half Moon Bay (HMB), Visalia Municipal Airport (VMA), and Chews Ridge Observatory (CRO). The air basins of California are bordered by light dashed lines with the San Joaquin Valley Air Basin (SJVAB) outlined in heavier solid black. Interstate highways and urban areas are shown in gray.*

This elevated "buffer layer" [*Faloona*, 2018] acts as a reservoir for ozone and other pollutants that can potentially be re-entrained to the surface or exported to other air basins. Subsidence generated by mountain-plains circulation and the persistent North Pacific High [*Trousdell et al.*,

2016], and to a lesser extent, latent heating associated with widespread agricultural irrigation [*Li et al.*, 2016], limits growth of the convective mixed layers (ML) in the central SJV to less than ≈0.8 km on most summer days [*Bianco et al.*, 2011]. Slightly deeper mixed layers form in the southern part of the valley where the converging up-valley flows are lifted by the Tehachapi Mountains [*Trousdell et al.*, 2016]. Ozone remaining in the residual layer left after the ML decays can be re-entrained the following day or turbulently mixed into the stable nocturnal boundary layer by the LLJ and destroyed at the surface [*Caputi et al.*, 2018] (https://www.arb.ca.gov/research/apr/past/14-308.pdf).

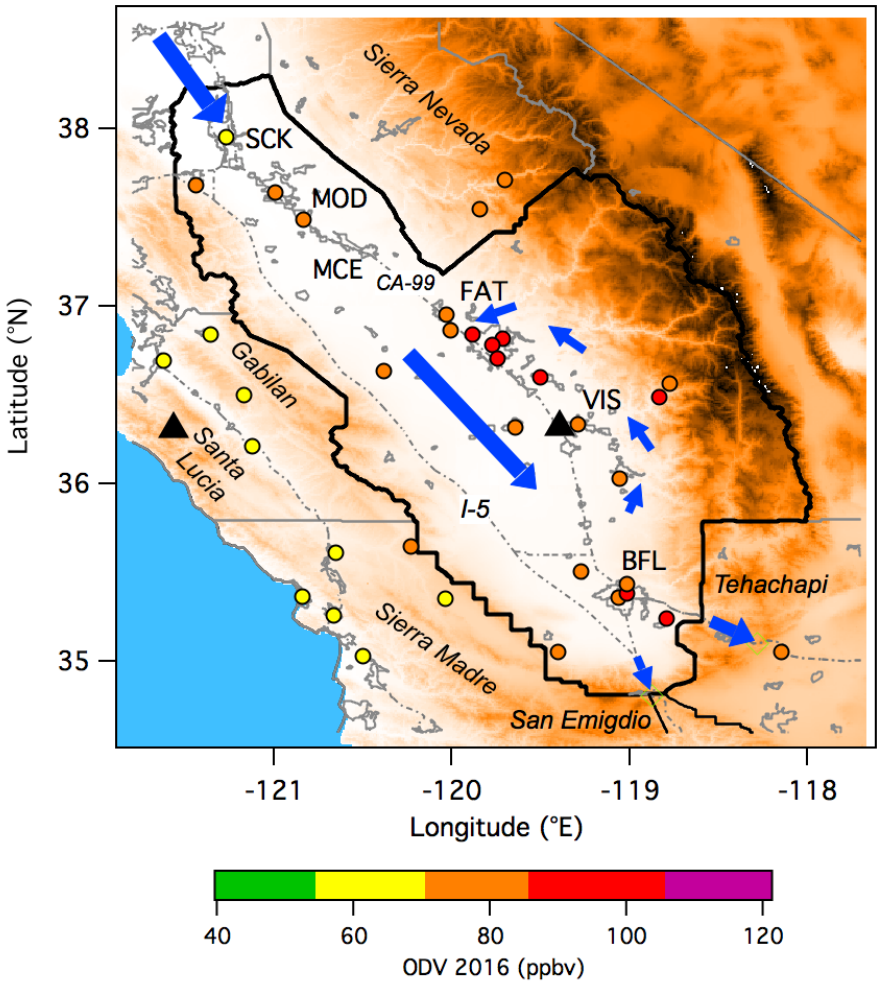

***Figure** 2. Enlarged view of the SJVAB showing regulatory O_3 monitors operated by CARB, the San Joaquin Valley Air Pollution Control District (SJVAPCD), and the U.S. National Park Service (USNPS). The monitors are color-coded by their 2016 ODV using the EPA 2015 Air Quality Index (AQI) scale. Monitors in orange ("Unhealthy for Sensitive Groups") and red ("Unhealthy") exceed the 2015 NAAQS. The CRO and VMA are represented by filled black triangles and urban areas*

are outlined in gray. The major cities labeled by their FAA airport codes are Stockton (SCK), Modesto (MOD), Merced (MCE), Fresno (FAT), Visalia (VIS), and Bakersfield (BFL). Mountain ranges are shown in italics. The blue arrows represent the primary airflows.

The large-scale subsidence associated with the Pacific High also inhibits cloud formation during summer, and the combination of hot weather and clear skies in July and August fosters rapid photochemical production of O_3 from NO_x and VOC precursors emitted in the San Francisco Bay Area and transported into the valley by the northerly flow, emitted by sources in Fresno and other urban areas of the SJV, or released by the dispersed transportation, agricultural, and petrochemical sources that pepper the SJV [*Pusede and Cohen*, 2012; *Pusede et al.*, 2014]. The Fresno eddy often recirculates these pollutants within the central SJV to create an ozone hotspot (cf. **Figure** 2) near Fresno [*Beaver and Palazoglu*, 2009].

3.3. Ozone Air Quality

The California Air Resources Board (CARB), San Joaquin Valley Unified Air Pollution Control District (SJVAPCD), and the U.S. National Park Service (USNPS) maintain a network of 25 EPA-compliant regulatory O_3 monitors within the SJVAB. **Figure** 2 shows that nearly all of the monitors in the SJVAB exceeded the 2015 NAAQS as of 2016, with the highest O_3 found along the eastern side of the valley between Fresno and Bakersfield, and into the Sierra foothills including Kings Canyon National Park. **Table** 1 shows that one or more of the regulatory monitors in the SJVAB exceeded the 2008 NAAQS (75 ppbv) on 60 days during 2016, and the 2015 NAAQS (70 ppbv) on 87 days (https://www.arb.ca.gov/adam/select8/sc8start.php).

Table 1. Ozone compliance in the San Joaquin Valley Air Basin (2013-2017)

Year	Days >75 ppbv	Days >70 ppbv	ODV	Max MDA8	Max 1-h
2013	56	81	94	106	123
2014	56	82	95	104	128
2015	55	73	93	110	135
2016	**60**	**87**	**94**	**101**	**131**
2017	54	85	92	112	143

The three SJV monitors with the most exceedance days during 2016 were the Sequoia and Kings Canyon National Parks' Ash Mountain monitor, which exceeded the 2008 NAAQS on 60 days, and the monitors at Parlier and Porterville, which exceeded the NAAQS on 52 days. **Table** 2 shows the number of 75 ppbv exceedance days recorded by each of the 7 monitors nearest (<60 km) the VMA between 2013 and 2017. The Sequoia and Kings Canyon (SQK) monitor at Ash Mountain is maintained by the U.S. National Park Service. The Hanford (HFD), Fresno-Drummond St. (FRD), Parlier (PRL), and Porterville (PRV) monitors are maintained by the

SJVAPCD and the Visalia (VIS) monitor by CARB. The Tachi-Yokut tribe operates the non-regulatory monitor at the Santa Rosa Rancheria (SRR). As is discussed in more detail below, the larger than average number of exceedance days in the SJVAB during 2016 may be due to the influence of the Soberanes Fire.

The number of exceedance days reported on the CARB and SJVAPCSD websites for each of the regulatory monitors is shown in Table 2. There were large year-to-year variations in the number of ozone exceedance days at most of the individual monitoring stations with the most pronounced variations at Porterville, where the number of exceedance days ranged from 52 in 2016 to none at all in 2014. The Porterville station used the same API/Teledyne 400 monitor from 2012 to 2016 with no issues reported in the annual Site Survey Reports and we can find no obvious reason for such large fluctuations. The corresponding values for Parlier, only 75 km to the northwest, were 52 and 36, and we note that this monitor also measured fewer exceedances in 2014. These spatial variations and interannual variability may be caused by changes in the synoptically-driven mesoscale transport associated with the thermal diurnal circulations and the Fresno eddy [*Beaver and Palazoglu*, 2009].

Table 2. Number of ozone exceedances* by monitors nearest the VMA

Year	SRR**	HFD	VIS	FRD	PRL	PRV	SQK
2013	N/A	25	2	24	50	23#	56
2014	N/A	14	10	20	36	0	51
2015	N/A	22	22	21	46	25#	52
2016	7	**20**	**7**	**32**	**52**	**52**	**60**
2017	5	22	32	17	47	17	54

* 2008 NAAQS. Data from ARB website.
** Non-regulatory. Data from AirNow.org
# Monitor offline for more than 10 days between June and August.
N/A Data unavailable

4. NOAA contributions to CABOTS

4.1 TOPAZ Lidar and supporting measurements

The primary contribution of NOAA/ESRL/CSD to CABOTS was the deployment and operation of the TOPAZ differential absorption lidar (DIAL) system at the Visalia Municipal Airport. TOPAZ was originally developed for profiling O_3 and particulate backscatter in the boundary layer and lower free troposphere from NOAA Twin Otter aircraft [*Alvarez et al.*, 2011; *Langford et al.*, 2012; *Langford et al.*, 2010; *Langford et al.*, 2011; *Senff et al.*, 2010]. The lidar was reconfigured and installed in a medium-duty truck after CalNex, and deployed in this configuration to several field campaigns including the 2013 Las Vegas Ozone Study (LVOS) [*Langford et al.*, 2015b] before CABOTS. The system is automated, but not autonomous, and safety considerations mandate that two operators always be present. This limits the data collection to no more than 10-12 hours on most days.

The TOPAZ lidar uses a low energy (≈100 μJ), high pulse rate (1 kHz) quadrupled Nd:YLF pumped Ce:LiCAF laser that is re-tuned between each pulse to generate light at three different wavelengths ranging from 286 to 294 nm reducing the effective repetition rate to 333 Hz [*Alvarez et al.*, 2011]. The low pulse energies and tunability of TOPAZ allow the system to be operated from airports and other locations where eye safety is a major concern and facilitate optimization of the wavelengths for lower tropospheric measurements. The laser pulses are transmitted and backscatter signals collected by a zenith viewing coaxial transmitter/receiver beneath an opening in the truck roof. A large scanning mirror inserted above the transceiver allows profile measurements at different slant angles (**Figure** 3). These slant profiles can be combined to create vertical profiles that begin much closer to the ground than conventional vertically staring lidar systems [*Proffitt and Langford*, 1997]. During CABOTS, the scanning mirror was moved sequentially between elevation angles of 90, 20, 6, and 2° with a 225-s averaging time at 90° and 75-s averaging times at the other 3 angles. The cycle was repeated approximately every 8 minutes and the vertical projections combined to create a composite vertical profile beginning 27.5 ± 5 m above ground level (AGL). This approach assumes the O_3 mixing ratios to be horizontally homogenous over a distance of up to 800 m during the 8 minutes required to complete the measurement cycle. This assumption is usually valid, but there are exceptions as discussed in more detail below.

The TOPAZ truck was parked on the west side of the VMA between the airport runway and CA-99 (**Figure** 4) and the lidar slant paths oriented parallel to the runway over open farmland to the southeast (135°) to avoid populated areas and the highway. Visalia was chosen because of its proximity to the Sequoia and Kings Canyon National Parks and location halfway between the Parlier and Porterville monitors which often measure the highest ozone in the SJV. The VMA was selected to facilitate intercomparison with the Scientific Aviation and NASA research aircraft and because of the co-located (160 m) San Joaquin Valley Air Pollution Control District (SJVAPCD) wind profiler and Radio Acoustic Sounding System (RASS) [*Bao et al.*, 2008]. Local boundary layer heights are derived from measurements made by the co-located SJVAPCD RASS. The hourly mean boundary layer height is estimated from the derivative of the virtual potential temperature profile measured at the top of each hour and then smoothed over a 3-hour

window. This method is relatively insensitive to assumptions about the gradient threshold, but only works well for heights up to about 1 km [*Bianco et al.*, 2011]. Independent estimates of the mixed layer height (MLH) were derived from direct measurements of the vertical velocity variance by an upward looking Doppler lidar deployed by NOAA ESRL to the VMA during the last two weeks of the second CABOTS IOP [*Bonin et al.* 2017].

In addition to the lidar, the truck is equipped with an *in-situ* O_3 monitor (2B Technologies Model 205) that samples air 5 m above the surface and an Airmar 150WX weather station to measure temperature, pressure, relative humidity, and wind speed and direction. The 2B ozone monitor operated continuously throughout the TOPAZ deployment with the system response checked during each IOP by an external mobile calibration source operated by CARB. These calibration checks revealed a 3% low bias in the 2B measurements that has been corrected in the data included in this report.

***Figure** 3. (Left) TOPAZ lidar truck parked at the Visalia Municipal Airport (VMA). The 2B sampling mast can be seen to the right of the scanning mirror and warning light. Note the traffic on CA-99 in the background. (Right) Composite vertical O_3 profile showing the altitude segments derived from each of the slant profiles.*

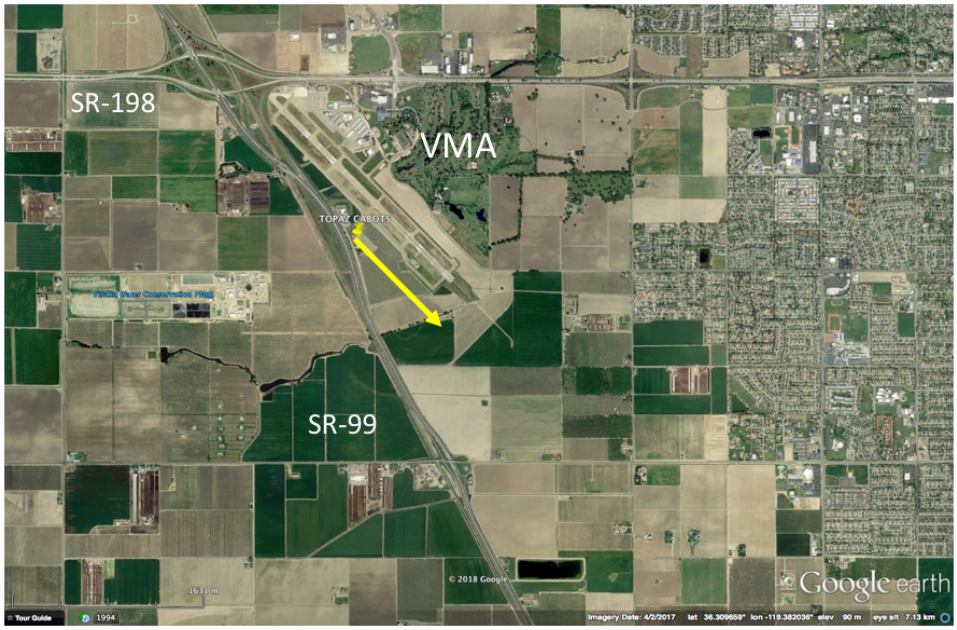

***Figure** 4. Aerial view of the Visalia Municipal Airport (VMA) showing the location of TOPAZ and the 1 km lidar slant path line of sight (yellow line).*

The O_3 and aerosol profiles were computed using the iterative technique described in [*Alvarez et al.*, 2011]. The O_3 profiles were retrieved using the shortest and longest wavelengths (≈287 and 294 nm) with 30 m range gates and a smoothing filter with a varying width that increased from 270 m at the minimum range (800 m) up to 1400 m at the maximum range (8 km). The aerosol profiles were computed from the 294-nm data at 30-m range resolution. The aerosol backscatter and extinction wavelength dependences, which are needed to correct differential aerosol effects in the O_3 calculation, are assumed to follow a power law. In most cases, a power-law exponent of 0 (no wavelength dependence) was used for the aerosol backscatter with an exponent of -0.5 for aerosol extinction. These values seem to be a good compromise for a wide range of aerosol types [*Völger et al.*, 1996]. In the first iteration step, O_3 profiles are calculated without differential aerosol backscatter and extinction corrections. These O_3 profiles are then used to correct ozone extinction in the 294-nm channel, from which first-cut aerosol profiles are calculated. In the second iteration step, O_3 profiles are computed with an aerosol correction based on the aerosol backscatter and extinction profiles from the first step. These O_3 profiles are then used to provide a more accurate O_3 extinction correction of the signal data at 294 nm, which in turn results in a more accurate aerosol profile retrieval. This iteration procedure is repeated until the O_3 profiles produced in successive iteration steps converge. Convergence is reached when the absolute difference between successive O_3 profiles is less than 2.5×10^{15} m^{-3} (corresponding to about 0.1 ppbv) at all range gates.

The DIAL calculations used National Centers for Environmental Prediction (NCEP) North American Regional Reanalysis (NARR) temperature and pressure profiles for the grid point closest to the TOPAZ lidar location to account for the temperature dependence of the O_3 cross

sections [*Malicet et al.*, 1995] and convert the retrieved O_3 number densities into mixing ratios. The 3-hourly NARR temperature and pressure profiles were interpolated to the exact time each individual O_3 profile was recorded. The total uncertainties in the 8-min ozone retrievals are estimated to increase from ±3 ppbv below 4 km, to ±10 ppbv at the top of the profile. The unpolarized single wavelength backscatter profiles provide a semiquantitative measure of the particulate spatial distribution, but do not distinguish between different particle types or size distributions.

A TOLNet lidar intercomparison at the 2014 Colorado DISCOVER-AQ campaign [*Wang et al.*, 2017] found that the performance of the original analog data acquisition system developed at NOAA for aircraft operations in 2004 had deteriorated. This system was accordingly replaced with a new commercial dual analog/photon counting system prior to CABOTS. This upgrade improved the stability of the lidar retrievals and greatly expanded the useful altitude range of TOPAZ compared to earlier studies. The maximum altitude achieved during CABOTS ranged from ~6 km during the day to more than 8 km at night depending on the lidar return signal-to-noise ratios, which varied with laser power, atmospheric extinction, and solar background light. The improved performance was confirmed during the TOLNet multi-lidar Southern California Ozone Observation Project (SCOOP) intercomparison at the NASA Jet Propulsion Laboratory (JPL) Table Mountain Facility (TMF) in the San Gabriel Mountains immediately after CABOTS [*Leblanc et al.*, 2018].

4.2 NOAA Model Analyses

The TOPAZ lidar measurements were guided by operational analyses from the NOAA National Environmental Satellite, Data, and Information System (NESDIS) Real-time Air Quality Modeling System (RAQMS) assimilation/forecast model [*Pierce et al.*, 2003; *Pierce et al.*, 2007] and the NOAA ESRL RAP-Chem model during the field campaign. Subsequent data interpretation has been guided by RAP-Chem and the FLEXPART particle dispersion model [*Stohl et al.*, 2005].

4.2.1 NOAA NESDIS RAQMS model

The NOAA/NESDIS RAQMS (Realtime Air Quality Modeling System) model is a unified (stratosphere-troposphere) online global chemical and aerosol assimilation/forecasting system developed specifically to support airborne field missions [*Pierce et al.*, 2003; *Pierce et al.*, 2007]. The meteorological forecasts are conducted using the University of Wisconsin Hybrid Model [*Schaack et al.*, 2004], and the chemical forecasts are initialized daily at 12 UT with real-time assimilation of Ozone Monitoring Instrument (OMI) cloud-cleared total column ozone and Microwave Limb Sounder (MLS) ozone profiles from the NASA *Aura* satellite, and MODIS aerosol optical depth from the NASA *Terra* and *Aqua* satellites. RAQMS has been run routinely in a forecast mode since 2010 with 2° x 2° resolution analyses and forecasts prior to 2012, and 1° x 1° analyses since 2012. The model predicts global O_3, CO, SO_4, and black organic carbon distributions at 6-hour intervals for the next 4 days. The real-time analyses are archived online (http://raqms-ops.ssec.wisc.edu).

4.2.2 NOAA ESRL RAP-Chem model

The NOAA ESRL Global Systems Division (GSD) RAP-Chem forecast system (https://rapidrefresh.noaa.gov/RAPchem/Welcome.cgi) uses the Weather Research and Forecasting model coupled to Chemistry (WRF-Chem) model [*Grell et al.*, 2005; *Pagowski et al.*, 2010] driven by meteorology from the NCEP's GFS analysis at 00 UTC and 6-hourly forecasts thereafter. This 13-km resolution North American model uses the Regional Atmospheric Chemistry Mechanism (RACM) [*Goliff et al.*, 2013] and aerosol scheme by *Ahmadov et al.* [*Ahmadov et al.*, 2012]. It incorporates MEGAN biogenic emissions [*Guenther et al.*, 2006], and the U.S EPA NEI-11 (CONUS) version-1 anthropogenic emission inventories with oil/gas sector emissions updated to version-2. Biomass burning emissions are derived from MODIS and GOES-West satellite observations.

The RAP-Chem model includes surface deposition, photolysis, and convective and turbulent chemical transport, and wet removal of aerosols by resolved and convective precipitation with advective chemical transport performed simultaneously with the meteorology. The lateral boundary conditions for chemistry are obtained from the RAQMS model [*Pierce et al.*, 2003]. Operational forecasts are run at 00 UTC at 3-h forecast intervals for up to 48 hours, and plots of the CO and O_3 distributions on the 500, 700, and 850 hPa and surface levels were archived for the entire CABOTS period by M. Pagowski of the NOAA ESRL Global Systems Division and the University of Colorado Cooperative Institute for Research in Environmental Sciences (CIRES).

4.2.3 FLEXPART particle dispersion model

FLEXPART [*Stohl et al.*, 2005] is a passive tracer model (no chemistry) that calculates the evolving distribution of a multitude of "particles" transported forward in time for up to 20 days from a specified source region. FLEXPART calculations played a key role in earlier TOPAZ studies of long-range transport and stratosphere-to-troposphere transport (STT) in the western U.S. [*Langford et al.*, 2012; *Langford et al.*, 2015b]. Asian pollution CO (ASCO), biomass burning CO (BBCO), and stratospheric O_3 (STO3) tracer distributions were calculated with 0.25° resolution over an output domain extending from 130 to 70°W and from 20 to 50°N at 3-h intervals. The particles were transported by winds from the European Centre for Medium-Range Weather Forecasts (ECMWF) operational (0.5° x 0.5°) model forecasts and by sub grid motions including convection and turbulence based on the parameterization schemes of *Emanuel and Zivkovic-Rothman* [*Emanuel and Zivkovic-Rothman*, 1999] and *Hanna* [*Hanna*, 1982] respectively. The tracer distributions were calculated at the surface (1 km above ground level) and on the 700hPa, 500hPa, 400hPa levels for June-August 2016.

The stratospheric O_3 tracer was represented by particles released into the stratosphere (>2 potential vorticity units or PVU) with the O_3 mixing ratios calculated using a linear relationship between O_3 and potential vorticity (60 ppbv/PVU) at the particle origin. The Asian CO tracer is based on the amount of CO released into the boundary layer from anthropogenic sources in East Asia using the EDGAR 3.2 fast track inventory [*Olivier et al.*, 2005]. Biomass burning CO emissions were calculated using the ECMWF Copernicus Atmosphere Monitoring System (CAMS) near-real time biomass burning emission estimates based on the Global Fire

Assimilation System (GFAS), which converts Fire Radiative Power (FRP) observations from MODIS satellites into smoke constituents [*Francesca Di et al.*, 2016]. Since CO is chemically inert over the timescale of the FLEXPART calculations, these two tracers show the relative importance and temporal evolution of these potential O_3 sources, but cannot be quantitatively compared to the stratospheric O_3 flux since FLEXPART does not include chemistry. The FLEXPART calculations used here were generously provided by S. Evan and J. Brioude of the Laboratoire de l'Atmosphere et des Cyclones (LACy), UMR 8105, CNRS, Université de La Réunion, Météo-France, Saint-Denis, La Reunion, France.

5. TOPAZ Measurements

TOPAZ measurements were conducted at the VMA over two 3-week intensive operating periods (IOPs) in the late spring (IOP1: May 27 to June 18) and summer (IOP2: July 18 to August 7) of 2016. The first IOP officially started on May 29, but measurements from May 27 and 28 are included in the following discussions. A total of 440 hours of lidar data were recorded during the first (1654 profiles over 22 days) and second (1686 8-min profiles over 21 days) IOPs with an average of more than 10 hours of nearly continuous measurements per day. The skies were mostly cloud-free during both IOPs, but a few profiles were truncated by high clouds during the passage of a cold front on June 11-12. **Table** 3 shows the TOPAZ temporal coverage during each IOP.

Table 3. TOPAZ temporal coverage during CABOTS

	IOP1		IOP2	
Start (PDT)	Days	Profiles	Days	Profiles
0	3	22	1	8
1	2	15	1	4
2	2	15	0	0
3	2	15	0	0
4	1	11	0	0
5	1	11	0	0
6	2	15	0	0
7	2	15	0	1
8	6	48	1	10
9	13	95	3	23
10	14	108	6	46
11	16	122	9	66
12	18	137	8	60
13	20	148	14	102
14	21	160	16	119
15	21	161	15	109
16	22	168	14	108
17	20	152	13	96
18	11	86	16	118
19	7	51	12	90
20	4	32	8	57
21	3	23	7	49
22	3	22	3	19
23	3	23	2	15

The O_3 and backscatter (ß) measurements from both IOPs are summarized as a series of time-height curtain plots in **Figures** 5 and 6, respectively. The scalloped appearance of the individual curtain plots is caused by increased solar background radiation near local noon, which reduces the lidar maximum range.

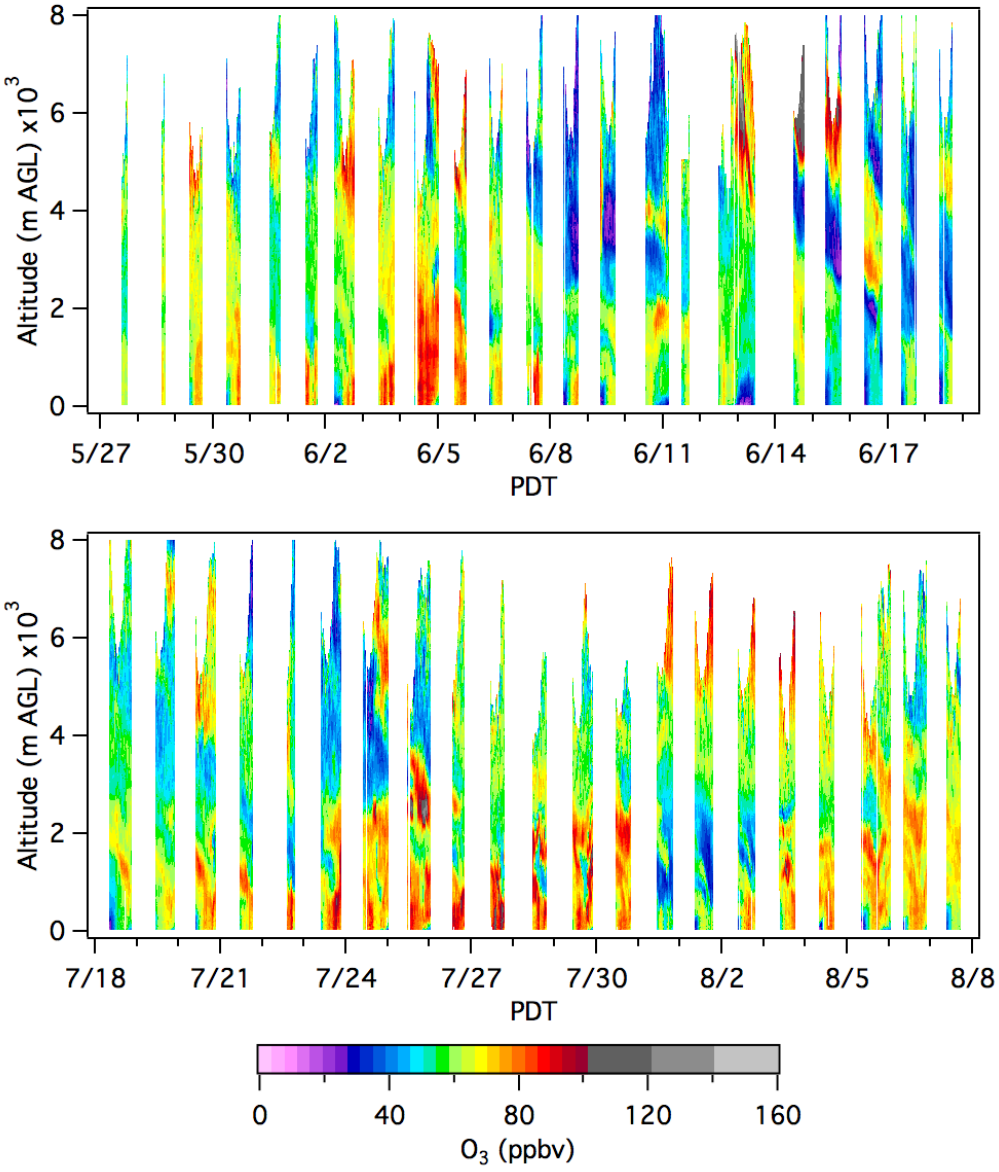

***Figure** 5: Time-height curtain plots of the O_3 concentrations measured by TOPAZ at the VMA during the first (top) and second (bottom) IOPs.*

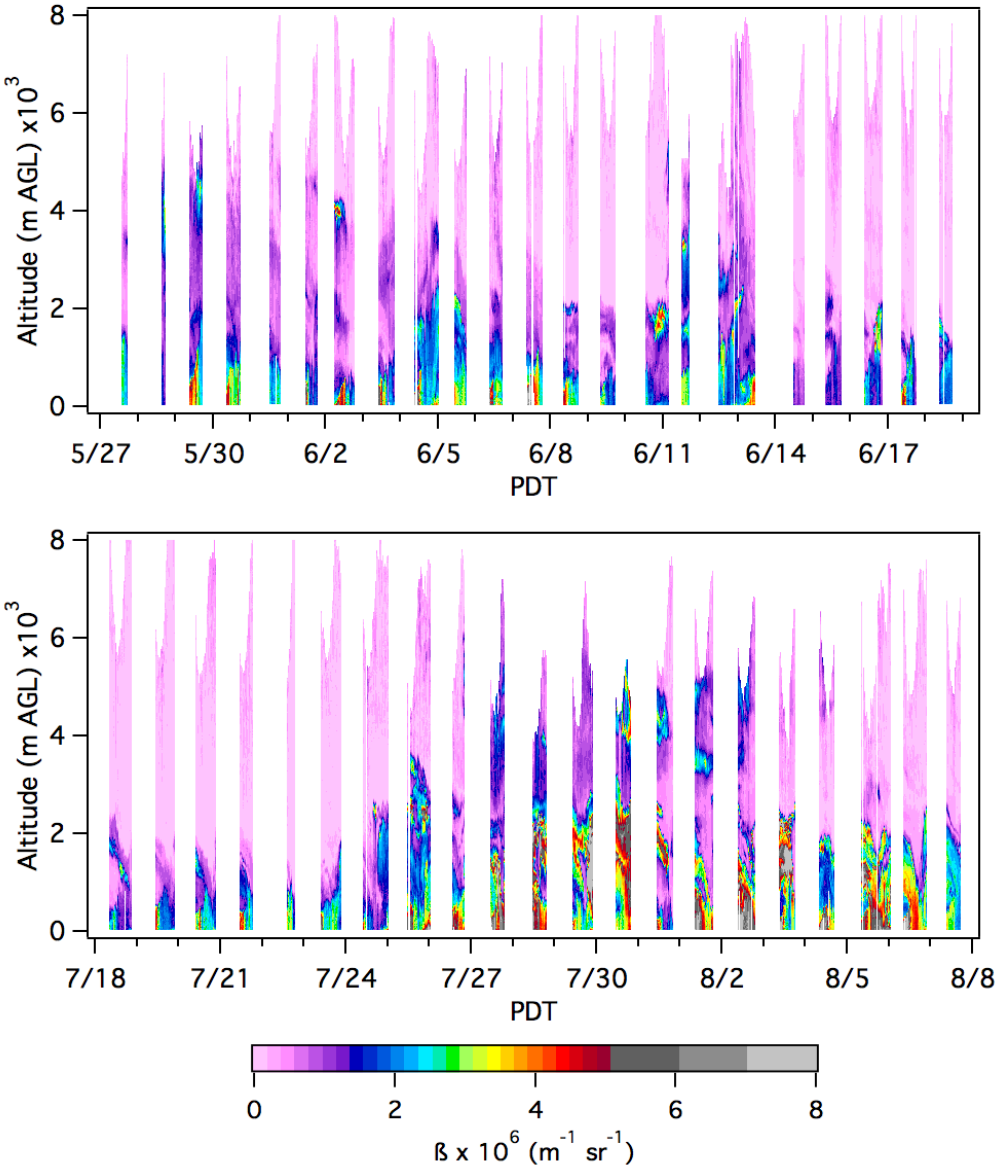

***Figure 6**: Time-height curtain plots of the particulate (smoke and aerosol) backscatter distributions measured by TOPAZ at the VMA during the first (top) and second (bottom) IOPs.*

The TOPAZ measurements are also shown as diurnally-averaged hourly-binned curtain plots for each IOP in **Figures** 7 and 8**.** Only times with at least 5 days of data are shown (cf. **Table** 3). The statistics are most robust for the hours between 1300 and 1900 PDT when the averages represent at least 12 days of measurements. The corresponding mean winds from the co-located SJVAPCD profiler are superimposed on each plot; wind speeds less than 2 m s^{-1} are represented by plus signs. The wind vectors show the horizontal wind direction with the top of the plot representing north and the right side east. The mean winds appear very similar to those shown in *Bao et al.* [2008] that were based on a 5-day period in late July and early August during the 2000 Central California Ozone Study. The heavy black line in each plot represents the boundary layer height calculated from the derivative of the RASS virtual potential temperature profiles using a threshold of +0.5 °C. Similar results were obtained if this threshold was changed by a factor of two in either direction. The dashed line in **Figure** 8 shows the boundary layer height (BLH) calculated from direct measurements of the vertical velocity variance by an experimental NOAA ESRL Doppler lidar deployed next to TOPAZ for the last two weeks of the campaign. These two BLH measurements are in very good agreement, and are also consistent with the gradient in the TOPAZ UV backscatter profiles. All three methods indicate that the mean BLH was about 500 m, in agreement with the earlier findings of *Bianco et al.* [2011].

The diurnally-averaged O_3 plot for IOP1 shows depletion in a shallow nocturnal boundary layer during the early morning hours followed by a buildup of O_3 in the boundary layer during the day. The corresponding backscatter measurements show the opposite behavior for aerosols. The profiler measurements show northwesterly (up-valley) winds driven by the Carquinez inflow in the lowest 1.5 km during the day that deepens to about 2.5 km in the late afternoon and then strengthens into a low-level jet (LLJ) during the night. The cluster of weak average winds around 0800 PDT in the lowest 500 m show the influence of the Fresno eddy.

The mean winds weaken above the LLJ in the late evening and higher mean O_3 and aerosol concentrations appear over the VMA between 1 and 2 km as pollution transported into the Sierra Nevada by the afternoon upslope winds is returned in an elevated “buffer layer” by the compensation flow closing this circulation [*Rampenelli et al.* 2004, *Zardi and Whiteman*, 2013]. These weak return flows disappear in the averaged plots, but can be seen in the VMA profiler measurements when the synoptic forcing is weak. The higher concentrations in the buffer layer reflect the fact that O_3 can persist there for days and is often present on days when the boundary layer is relatively clean. The generally weak mean winds around 2 km explain this persistence.

There were fewer early morning measurements during the second IOP, but the overall appearances of the diurnal plots are qualitatively similar. The O_3 and backscatter were greatly increased, however, both within and above the boundary layer as smoke plumes from the Soberanes Fire made their way into the Visalia area (**Section** 8).

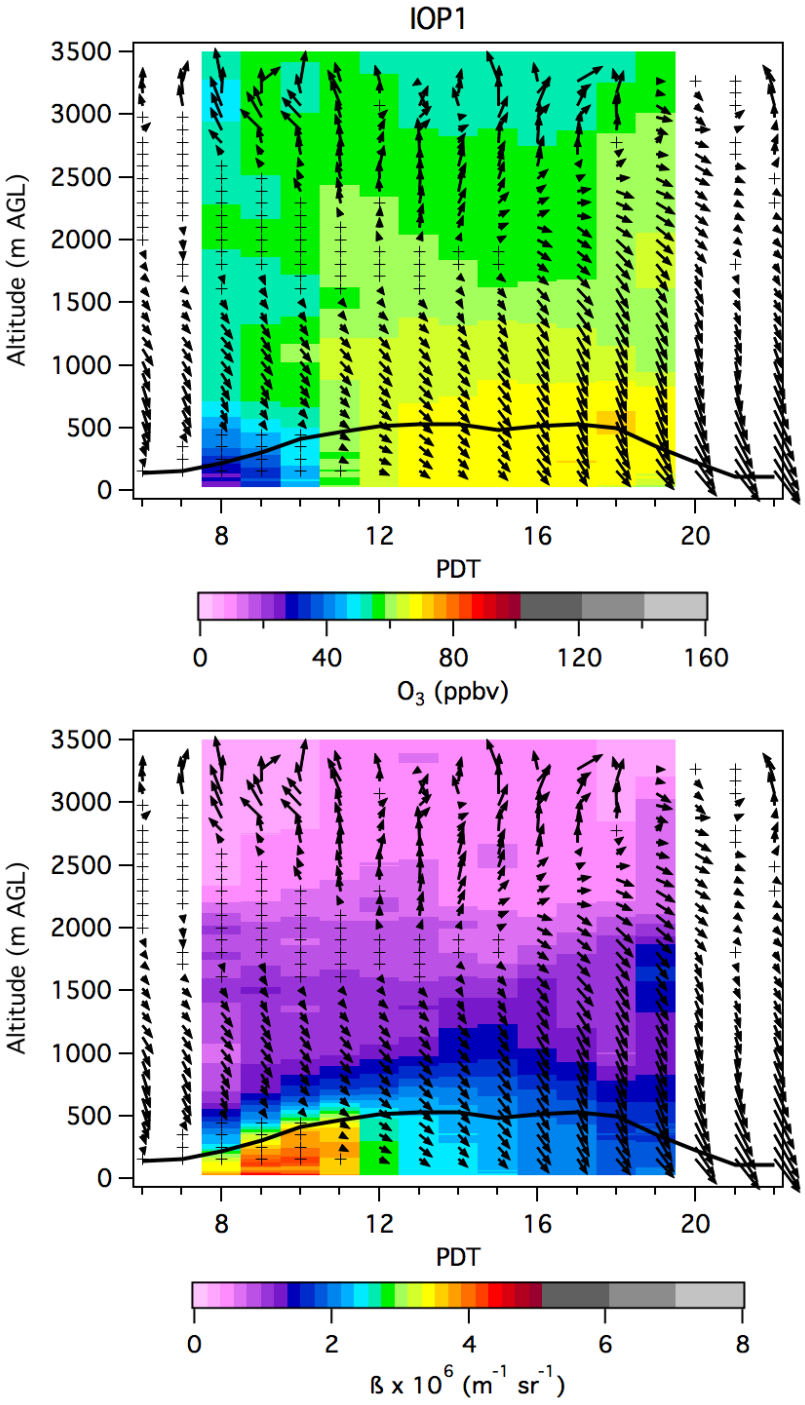

***Figure** 7. Diurnally-averaged ozone (top) and backscatter (bottom) measured by TOPAZ at the VMA during the first IOP with the mean winds from the co-located SJVAPCD profiler superimposed. The heavy black line shows the mean boundary layer height inferred from the co-located RASS temperature gradients. The dashed black line shows the boundary layer height derived from the vertical velocity variance measured by the co-located NOAA Doppler lidar.*

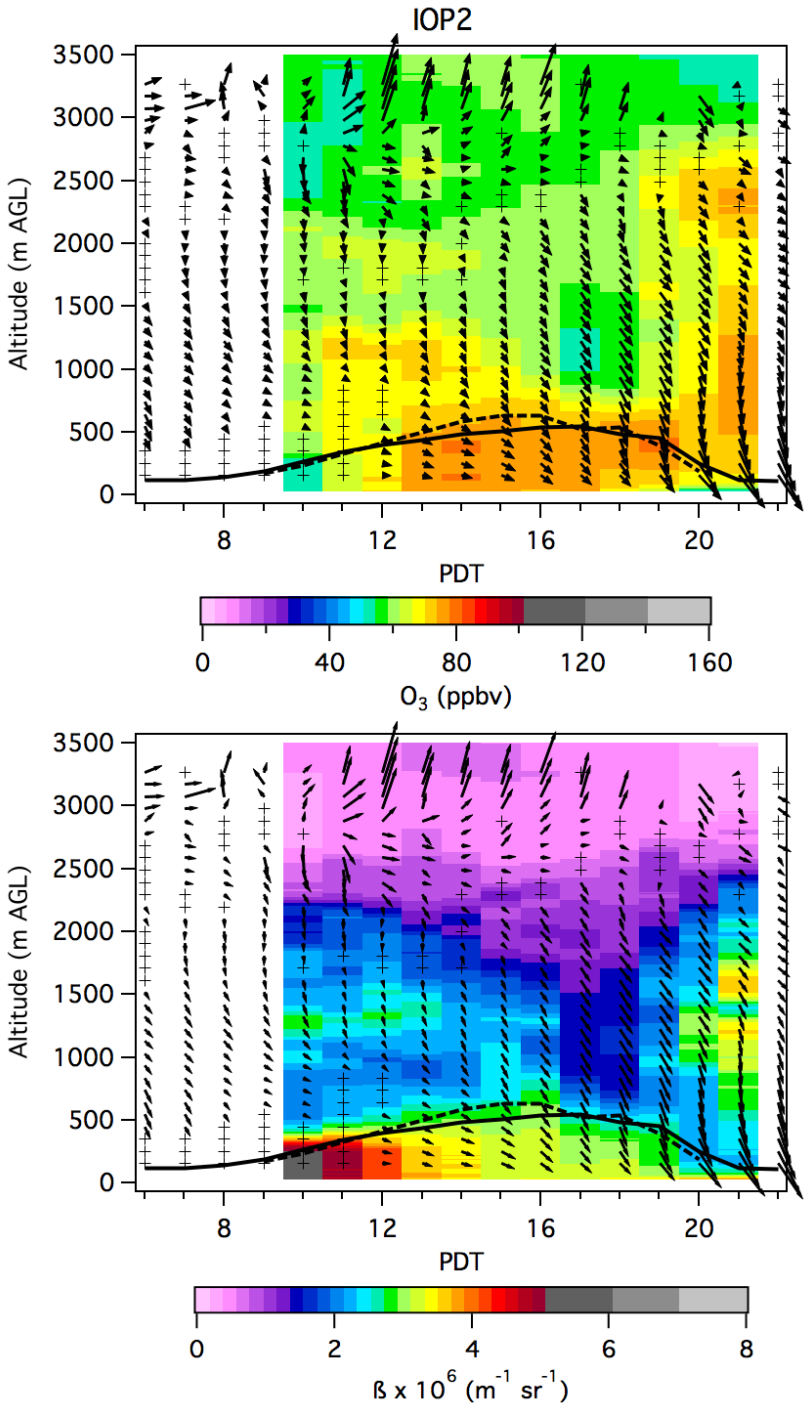

***Figure** 8. Diurnally-averaged ozone (top) and backscatter (bottom) measured by TOPAZ at the VMA during the second IOP with the mean winds from the co-located SJVAPCD profiler superimposed. The heavy black line shows the mean boundary layer height inferred from the co-located RASS temperature gradients. The dashed black line shows the boundary layer height derived from the vertical velocity variance measured by the co-located NOAA Doppler lidar.*

6. TOPAZ Results and Validation

6.1 Comparison to surface measurements

The representativeness of the VMA sampling site can be assessed by comparing the in-situ and low elevation TOPAZ measurements with measurements from nearby O_3 monitors. These routine air quality measurements also provide important context for the CABOTS measurements. The filled circles in **Figure** 9 show the locations of the nearest operational O_3 monitors along the valley floor during CABOTS. The circle colors show the AQI categories for the mean MDA8 measured during the (a) first, and (b) second, IOP respectively. The Hanford (HFD), Fresno-Drummond St. (FRD), Parlier (PRL), and Porterville (PRV) monitors are maintained by the SJVAPCD and the Visalia (VIS) monitor by CARB. The Tachi-Yokut tribe operates the non-regulatory monitor at the Santa Rosa Rancheria (SRR). The nearest monitors to the VMA are the CARB (API/Teledyne 400) monitor about 10 km east of the VMA on N. Church Street in Visalia (102 m ASL) and the SJVAPCD (API/Teledyne 400) monitor about 22 km to the west of VMA in Hanford (82 m ASL). These monitors sample air 7 and 5 m above the ground, respectively.

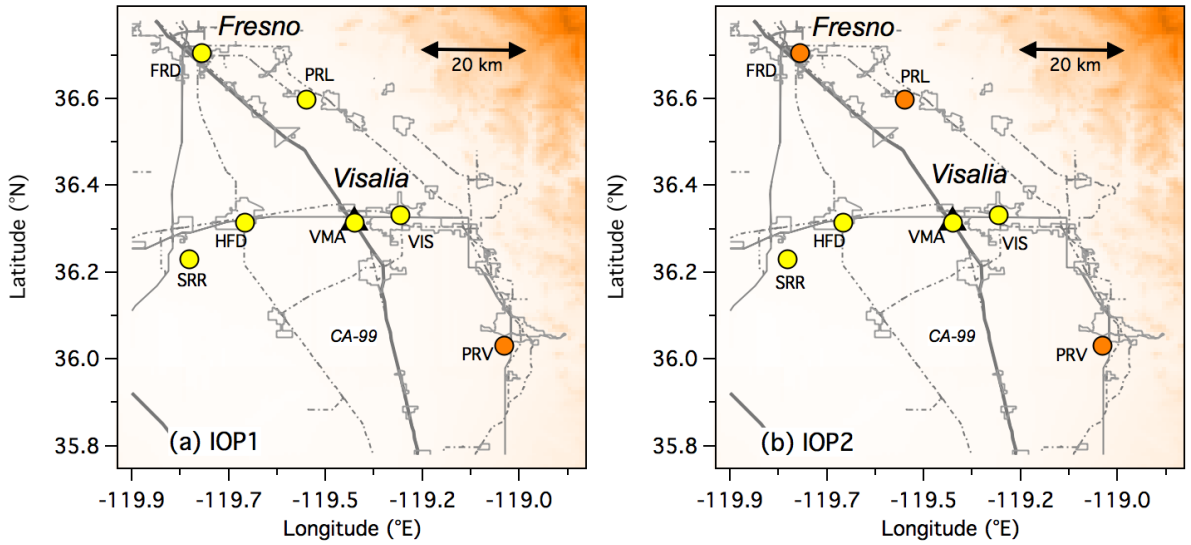

***Figure** 9. Enlarged view of the Visalia area showing the nearest active O_3 monitors in the valley (filled circles) during CABOTS. The colors show the AQI category (cf. **Figure** 2) corresponding to the mean MDA8 O_3 measured during the first (a), and second (b), IOP. Yellow corresponds to "moderate" and orange to "Unhealthy for Sensitive Groups" concentrations. The solid and dot-dash gray lines represent the major highways and railroads, respectively. Urban areas are outlined in light gray.*

Figure 10 plots the MDA8 O_3 concentrations measured by the NOAA 2B monitor at the VMA and by each of the monitors in **Figure** 9 during each of the IOPs. The upper panel (a) shows a

broad maximum in the MDA8 across the SJV during the first week of June when TOPAZ also measured high O_3 in the lower troposphere (**Figure** 5). The highest MDA8 values were measured at Parlier and Porterville, but the monitor-to-monitor differences were relatively small. At least one of the 5 regulatory monitors in the east-central SJV exceeded both the 2015 and 2008 NAAQS on 8 of the 22 days during IOP1.

The surface O_3 concentrations were generally higher and the monitor-to-monitor differences greater during the second IOP when the NAAQS was exceeded by one or more monitors on 13 out of 20 days. **Figure** 5 shows that the lower tropospheric O_3 measured by TOPAZ was also higher. The highest overall concentrations were measured at Parlier near the middle of the IOP (July 26-29). All 6 monitors (and the VMA) exceeded the NAAQS on July 27 when Parlier reported an MDA8 of 101 ppbv, the highest value recorded in all of the SJVAB during 2016. These high concentrations occurred soon after the start of the Soberanes Fire, which scorched nearly 57,800 acres about 200 km west of Visalia near Big Sur before the end of the second IOP, and burned a total of 132,127 acres of chaparral, tall grass, and timber before it was extinguished on 12 October. The Soberanes influence may explain the greater monitor-to-monitor variability during the second IOP and the increase in exceedance days compared to recent years (**Table** 2). The measurements from both IOPs show a general increase in O_3 from the center of the valley to the Sierra foothills with the lowest concentrations typically measured at Santa Rosa Rancheria.

Figure 11 compares the 1-min averaged VMA 2B *in-situ* surface mixing ratios (dots) measured during each IOP together with the TOPAZ mixing ratios retrieved from a height of 27.5±5 m (red line) and at a range of ≈800 m along the slant path above the agricultural fields to the southeast (cf. **Figure** 4). The MDA8 O_3 from the VMA and the Hanford regulatory monitor are also shown.

Figure 12a displays an enlarged view of the VMA surface measurements (gray line) from June 9-13 together with the mixing ratios from the 27.5 m TOPAZ measurements (filled black circles). Also plotted are the 1-h average ozone mixing ratios from the Visalia and Hanford monitors. The four sets of measurements agreed fairly well during the day but diverge markedly at night and in the early morning when ozone was removed by surface deposition and titration by NO_x within the surface layer. The losses were greatest at the VMA monitor located next to the heavily-trafficked CA-99 and SJVR railroad line. Much smaller losses were measured by the rural Hanford monitor and intermediate losses were measured by the Visalia monitor which is located on a downtown rooftop.

Figure 12b shows that while the 27.5 m TOPAZ measurements were usually larger than the VMA *in-situ* measurements, the correspondence approaches 1:1 when the comparison is restricted to daytime measurements made after the nocturnal inversion had dissipated (0900 to 1800 Pacific Daylight Time, PDT or UT-7 h) and the comparison restricted to periods with southeasterly winds greater than 2.5 m s^{-1} (cf. **Figure** 4) to exclude local influences (e.g. CA-99) and ensure that the downrange lidar and in-situ monitor were sampling the same air mass.

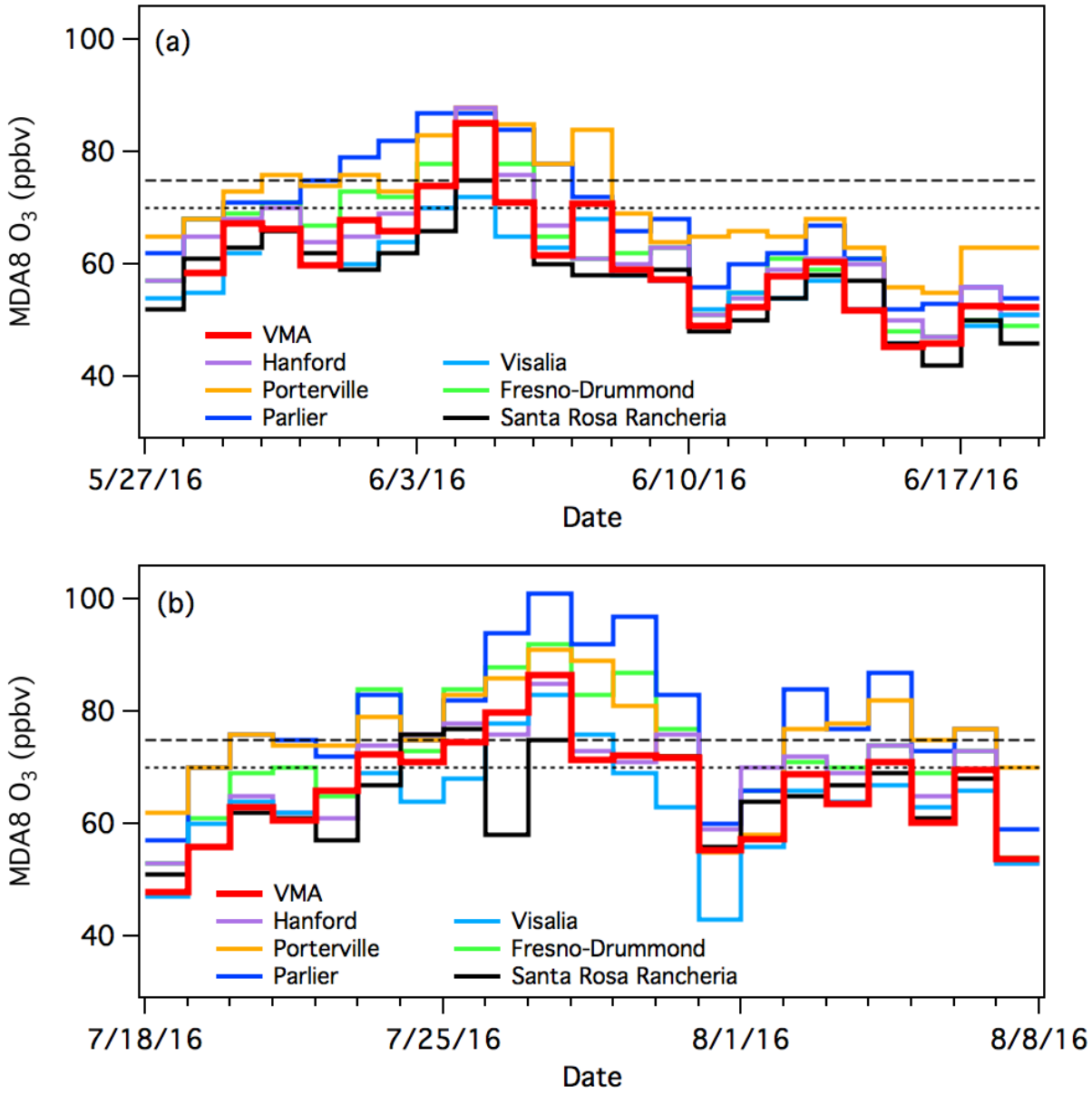

***Figure** 10. MDA8 O_3 measured by the TOPAZ in-situ monitor (VMA) and the nearby CARB, SJVAPCD, and Tachi-Yokut monitors shown in **Figure** 9 during the first (a), and second (b), CABOTS IOPs. The dashed and dotted horizontal black lines show the 2008 and 2015 NAAQS, respectively.*

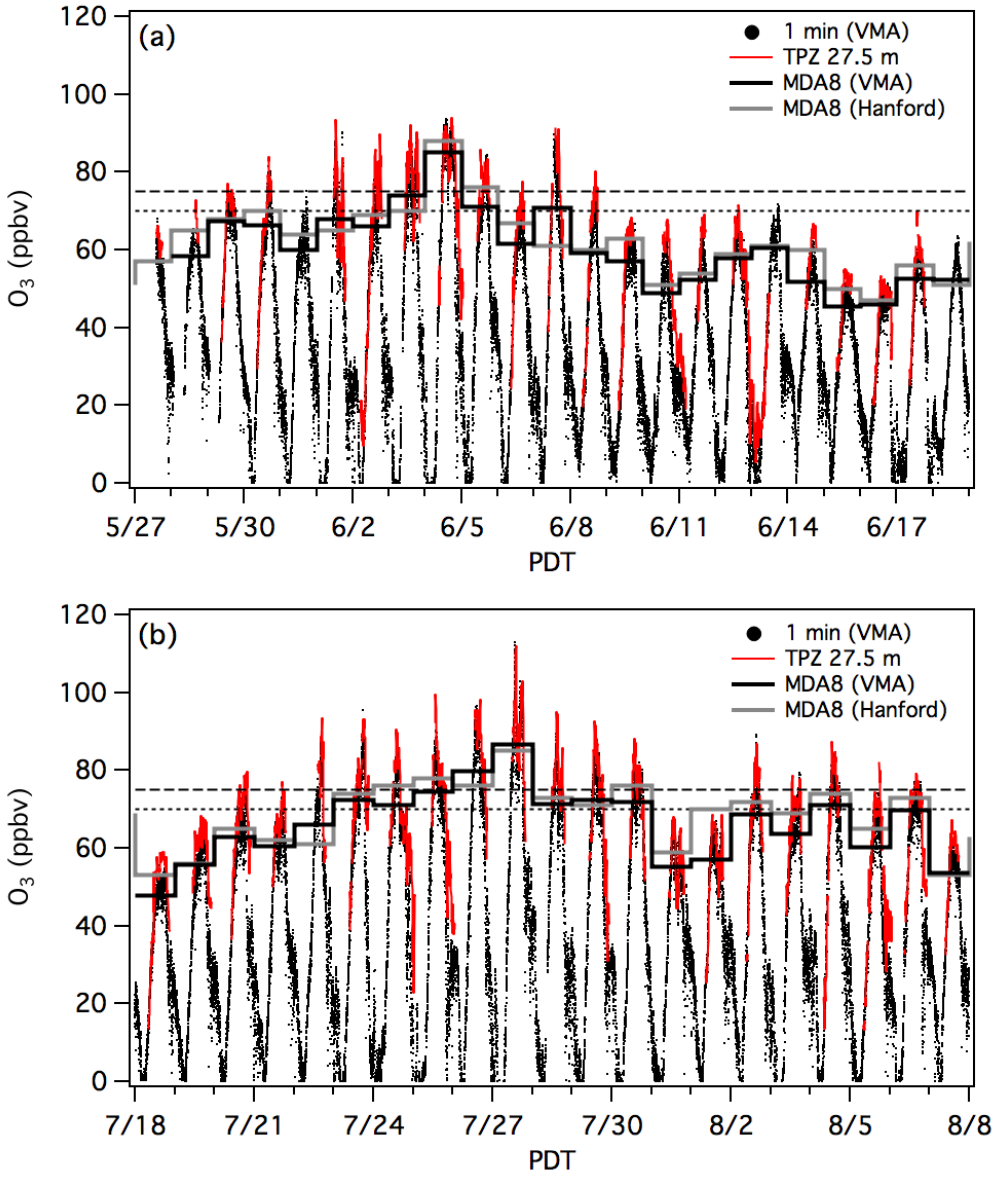

***Figure** 11. Time series plots of the VMA in-situ (gray dots) and TOPAZ O_3 concentrations measured at 27.5 m (red line) during the first (a), and second (b) CABOTS IOPs. The black and gray staircase lines represent the VMA and Hanford MDA8 O_3. The horizontal dashed and dotted lines show the 2008 NAAQS, and 2015 NAAQS/CARB 8-h standards, respectively.*

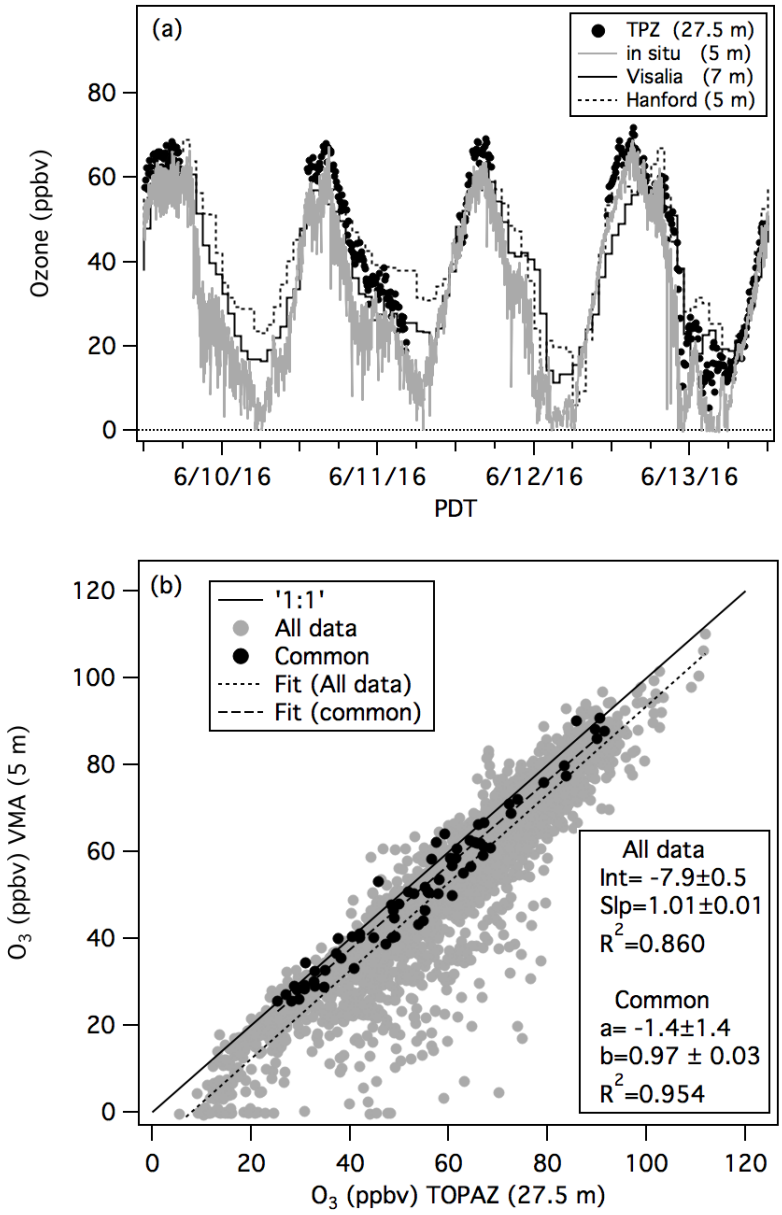

***Figure** 12. (a) Four-day time series comparing the O_3 mixing ratios measured by the 2B monitor in the TOPAZ truck (gray line) and retrieved by TOPAZ 800 m downrange and 27.5±5 m above the ground (filled black circles). The solid and dotted black lines show the 1-h measurements from the Visalia and Hanford monitors. (b) Scatter plot comparing the 27.5 m TOPAZ measurements to the interpolated 5 m in-situ measurements. The filled gray circles (dotted fit) show the entire CABOTS data set and the filled black circles (dashed fit) daytime measurements (0900 to 1800 PDT) and southeasterly (125 to 145°) winds greater than 2.5 m s^{-1}.*

Figure 13 compares the lowest elevation (27.5 m AGL) TOPAZ O_3 measurements to the regulatory O_3 surface measurements from the monitors at Visalia (8.5 km) and Hanford (24 km) described above, and from the slightly more distant SJVAPCD monitors at Parlier (34 km) and Porterville (43 km). The TOPAZ mixing ratios were slightly higher than those at Visalia and Hanford, but lower than those at Parlier and Porterville, which are closer to the Sierra foothills and measure some of the highest O_3 concentrations in the SJVAB. The degree of correlation decreased with distance as expected, and the concentrations were generally higher near the foothills, but the O_3 measurements acquired at the VMA during CABOTS appear to be fairly representative of the central San Joaquin Valley.

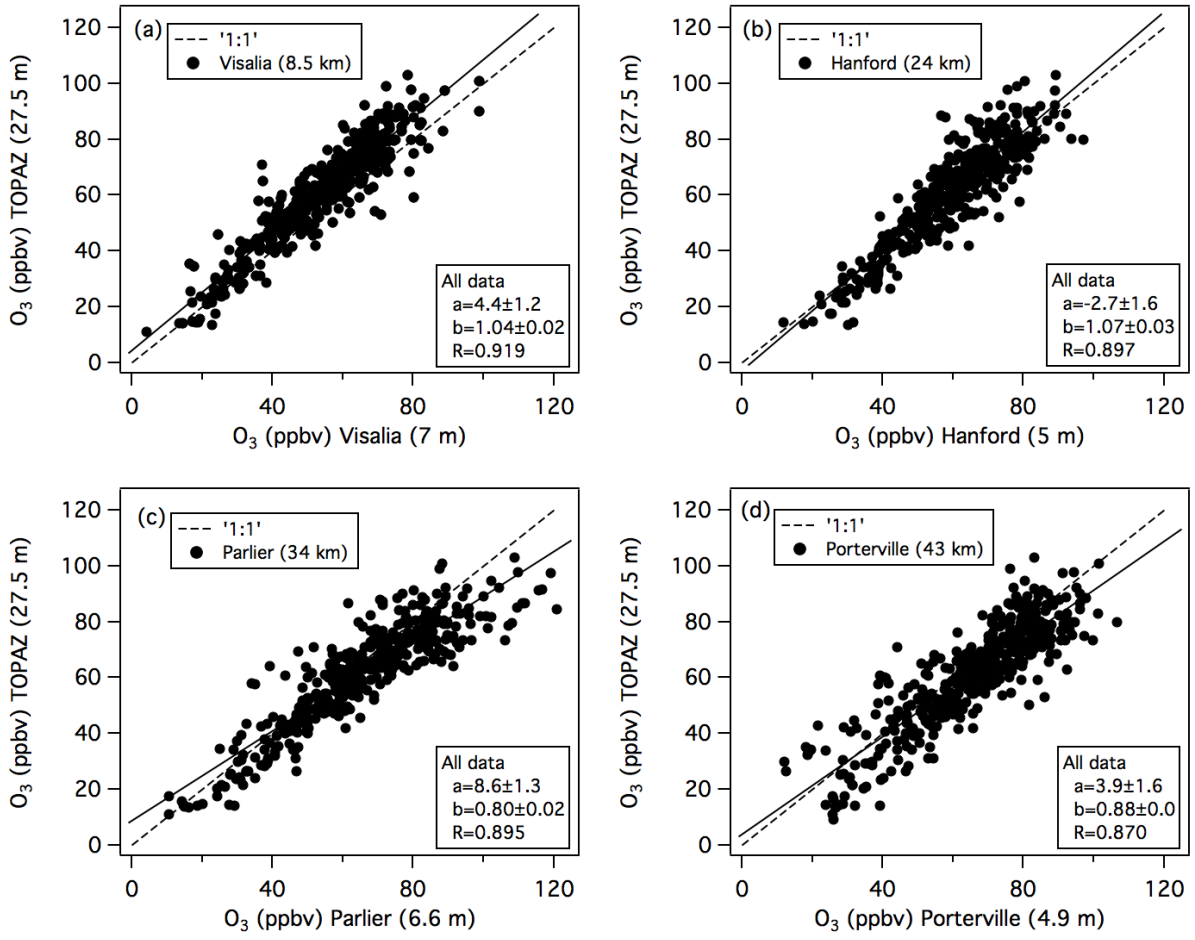

***Figure** 13. Scatter plots comparing the 27.5 m TOPAZ measurements with the 1-h measurements from the regulatory monitors at (a) Visalia-N. Church Street, (b) Hanford, (c) Parlier, and (d) Porterville. The measurements in the upper box and x-axis label refer to the distance from the VMA and sampling height above ground, respectively. The Visalia monitor is operated by the California Resources Board. The remaining three are operated by the SJVAPCD. The TOPAZ measurements are interpolated to the 1-h time base of the regulatory measurements for the comparison.*

Lidar backscatter measurements have long been used to map the distribution of particulates (dust, cloud, smoke, aerosols) in the atmosphere. Single wavelength backscatter provides no quantitative information about particle size distributions or composition, but it is roughly proportional to the total aerosol mass under cloud-free conditions and thus provide a useful diagnostic tool for assessing air mass origins. The ultraviolet wavelengths (≈0.3 µm) used by TOPAZ should be more sensitive to smaller particles like smoke [*Reid et al.*, 2005] than the visible or near-infrared wavelengths used by most lidars and ceilometers.

Figure 14 compares the 27.5 m AGL TOPAZ backscatter measurements with the hourly in-situ $PM_{2.5}$ measurements from the Visalia and Hanford $PM_{2.5}$ monitors. Only measurements made after local noon are shown to minimize the influence of shallow nocturnal boundary layers. The VMA backscatter measurements are surprisingly well correlated with the surface $PM_{2.5}$ measurements, particularly those made at Hanford, showing that the particles did not originate from CA-99 or other sources near the VMA. The closed and open symbols distinguish measurements made before and after July 22 to emphasize the impact of the Soberanes Fire on surface air quality in the SJV. Nearly all of the $PM_{2.5}$ measurements exceeding 20 µg m^{-3} occurred after the start of the Soberanes Fire when the VMA was noticeably smoky (see below).

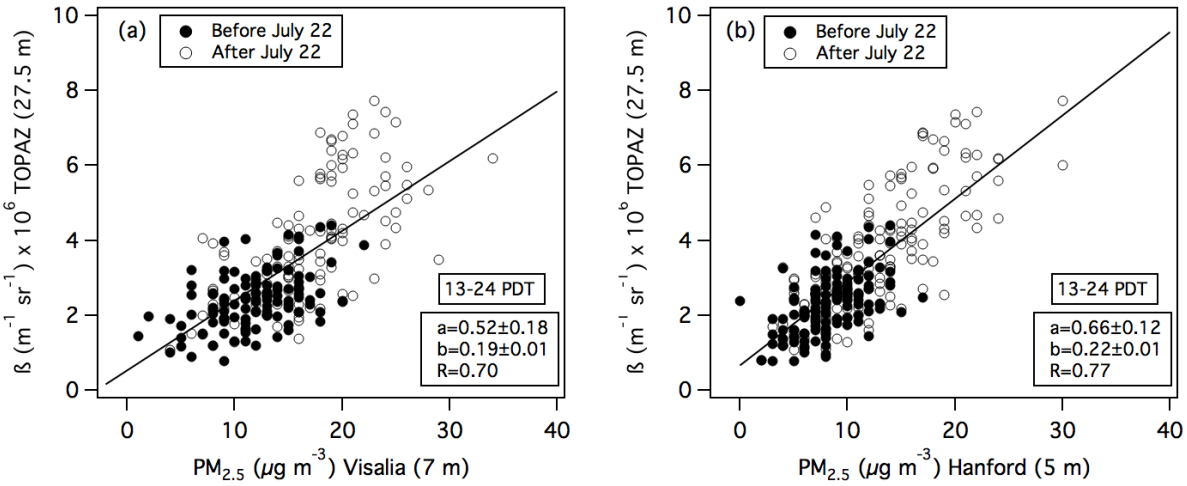

***Figure** 14. TOPAZ backscatter (27.5 m AGL) compared to the hourly $PM_{2.5}$ measurements from the (a) Visalia and (b) Hanford monitors. The closed and open symbols represent measurements made before and after the start of the Soberanes Fire on July 22, respectively. The linear regressions correspond to all the measurements.*

6.2. Comparisons with aircraft measurements

6.2.1 UC Davis/Scientific Aviation

The University of California at Davis, in collaboration with Scientific Aviation, Inc. (http://www.scientificaviation.com), conducted a series of research flights above the SJV during the summer of 2016 using a single-engine Mooney TLS or Ovation aircraft as part of the CARB-supported Residual Layer Ozone Study (RLO) (https://www.arb.ca.gov/research/apr/past/14-308.pdf) with 12 additional flights funded by the U.S. EPA and the Bay Area Air Quality Management District (BAAQMD). The Mooney carried a 2B Technologies Model 205 O_3 monitor, an Eco Physics Model CLD 88 (NO) with a photolytic converter to measure NO and NO_2, and a Picarro 2301f Cavity Ring-Down Spectrometer (CRDS) to measure CO_2, CH_4, and H_2O [*Trousdell et al.*, 2016]. The 2B O_3 data were sampled every 2 s, or about every 150 m at the typical level leg flight speed of 75 m s^{-1}.

The RLO flights were executed as a series of 2 to 3-day deployments with as many as 4 flights of 2-3 hours duration between Fresno and Bakersfield each day. Two of these deployments, RLO2 (June 2-4), and RLO4 (July 24-26), occurred during the highest O_3 episodes of both the first and second TOPAZ IOPs, respectively, and included several spiral profiles near VMA with low approaches on most of the flights between Fresno and Bakersfield.

Figure 15 (top) plots the combined tracks from all of the Mooney flights during the RLO2 (pink) and RLO4 (blue) deployments. RLO4 (in blue) originated just north of Sacramento in Lincoln, CA and included spiral profiles near Bodega Bay and Half Moon Bay en route to Fresno that are not shown on the map. The two EPA/BAAQMD deployments (July 27-29 and August 4-5) also coincided with the second TOPAZ IOP and were of longer duration with morning and afternoon flights that placed more emphasis on cross-valley measurements and transects to the coast (**Figure** 15, bottom) including profiles above the South Bay (EPA1, green) and Chews Ridge (EPA2, purple). The afternoon flights during both series included legs to Visalia.

Figure 16 shows the sections of the RLO and EPA/BAAQMD flight tracks that passed within 5 km of TOPAZ (red triangle) and **Figure** 17 plots the altitude profiles of these flights (dashed lines) with the sections within 5 km of TOPAZ highlighted by square markers. Most of these flights included low passes along the VMA runway that approached to within ≈350 m of the TOPAZ truck, and were 800 to 1200 m from the center of the TOPAZ 27.5 m AGL slant path measurements (cf. **Figure** 4).

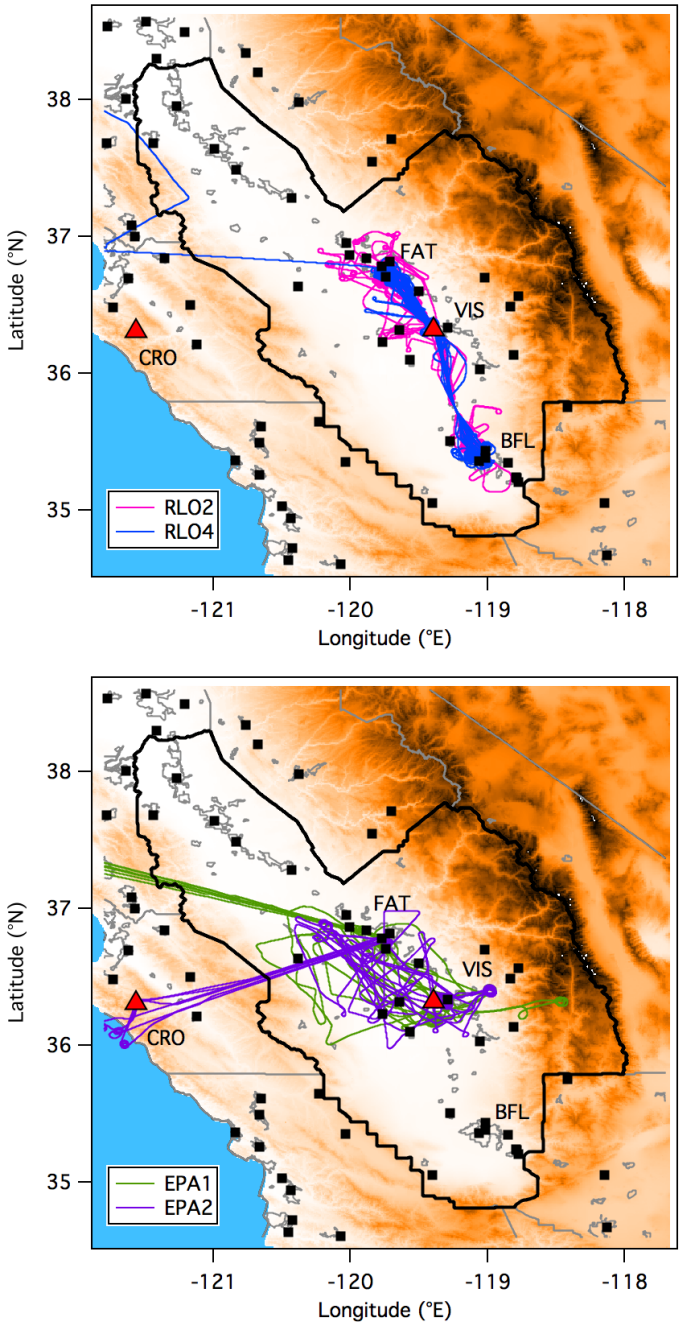

***Figure** 15. Maps of the SJVAB showing the UC Davis/Scientific Aviation RLO (top) and EPA/BAAQMD (bottom) flight tracks coincident with the TOPAZ measurements. The filled black squares show regulatory surface monitors. The CABOTS sampling sites at CRO and VMA are marked by red triangles. The other abbreviations are the Fresno (FAT), Visalia (VIS), and Bakersfield (BFL) airport codes.*

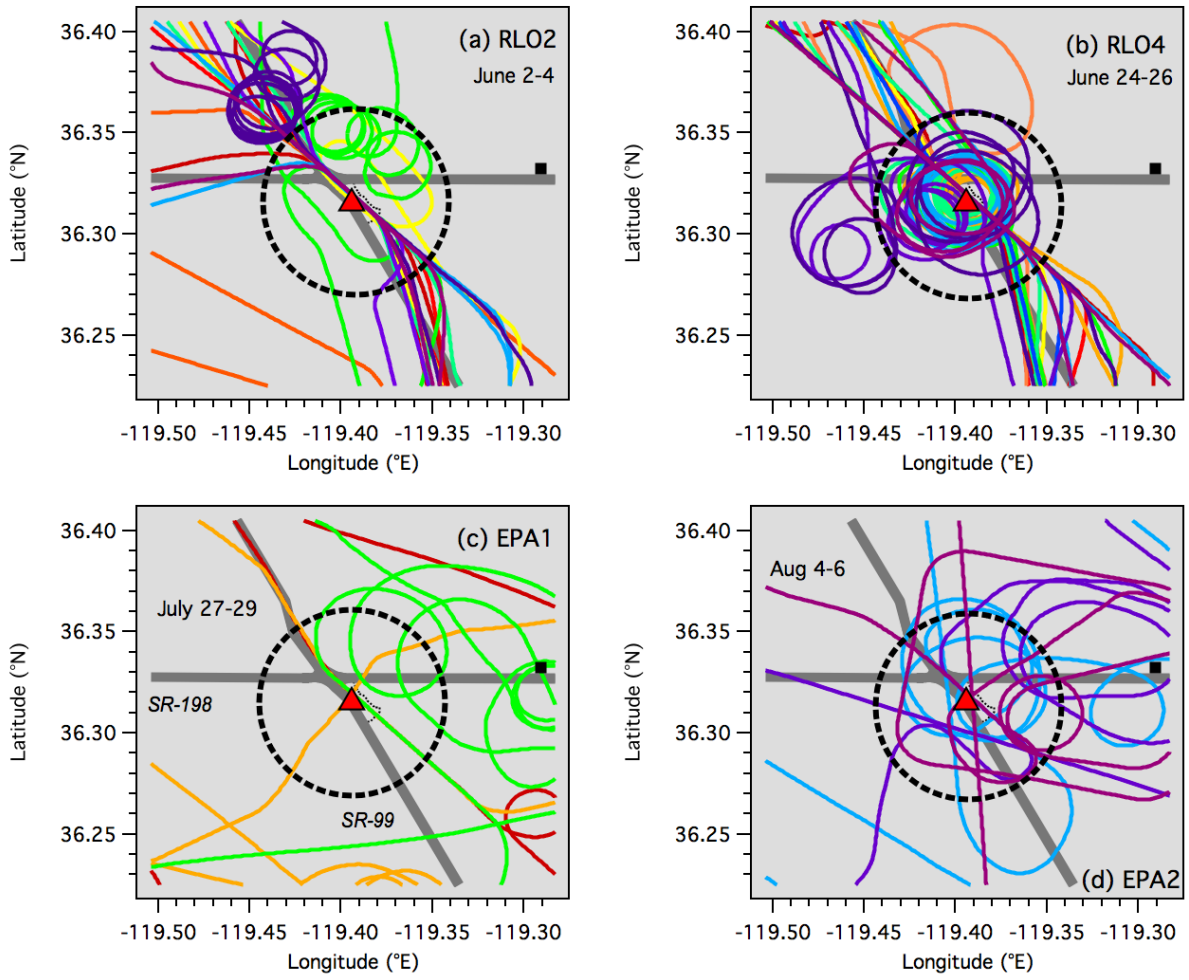

***Figure** 16. RLO and EPA/BAAQMS flight tracks in the vicinity of TOPAZ. (a) RLO2 (June 2-4), (b) RLO4 (July 24-26), (c) EPA1 (27-29 July), and (d) EPA2 (4-6 August). The red triangle marks the location of TOPAZ and the dashed black circles show the 5 km radius used for the profile comparisons. The black filled square marks the location of the Visalia-N. Church St. ozone monitor. The color scheme identifying the individual flights is shown in **Figure** 17.*

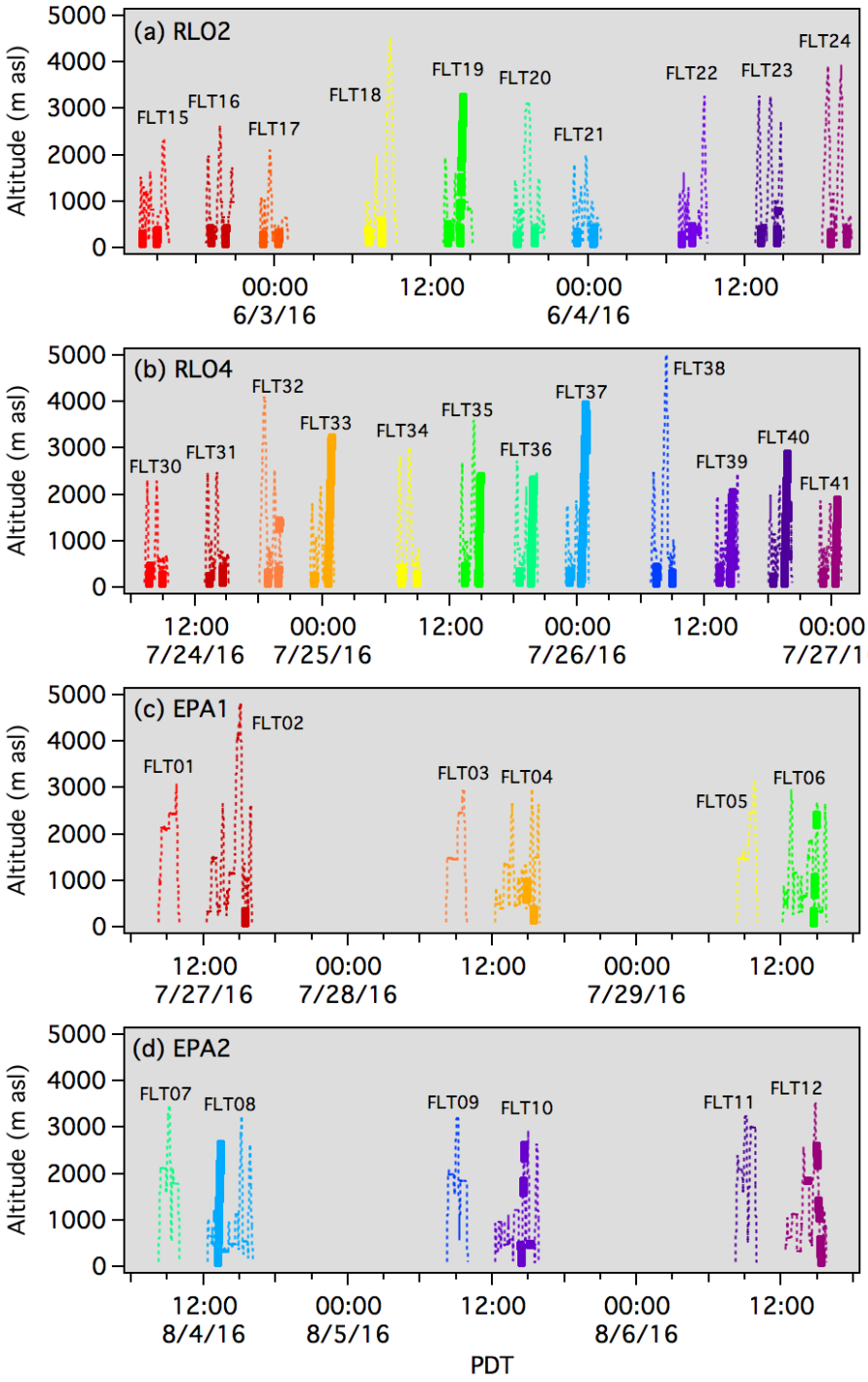

***Figure** 17. Time-altitude plots of the Scientific Aviation Mooney flight tracks during the RLO and EPA/BAAQMS flights (dashed lines). The flight segments lying within a 5 km radius of TOPAZ are highlighted by filled squares.*

Figure 18 plots time series of the 27.5 m TOPAZ and 5 m *in-situ* measurements during all of the RLO and EPA/BAAQMD low approaches together with the ozone measured by the aircraft between the surface and 25 m AGL. All of the aircraft measurements lie within 10% of the O_3 retrieved by TOPAZ with the notable exception of the much higher values (>100 ppbv) measured by the Mooney around 1400 PDT on June 3 (**Figure** 18a).

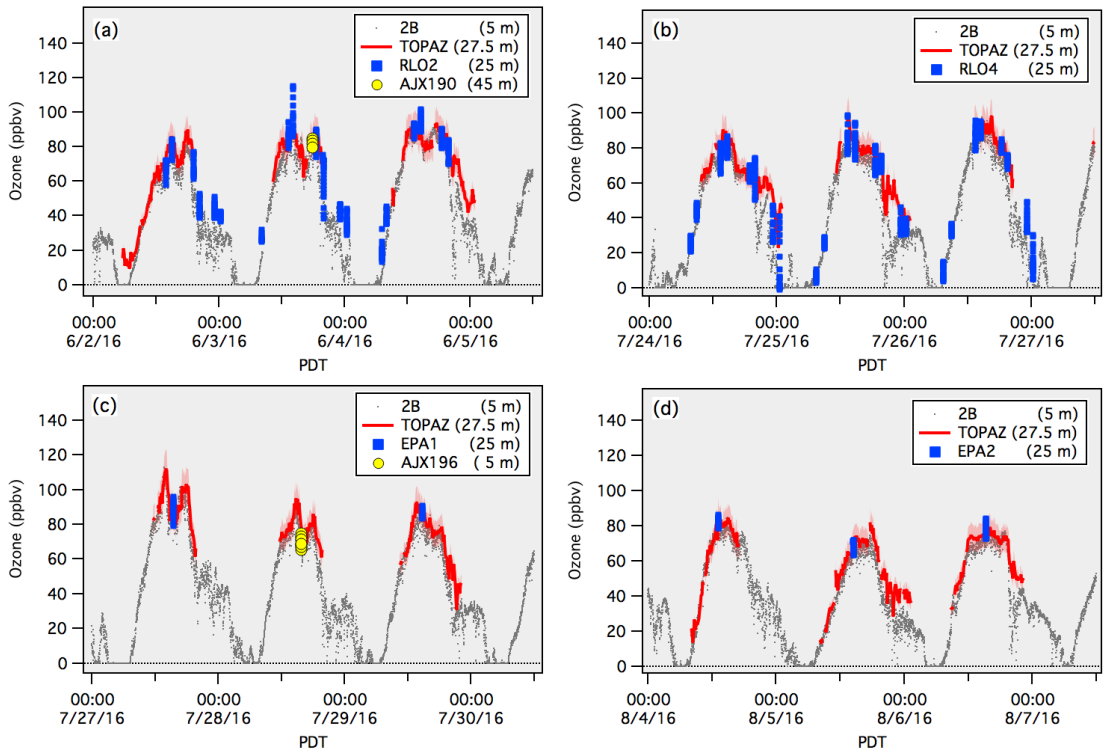

***Figure** 18. Time series of the surface in-situ O_3 (gray dots) and 27.5 m TOPAZ O_3 (red line) measured during the RLO and EPA/BAAQMD low approaches. The light red envelope shows the ±10% limits of the TOPAZ measurements. The blue squares represent the 1-s Scientific Aviation measurements made between the surface and 25 m AGL. The filled yellow circles in (a) and (c) show 2-s measurements from AJAX low approaches (see text).*

Figure 17 shows that the UC Davis/Scientific Aviation Mooney also conducted profiles in the TOPAZ vicinity from the surface to more than 3 km on FLT19 (June 3), FLT33 (July 25), and FLT37 (July 26), and these profiles are plotted in **Figure** 19 along with the TOPAZ measurements acquired during the 15 to 30 min period required for the Mooney to reach the top of the spiral at a climb rate of ≈2.2 m s^{-1}. The narrow layers seen near the bottom of the June 3 aircraft profile (**Figure** 19a) (and the corresponding ozone spike in **Figure** 18a) show that there were strong horizontal gradients in the O_3 mixing ratios near the surface during this early afternoon comparison. The rapid variations around 800 m seen in the four sequential 8-min composite vertical lidar profiles plotted in **Figure** 19a may have been caused by these horizontal gradients

since this altitude range relies heavily on the 20° slant profile measurements, but it is also possible that they are real vertical changes caused by gravity wave activity.

The July 25 and 26 comparisons (**Figures** 19b and 19c) were conducted just after local midnight and both the lidar and aircraft measurements show sharp decreases in ozone below 500 m from chemical destruction and surface deposition. The lidar measurements from July 26 show rapid changes near 400 m, but little variation at higher altitudes. The agreement between the aircraft and lidar measurements is generally quite good with the greatest differences arising from the much coarser vertical resolution of the lidar above 1 km. This is evident in the July 26 profiles (**Figure** 19c) where several narrow layers detected by the aircraft between 2 and 3 km are smoothed into one broad layer by the lidar. However, the measurements below 1 km demonstrate the much higher effective vertical resolution of TOPAZ at low altitudes where the slant path measurements are used.

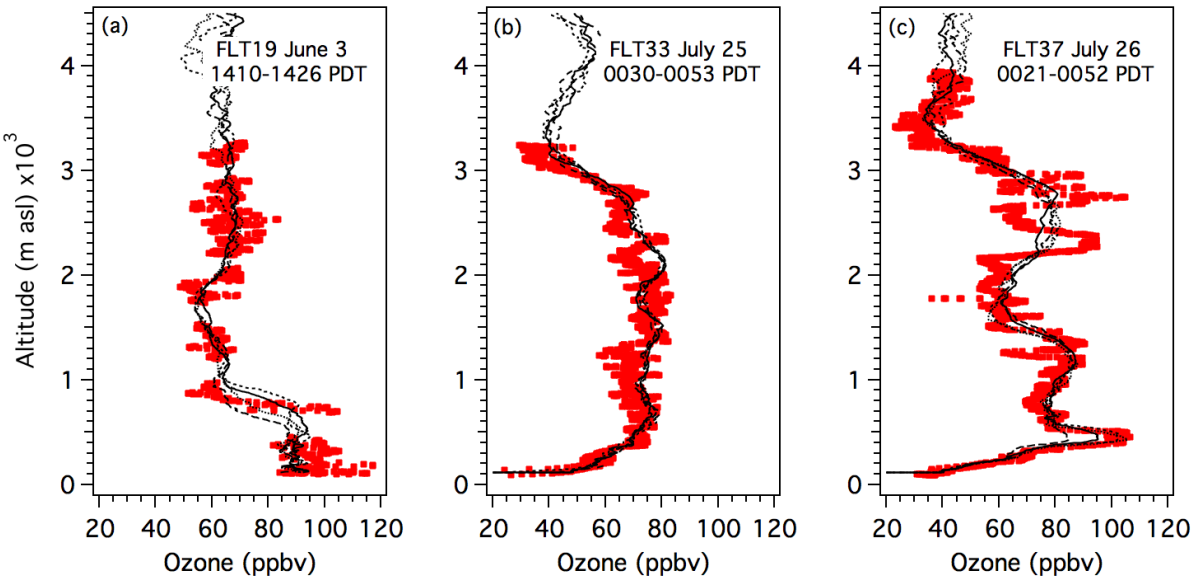

***Figure** 19. Profile plots comparing the TOPAZ (black lines) and Scientific Aviation (red squares) O_3 measurements on (a) FLT19, June 3, (b) FLT33, 25 July, and (c) FLT 37, July 26. The dotted, short dash, solid, and long dash lines show the order of the coincident 8-min lidar profiles.*

6.2.2 NASA Alpha Jet Atmospheric eXperiment (AJAX)

The NASA Ames Alpha Jet Atmospheric eXperiment (AJAX) [*Hamill et al.*, 2016] sampled O_3 and other tropospheric constituents above California during CABOTS using a two-person trainer fighter jet based at Moffett Field, CA (MF, 37.415° N, -122.050° E). The Alpha Jet carried an external wing pod with a modified commercial UV absorption monitor (2B Technologies Inc., model 205) to measure O_3 [*Ryoo et al.*, 2017; *Yates et al.*, 2015; *Yates et al.*, 2013] and a

(Picarro model 2301-m) cavity ringdown analyzer to measure CO_2, CH_4, and H_2O [*Tanaka et al.*, 2016]. A second wing pod carried a non-resonant laser-induced fluorescence instrument to measure formaldehyde (CH_2O) [*St. Clair et al.*, 2017]. The aircraft is also equipped with GPS and inertial navigation systems to provide altitude and position information, and the NASA Ames developed Meteorological Measurement Systems (MMS) to provide highly accurate pressure, temperature, and 3-D wind data. The 2B O_3 data, taken every 2 s, are averaged over 10 s to increase the signal-to-noise ratio, giving an overall ozone uncertainty of 3 ppbv at 10-s resolution. The overall uncertainties for the CO_2 and CH_4 measurements are typically less than 0.16 ppmv and 2.2 ppbv, respectively, when the 3-Hz data are binned to 3 s [*Tanaka et al.*, 2016].

AJAX conducted 4 research flights over the SJV while TOPAZ was operational with 2 additional flights (21 June and 7 July) between the two IOPs. **Figures** 20 and 21 are similar to **Figures** 15 and 16, but instead show the AJAX flight tracks.

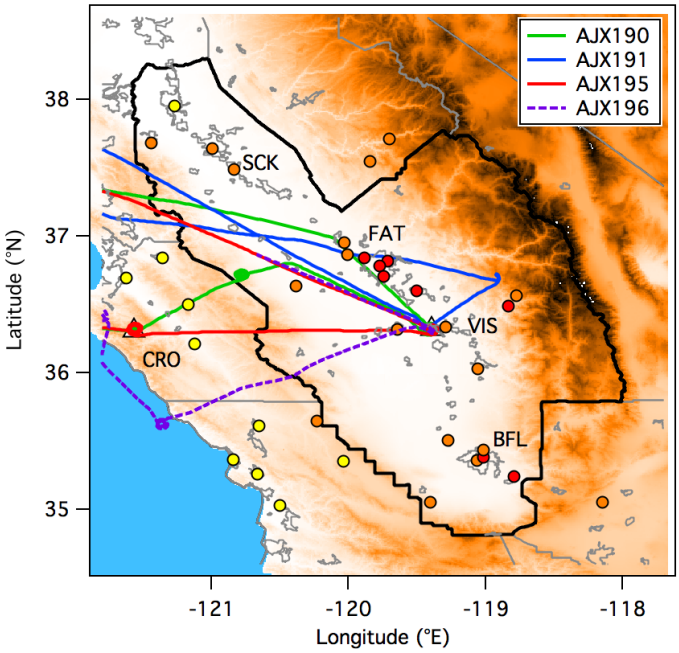

***Figure** 20. Map of the San Joaquin Valley similar to Figure 15 showing the AJAX flight tracks on June 3 (AJX190), June 15 (AJX191), July 21 (AJX195), and July 28 (AJX196).*

The Alpha Jet executed descending spiral profiles from 4 to 5 km down to the surface that ended in low approaches on three of these flights: AJX190 on June 3, AJX191 on June 15, and AJX195 on July 21. The aircraft also conducted a very low approach (≈5 m) at VMA on July 28 (AJX196) but did not execute a full profile. The first and last flights (AJX190 and AJX196) coincided with the high ozone episodes mentioned earlier and the third flight (AJX195) also occurred during a period of higher than normal pressure. The second flight (AJX191) was

conducted as a deep closed low moved into the Pacific Northwest, however, bringing unseasonably cool temperatures (26 °C) and strong surface winds to the SJV. This cyclonic system advected a large Asian pollution plume across the valley in the middle troposphere, but surface ozone remained low with a peak MDA8 O_3 of 59 ppbv at the Sequoia-Kings Canyon monitor.

The first AJAX flight (AJX190) on June 3 during IOP1 overlapped with the UC Davis/Scientific Aviation RLO2 deployment. AJX191 took place about two weeks later in IOP1, and AJX195 occurred several days prior to the RLO4 deployment in IOP2. AJAX also executed profiles (not shown here) above and upwind of Chews Ridge on AJX190 and AJX191 and near Bodega Bay on AJX191 and 195 and sampled the Soberanes Fire plume on AJX196.

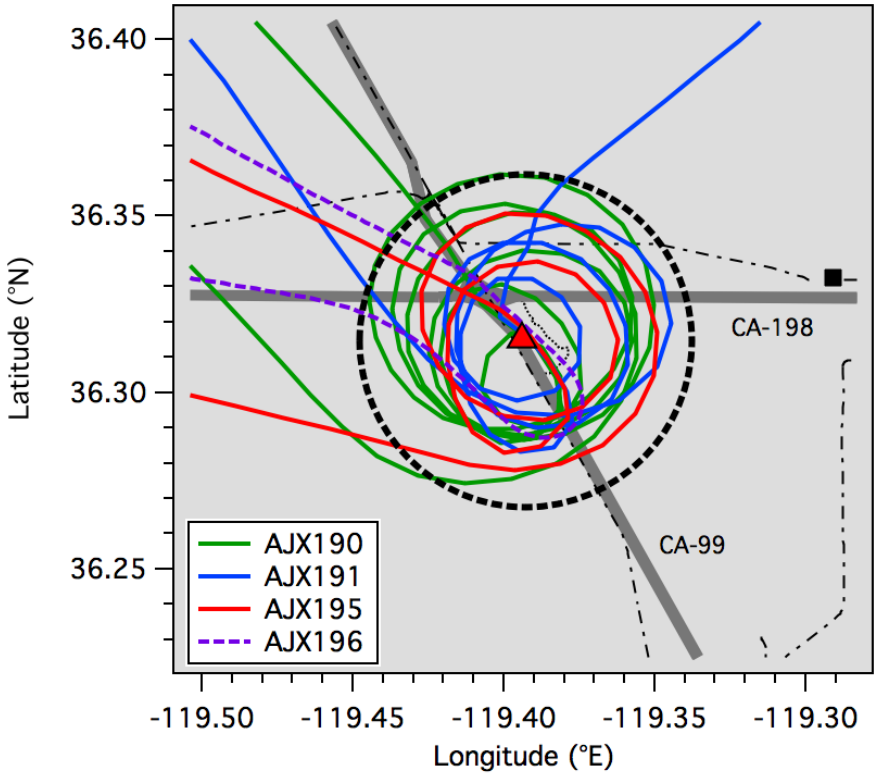

***Figure** 21. AJAX flight tracks in the vicinity of TOPAZ (red triangle). The dashed black circle marks the 5 km radius window used for the profile comparisons.*

Figure 22 displays the AJAX and coincident TOPAZ profiles in plots similar to those shown for the Mooney in **Figure** 19, but with an extended vertical axis to reflect the higher range of these profiles. The points in **Figure** 22 are sparser than those in **Figure** 19 in part because of the 10-s averaging time, and in part because the Alpha Jet executed its profiles with an airspeed of about 110 m s^{-1} and a climb rate of 8 m s^{-1} compared to 60 m s^{-1} and 2.2 m s^{-1} for the Mooney.

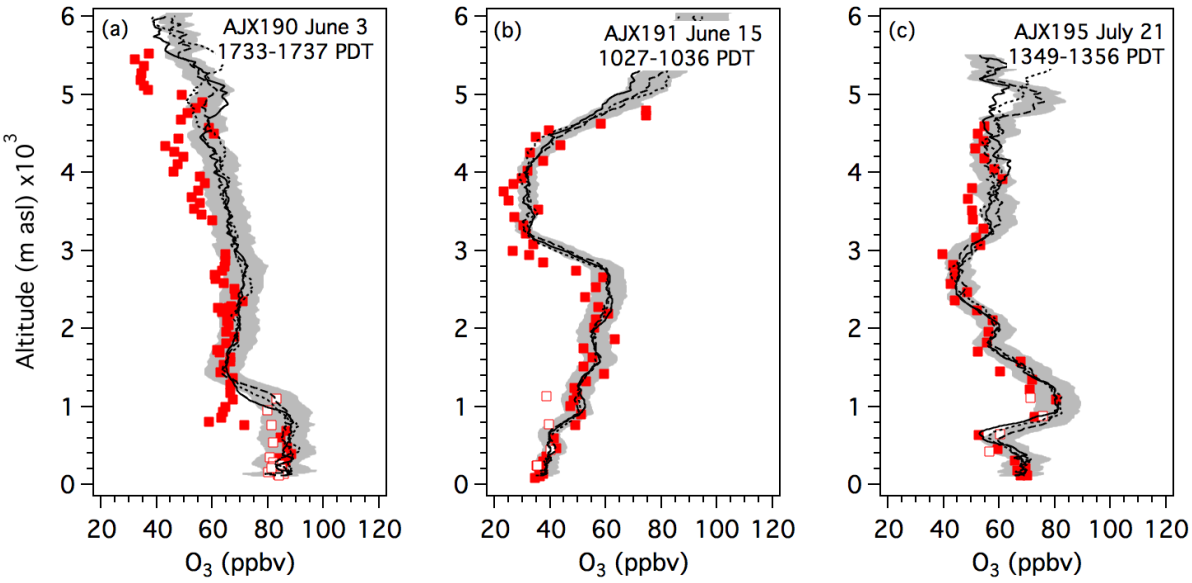

***Figure** 22. Profile plots comparing the TOPAZ (black lines) and 10-s AJAX (red squares) measurements on (a) AJX190, June 3, (b) AJX191, June 15, and (c) AJX195, July 21. The closed squares correspond to the Alpha Jet descent and the open squares the subsequent climb out. The dotted, dashed, and solid lines show the order of the three 8-min lidar profiles that bracket the AJAX profile. The gray envelope shows the middle lidar profile ±10%.*

The agreement between the Alpha Jet and TOPAZ measurements is generally within the combined uncertainties with the exception of June 3 (**Figure** 22a) when the measured aircraft and retrieved lidar concentrations differ by as much as 12 ppbv (20%) at 2.5 km ASL and 20 ppbv (≈50%) at 5.2 km ASL. The Alpha Jet arrived on station at VMA about 3 hours after the Mooney completed its profile (cf. **Figure** 19a), which showed strong horizontal gradients near the surface. The Alpha Jet measurements made during the close approach also show significant horizontal gradients near the top of the mixed layer, but the variations in the lidar profiles and differences between the aircraft and lidar measurements are smaller than those seen earlier in the day and the unaveraged 2-s O_3 measurement made during the Alpha Jet low approach on June 3 (filled yellow circle in **Figure** 18a) agrees well with both the lidar and surface measurements. The plots in **Figure** 23 suggests that the differences between the two profiles at the lower altitudes are probably due to fine-scale horizontal variability in the O_3 distribution during the measurements. Spatial variability may also be a factor in the differences at higher altitudes.

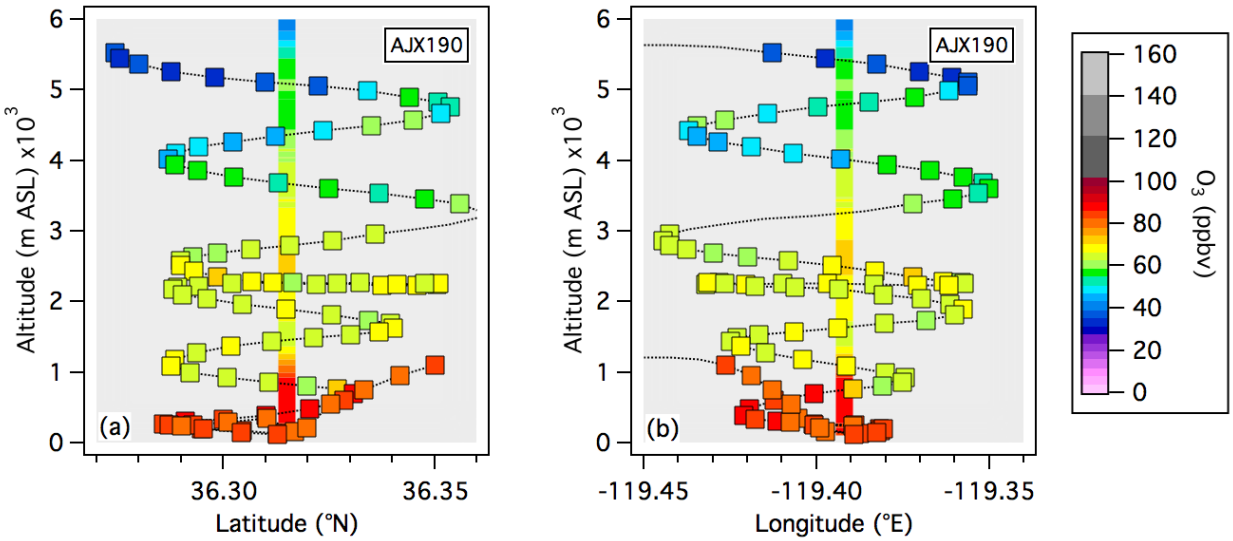

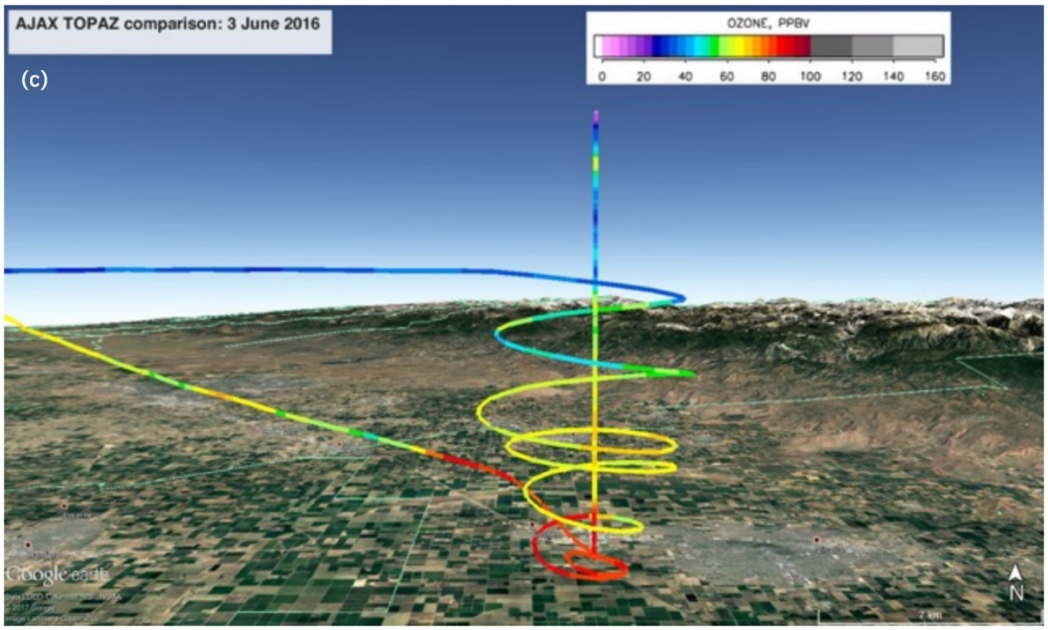

***Figure** 23. TOPAZ profile and AJAX flight track colorized by the O_3 mixing ratios measured during the AJX190 low approach and profile on June 3. (a) Latitude-altitude profile, (b) Longitude-altitude profile, (c) Google Earth image giving a 3-D view of the lidar (vertical line) and aircraft measurements.*

7. Origins of the free tropospheric O_3 layers above the SJV during CABOTS

The summary curtain plot in **Figure** 5 shows that high O_3 layers consistent with stratospheric intrusions, transported pollution, or biomass burning plumes frequently appeared in the free troposphere over the SJV during both CABOTS IOPs. This O_3 lies well above the shallow mixed layers of the SJV [*Bianco et al.*, 2011], and is too high to be local or regional pollution orographically lifted by the Sierra Nevada [*Fast et al.*, 2012; *Langford et al.*, 2010]. Some of the layers appear to be actively descending (e.g. June 12) while others are quasi-horizontal (e.g. June 15). In a few instances, the layers descend all the way to the top of the boundary layer (e.g. August 5-6). Elevated O_3 layers have been observed over California in previous studies (e.g. [*Cooper et al.*, 2011; *Ryerson et al.*, 2013]), but their influence on surface O_3 in the SJV has not been established.

The simultaneous backscatter measurements in **Figure** 6 provide some insight into the origin of the elevated O_3 layers since biomass burning plumes and stratospheric intrusions usually have very high and very low backscatter, respectively. For example, the areas of elevated backscatter near the high O_3 layers on May 29 and June 2 are consistent with a biomass burning origin, but the very low backscatter surrounding the high O_3 layer on June 5-6 suggests a stratospheric origin. Asian pollution plumes lie somewhere between these two extremes, however, with aerosol loadings that vary with the plume source [*Jaffe et al.*, 2003b] and history [*Brock et al.*, 2004]. The potential importance of these three sources can be estimated by comparing the lidar measurements to the FLEXPART STO3, ASCO, and BBCO tracer distributions. FLEXPART tracer distributions have previously been used to help interpret TOPAZ measurements from the CalNex [*Langford et al.*, 2012] and LVOS [*Langford et al.*, 2015b] field campaigns.

Figures 24 and 25 display time-height curtain plots of the FLEXPART STO3, ASCO, and BBCO tracer distributions above the VMA during the first and second IOPs, respectively. The distributions are shown for the 0.25° receptor grid point (36.25°N, -119.5°E) nearest the VMA (36.315°N, -119.392°E), and are plotted on roughly the same horizontal and vertical scales as the TOPAZ O_3 and ß measurements in **Figures** 5 and 6. All three tracers are plotted with the same color scale of 0 to 50 ppbv. The top panel (a) in **Figure** 24 shows large downward sloping stratospheric intrusions on June 5-6 and June 12-13 that correspond closely with measured structures in **Figure** 5. The STO3 tracer calculations also shows the second intrusion bringing more than 10 ppbv of O_3 down to the top of the boundary layer on June 13. As expected, the STO3 tracer concentrations for the second IOP are much smaller (**Figure** 25a).

The ASCO tracer in **Figure** 24b shows tongues of Asian pollution descending into the middle troposphere before or after each of the major stratospheric intrusions in IOP1. This interleaving of descending stratospheric air in the tropopause folds with Asian pollution ingested by the warm conveyor belt of developing cyclones over East Asia has been described previously [*Lin et al.*, 2012a; *Lin et al.*, 2012b]. **Figure** 24b also shows ASCO tracer concentrations of 2-8 ppbv throughout the free troposphere during the first IOP that are unrelated to specific transport events. Although FLEXPART is a passive model with no chemistry, equivalent O_3 concentrations for the ASCO tracer can be approximated using the published O_3-to-CO ratios of 0.2 to 0.5 mol

mol^{-1} from plumes sampled by aircraft above California and the eastern Pacific [*Hudman et al.*, 2004; *Nowak et al.*, 2004; *Price et al.*, 2004]. This conversion factor implies transported Asian pollution contributed only 1-4 ppbv to the surface O_3 in the SJV during IOP1. The ASCO tracer concentrations were also much smaller for the second IOP (**Figure** 25b).

The BBCO tracer in **Figure** 24c shows essentially no biomass burning contributions during the first IOP despite the appearance of the high backscatter on May 29 and June 2 that are most likely related to a series of fires burning in northern Arizona. This likely reflects the limitations of basing biomass burning emissions on fire radiative power (FRP) measurements [*Francesca Di et al.*, 2016] which can be masked by dense smoke plumes. The biomass burning contributions during the second IOP (**Figure** 25c) are much larger, however, and coincide with the start of the Soberanes Fire. A review of published measurements from biomass burning plumes [*Jaffe and Wigder*, 2012] suggests a mean O_3-to-CO ratio of about 0.15 mol mol^{-1} for aged plumes originating from temperate forests. This implies O_3 enhancements on the order of 10 ppbv in the Soberanes Fire plume (see below).

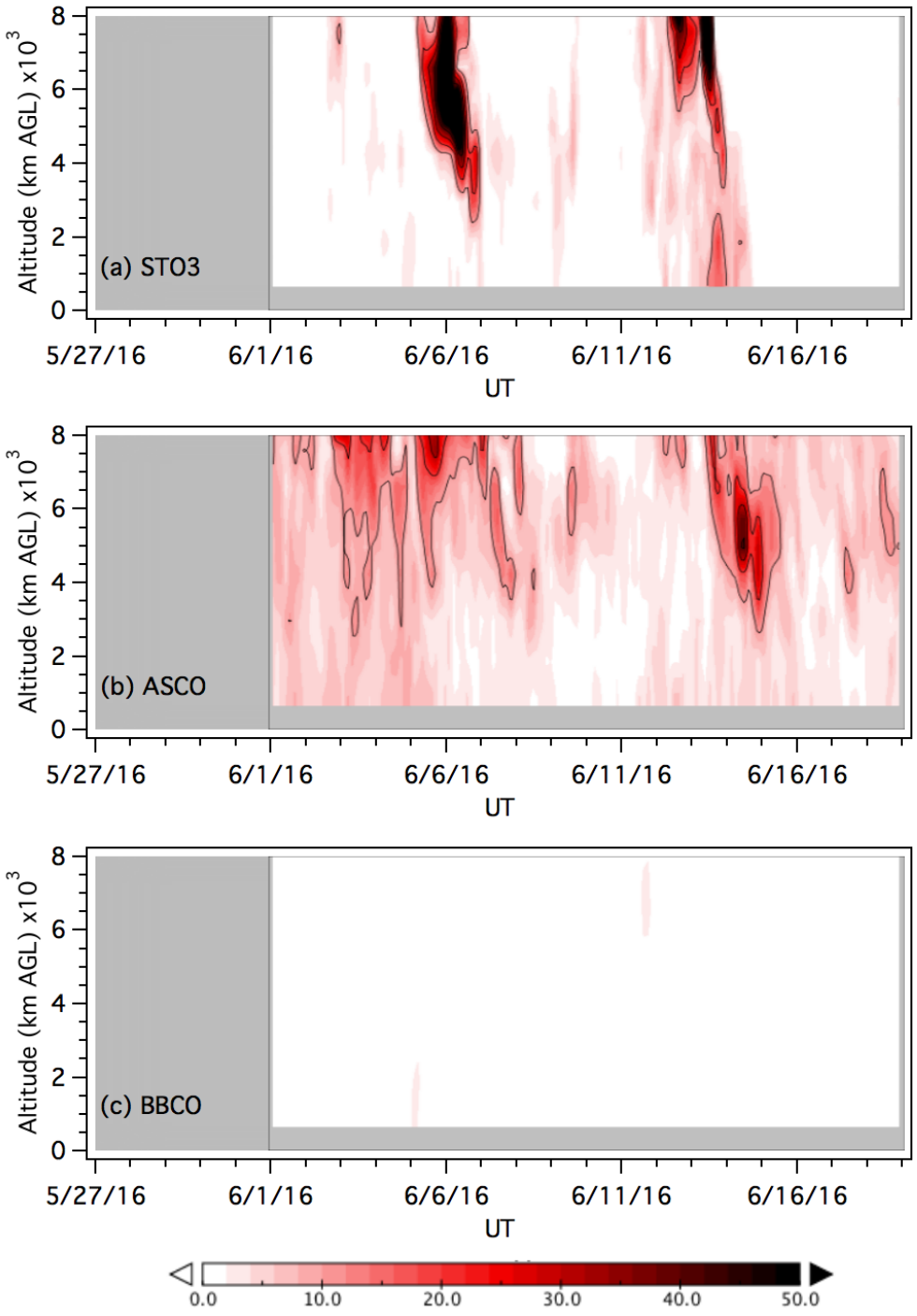

***Figure** 24: Time-height curtain plots of the FLEXPART (a) STO3, (b) ASCO, and (c) BBCO tracers above the receptor grid point nearest Visalia (36.25°N, -119.5°E) during the first IOP. The black contour lines are separated by 10 ppbv. Calculations for May are unavailable.*

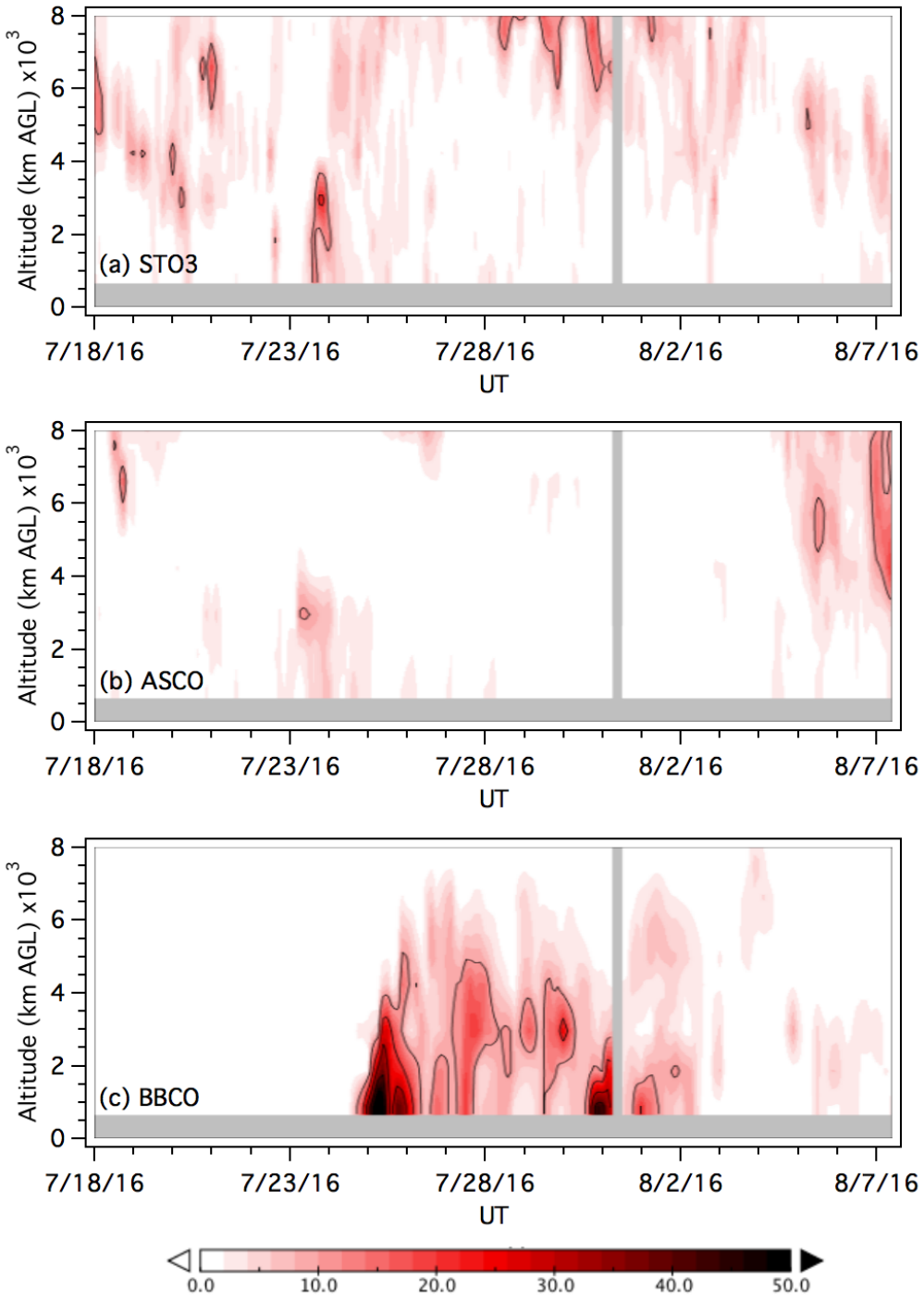

***Figure** 25: Time-height curtain plots of the FLEXPART (a) STO3, (b) ASCO, and (c) BBCO tracers above the receptor grid point nearest Visalia (36.25°N, -119.5°E) during the second IOP. The black contour lines are separated by 10 ppbv.*

8. Stratospheric Intrusions, Asian pollution, and surface O_3 in the SJV during CABOTS

Stratospheric intrusions and synoptic-scale transport layers are typically many tens or even hundreds of kilometers wide and thus are likely to affect multiple monitors if they reach the surface in an area like the San Joaquin Valley which has a dense observational network. In this section, we take a closer look at the potential contributions of stratospheric intrusions and transported Asian pollution to surface O_3 during three 6-day periods (June 2-7, June 12-17, and August 2-7) of CABOTS when lower stratospheric air and/or Asian pollution may have reached the surface.

8.1 Example 1: June 2-7, 2016

A strong high-pressure ridge (**Figure** 26) dominated the Southwestern U.S. at the beginning of June and brought unseasonably warm temperatures (>40°C) and stagnant conditions to Southern California and the San Joaquin Valley. The ridge advanced behind an upper level low (seen centered over Texas on June 3) and was displaced by a second, much shallower low that developed a modest tropopause fold which moved into northern California on June 5-6. The ridge fostered the buildup of surface O_3 and aerosols from regional sources that culminated in a peak MDA8 of 91 ppbv at Clovis on June 4 (cf. **Figure** 10). This buildup and the subsequent descent of the stratospheric intrusion are easily seen in the expanded TOPAZ curtain plots of **Figure** 27.

The high temperatures and weak anticyclonic winds attendant with the high-pressure ridge allowed strong upslope flow to develop along the foothills of the Sierra Nevada. **Figure** 28 shows westerly flow consistent with this hypothesis within the lowest kilometer from late morning until late afternoon when the northerly up-valley flow began to dominate. The upslope flow transported O_3 and aerosols from the valley into the western slopes of the Sierra Nevada mountains. The associated easterly compensation flow then returned some of this polluted air out over the valley between 1 and 2 km in the evening (**Figure** 28). This return flow was lifted upwards over the valley by a layer of much cleaner air (low O_3 and ß) that lay over the valley during the day. The weak radar return signals from this layer shows that it was highly laminar with little embedded turbulence which is consistent with a marine origin.

The dashed and dotted lines in **Figure** 27 roughly correspond to the 500 and 700 hPa surfaces in **Figure** 29, which plots the afternoon (17 PDT or 00 UT) O_3 analyses from the NOAA/ESRL/GSD RAP-Chem model. **Figure** 29a shows O_3-rich lower stratospheric air in the dry airstream (DA) and O_3-poor subtropical marine boundary layer air in the warm conveyor belt (WCB) wrapping around the trough as the tropopause fold develops over the eastern Pacific Ocean. The intrusion lies just off the coast on June 4 (**Figure** 29c) and over central California on June 5 (**Figure** 29e) in agreement with the FLEXPART STO3 tracer in **Figure** 24. The relatively shallow fold is just visible on the 700 hPa surface off the coast of Los Angeles on June 5 (**Figure** 29f). The corresponding CO analyses in **Figure** 30 show some CO of presumed Asian origin mingled with the DA at 500 hPa over the Pacific on June 3, but the CO at 500 hPa decreased when the trough moved ashore. Both the O_3 and CO concentrations at 700 hPa (≈3.1 km ASL) peaked on June 4,

and then decreased as the trough moved ashore over the following day (**Figures** 29f and 30f) in agreement with the O_3 surface measurements in the SJVAB (cf. **Figure** 10).

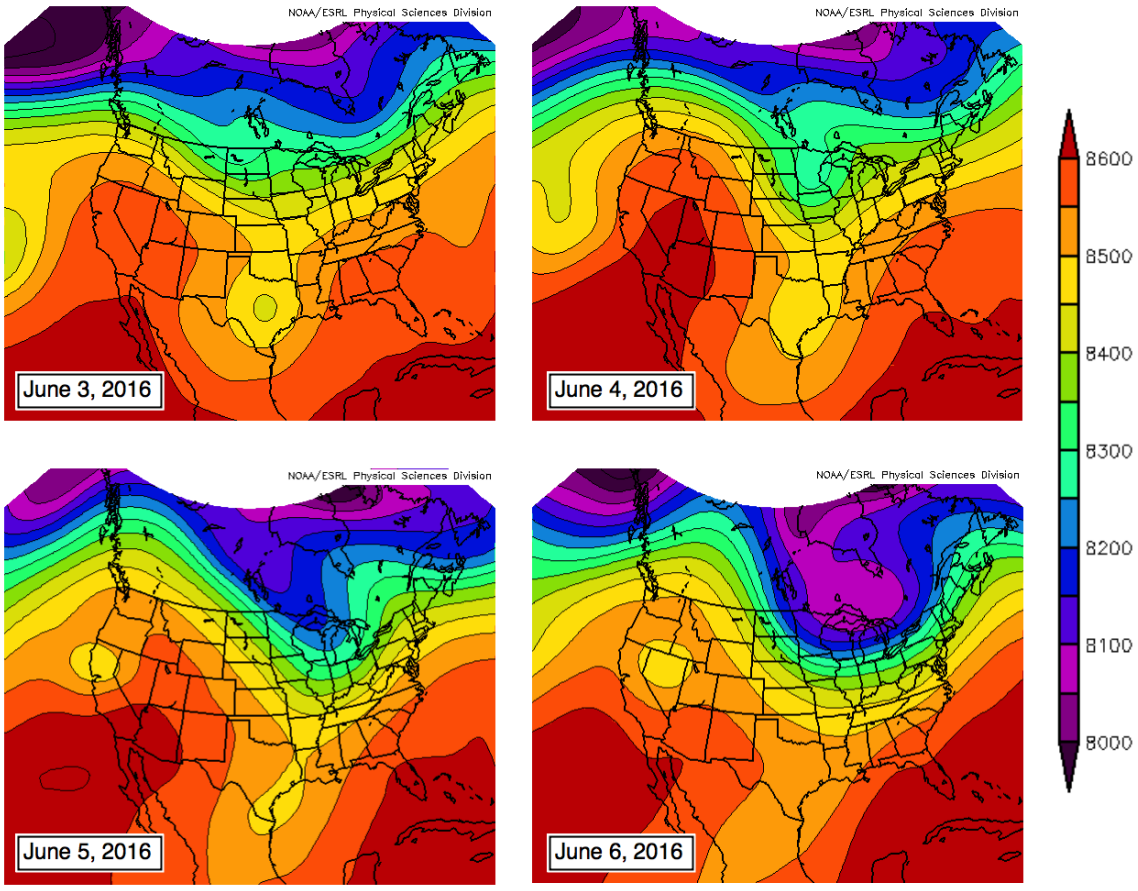

***Figure** 26. 24-hour composite North American Reanalysis (NARR) 350 hPa geopotential heights (m) for June 3-6, 2016.*

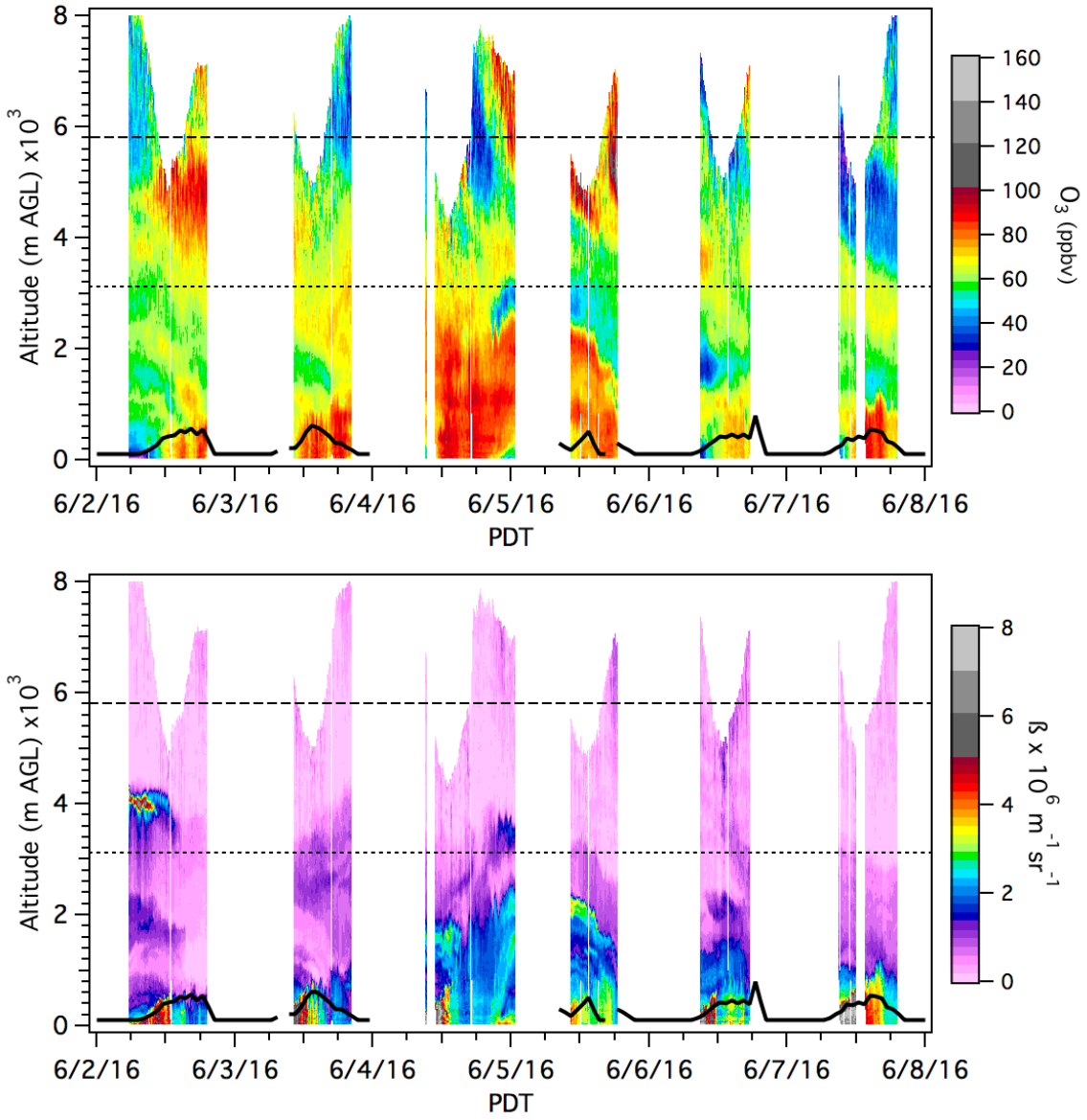

***Figure** 27: Time-height curtain plots showing the TOPAZ O_3 concentrations (top) and ß (bottom) from June 2 to 8. The dashed and dotted horizontal lines approximate the 500 and 700 hPa surface heights. The heavy black curves show the boundary layer heights derived from the co-located SJVAPCD RASS (no RASS or wind measurements were available for June 4).*

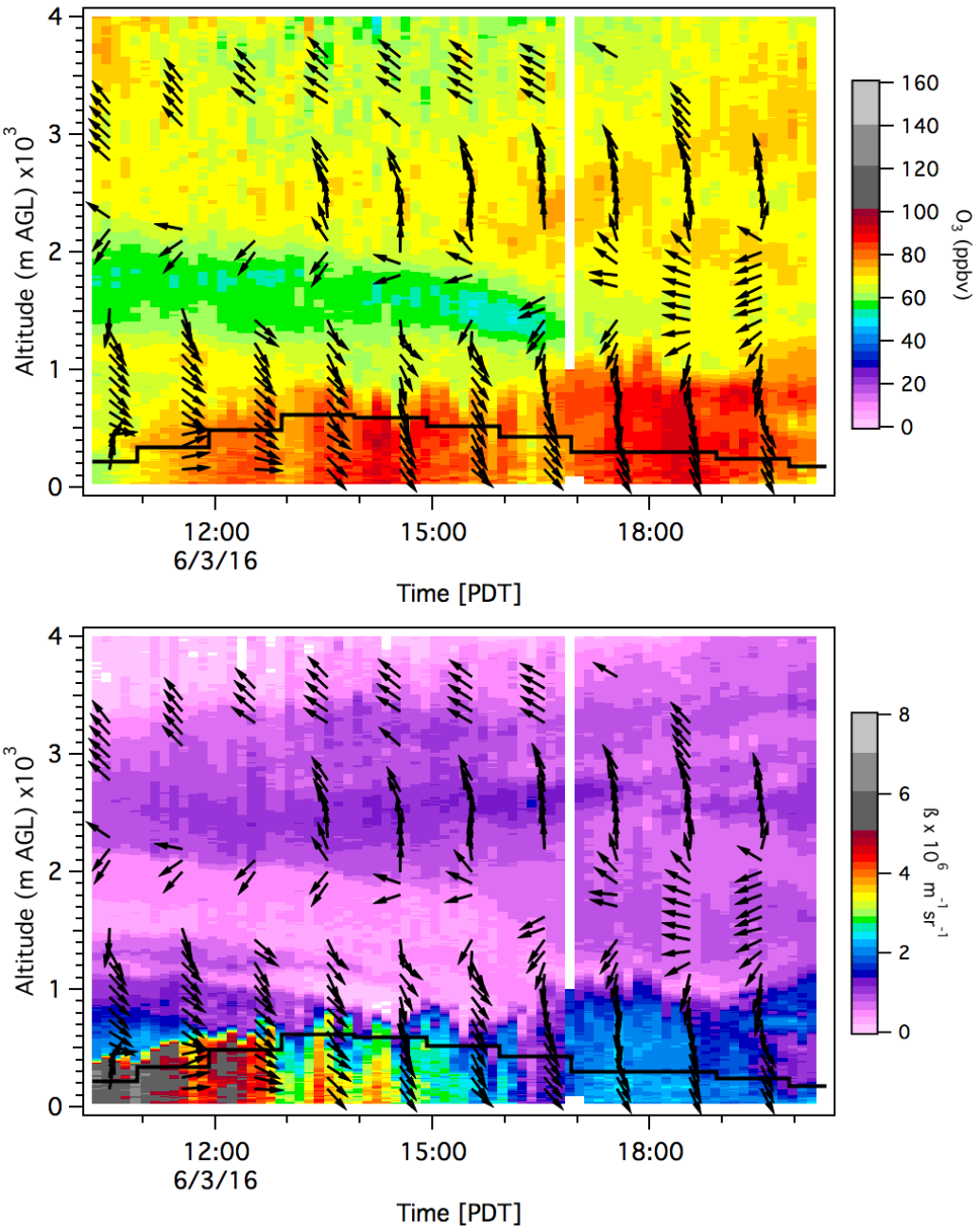

***Figure** 28: Time-height curtain plots showing the TOPAZ O_3 concentrations (top) and ß (bottom) from June 2 with the SJVAPCD profiler winds superimposed. The heavy black curves show the boundary layer heights derived from the co-located SJVAPCD RASS.*

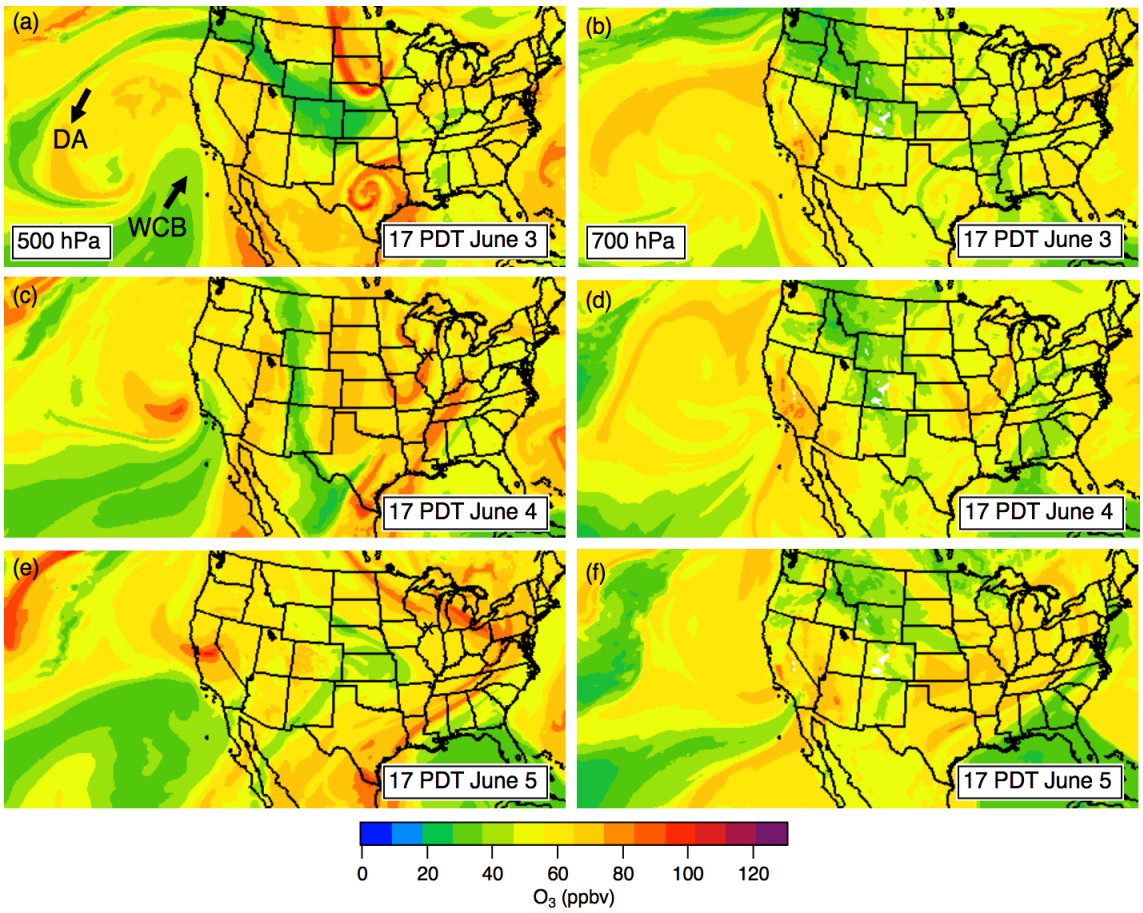

***Figure** 29: RAP-Chem model total O_3 distributions on the 500 hPa (left) and 700 hPa (right) surfaces for the afternoons of June 3-5 (00 UT on June 4-6).*

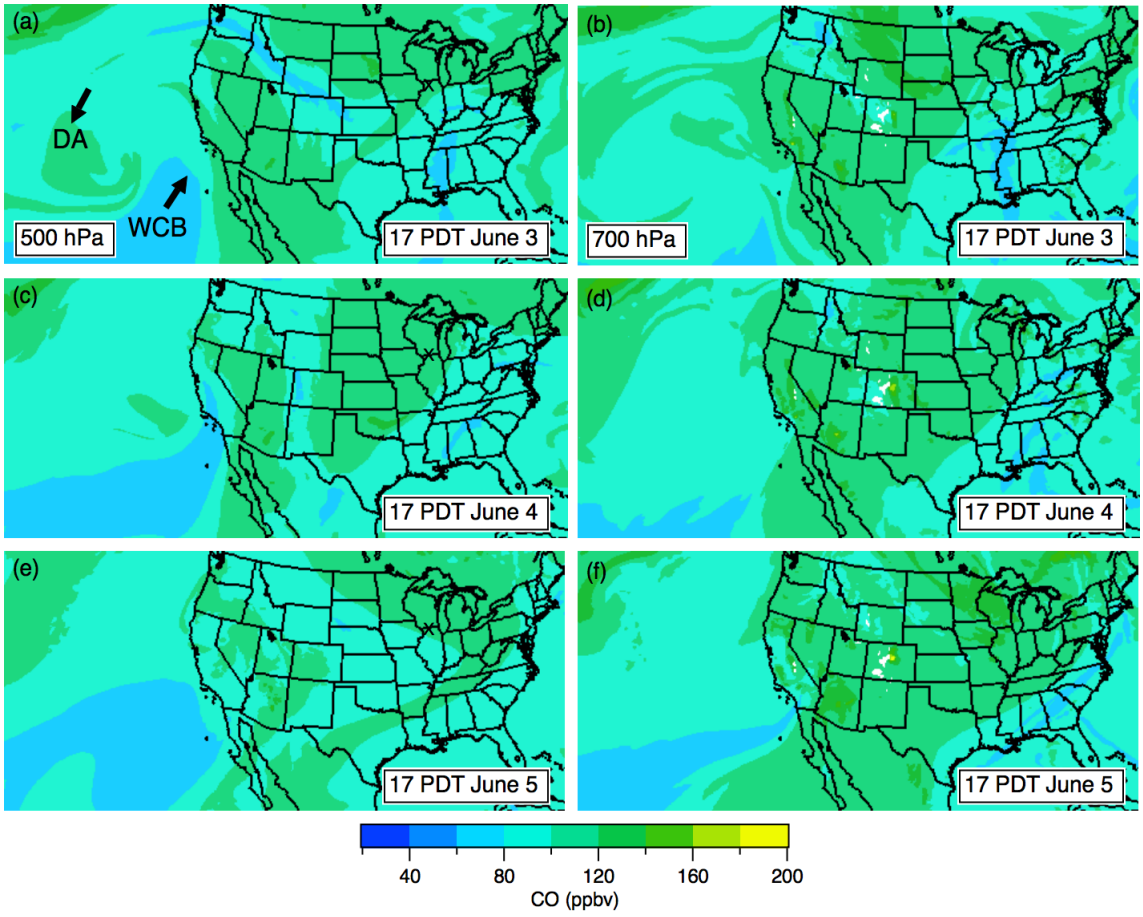

***Figure** 30: RAP-Chem model total CO distributions on the 500 hPa (left) and 700 hPa (right) surfaces for the afternoons of June 3-5 (00 UT on June 4-6).*

Figure 31 is an expanded version of the FLEXPART STO3 (top) and ASCO (bottom) tracer curtain plots for June 2-8 with the 5.5±0.5 km AGL TOPAZ and surface measurements superimposed. The STO3 tracer reproduces the timing of the peak seen in the TOPAZ measurements on the afternoon of June 5 (the high O_3 measured on the afternoon of June 2 is attributed to biomass burning). The intrusion approached the surface on June 6, well after the peak in surface O_3 on June 4 and coincided with a minimum in the surface concentrations. The surface contribution of the ASCO tracer peaked earlier on June 4, but the maximum tracer contribution was only 8 ppbv and the corresponding O_3 contribution even smaller.

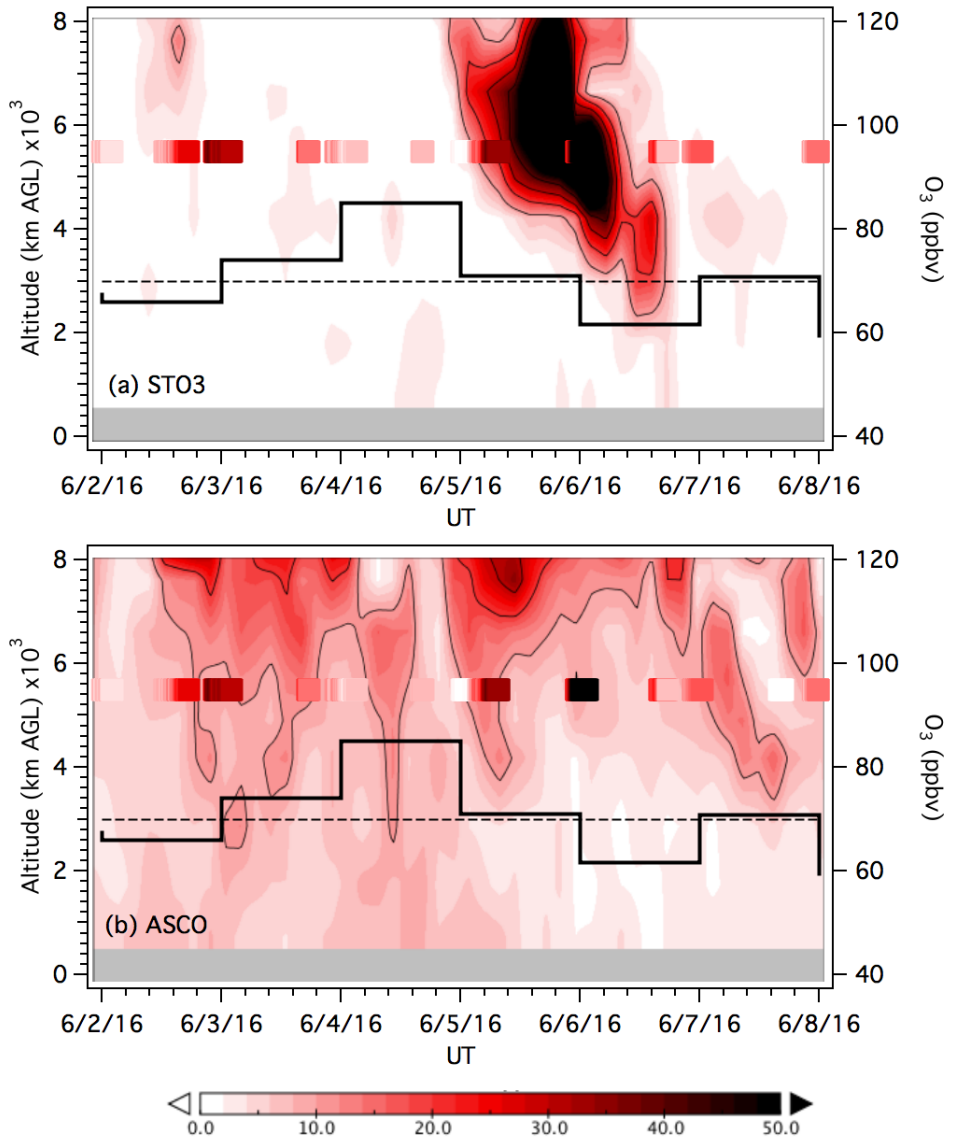

***Figure** 31: Time-height curtain plots showing the FLEXPART STO3 (top) and ASCO (bottom) tracer concentrations between June 2 and 8. The first contour line in both plots corresponds to 10 ppbv. The black staircase (right axis) shows the MDA8 O_3 measured at the VMA and the horizontal dashed line the 2015 NAAQS. The superimposed squares show the TOPAZ measurements at 5.5±0.5 km AGL using the same color scale but offset by 40 ppbv to approximate the background contribution.*

8.2 Example 2: June 12-17, 2016

The FLEXPART STO3 tracer in **Figure** 24 shows a much larger surface contribution on June 13 associated with a much larger low-pressure system that developed into a deep elongated trough as it swept across California (**Figure** 32). The accompanying cold front brought high clouds, cooler temperatures, and strong winds to the SJV which cleared out most of the local and regional pollution and resulted in much lower surface O_3 concentrations as shown in **Figures** 10 and 11. **Figure** 33 shows an expanded view of the TOPAZ measurements.

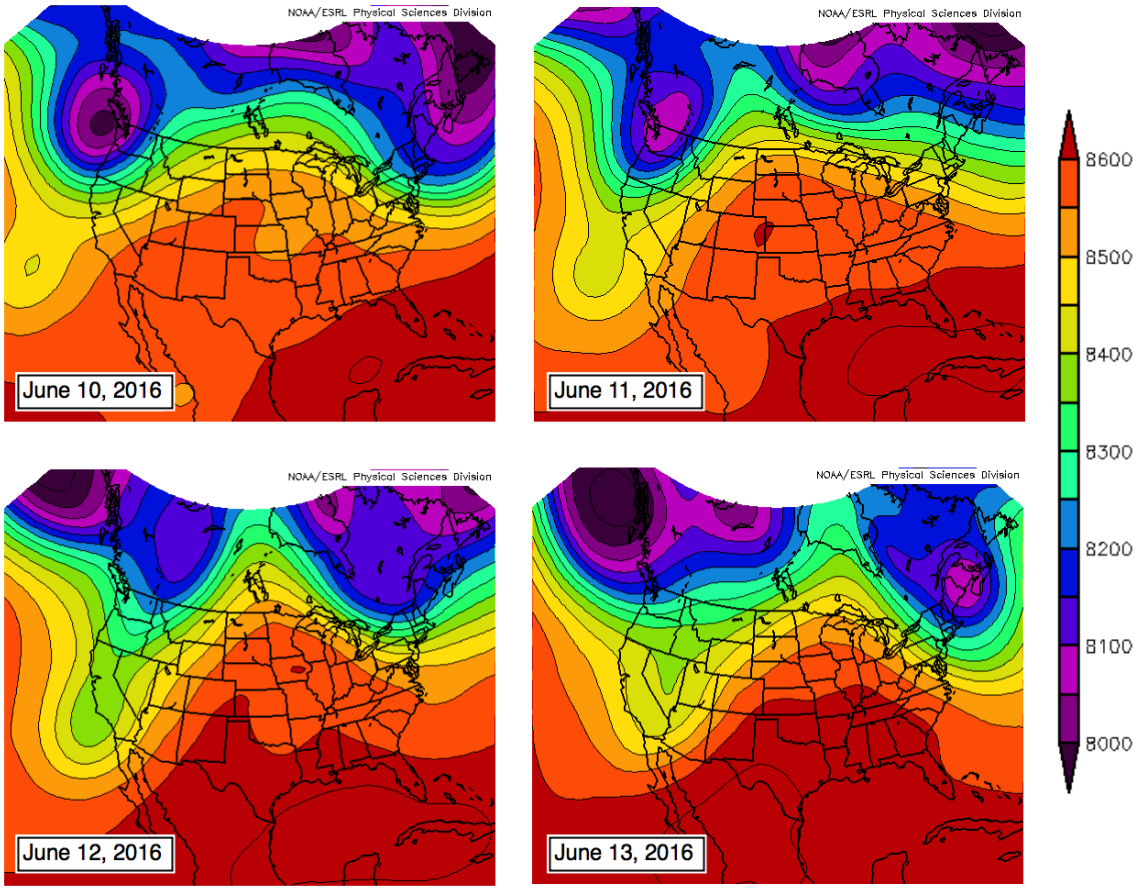

***Figure** 32. 24-hour composite North American Reanalysis (NARR) 350 hPa geopotential heights (m) for June 10-13, 2016.*

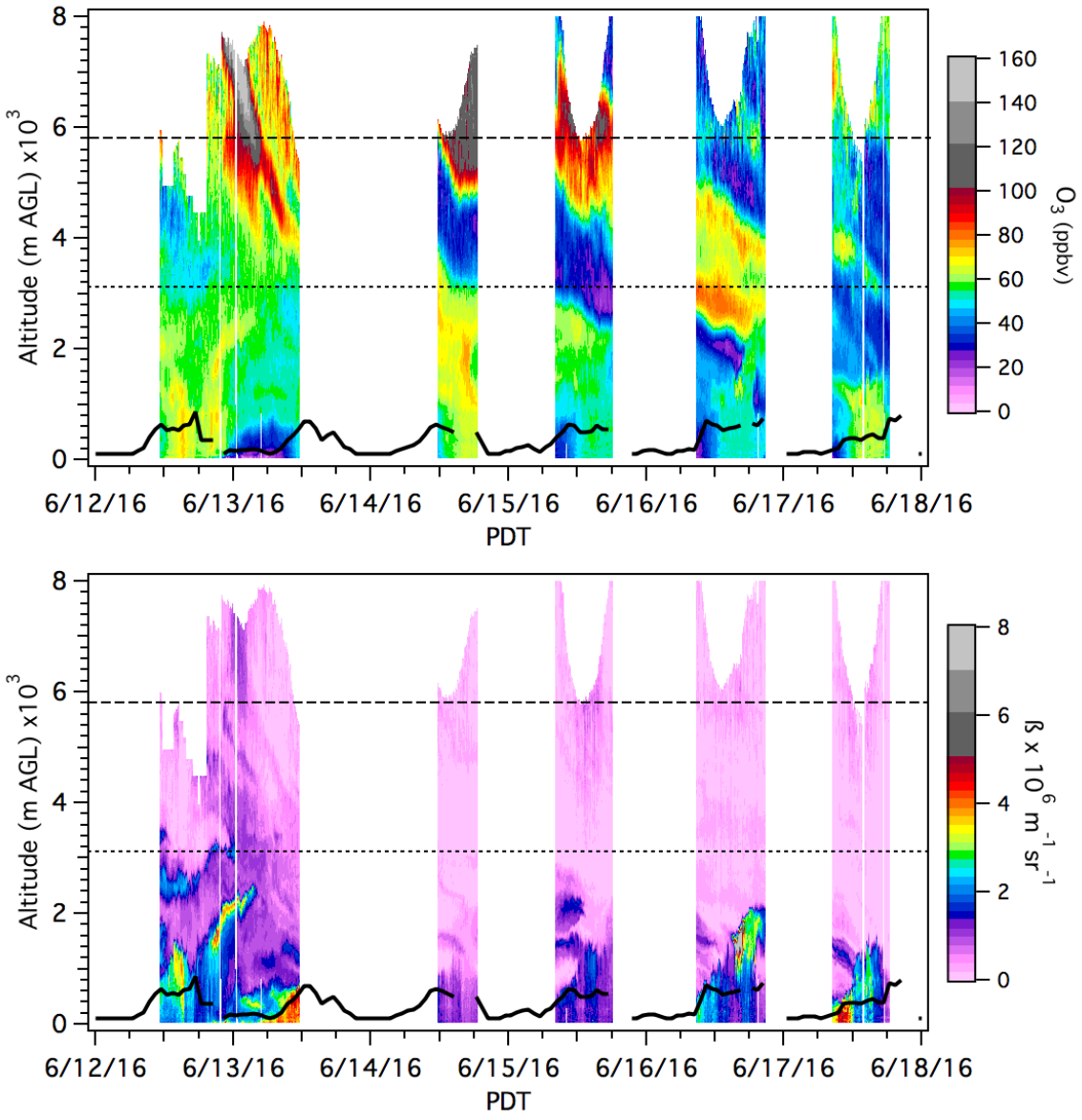

***Figure** 33: Time-height curtain plots showing the O_3 concentrations(top) and ß (bottom) measured by TOPAZ during the second STT event. The dashed and dotted horizontal lines show the approximate heights of the 500 and 700 hPa surfaces shown in the RAP-Chem analyses. The heavy solid black curves show the boundary layer heights derived from the co-located SJVAPCD RASS.*

The RAP-Chem O_3 500 hPa analyses for June 11-13 (**Figure** 34) show a region of high O_3 (>85 ppbv) sweeping eastward into Northern California on June 11 (**Figure** 34a) with two filaments of high O_3 crossing the state on June 12 (**Figure** 34c). The 700 hPa analyses show the deepest part of the intrusion remaining offshore before moving inland over Baja California on June 13 (**Figure** 34d and 34e). The 700 hPa O_3 concentrations remained relatively low (<60 ppbv) across

all of California throughout the event. The RAP-Chem CO analyses (**Figure** 35) show significant amounts of CO accompanying the O_3-rich airmasses on both the 500 and 700 hPa surfaces.

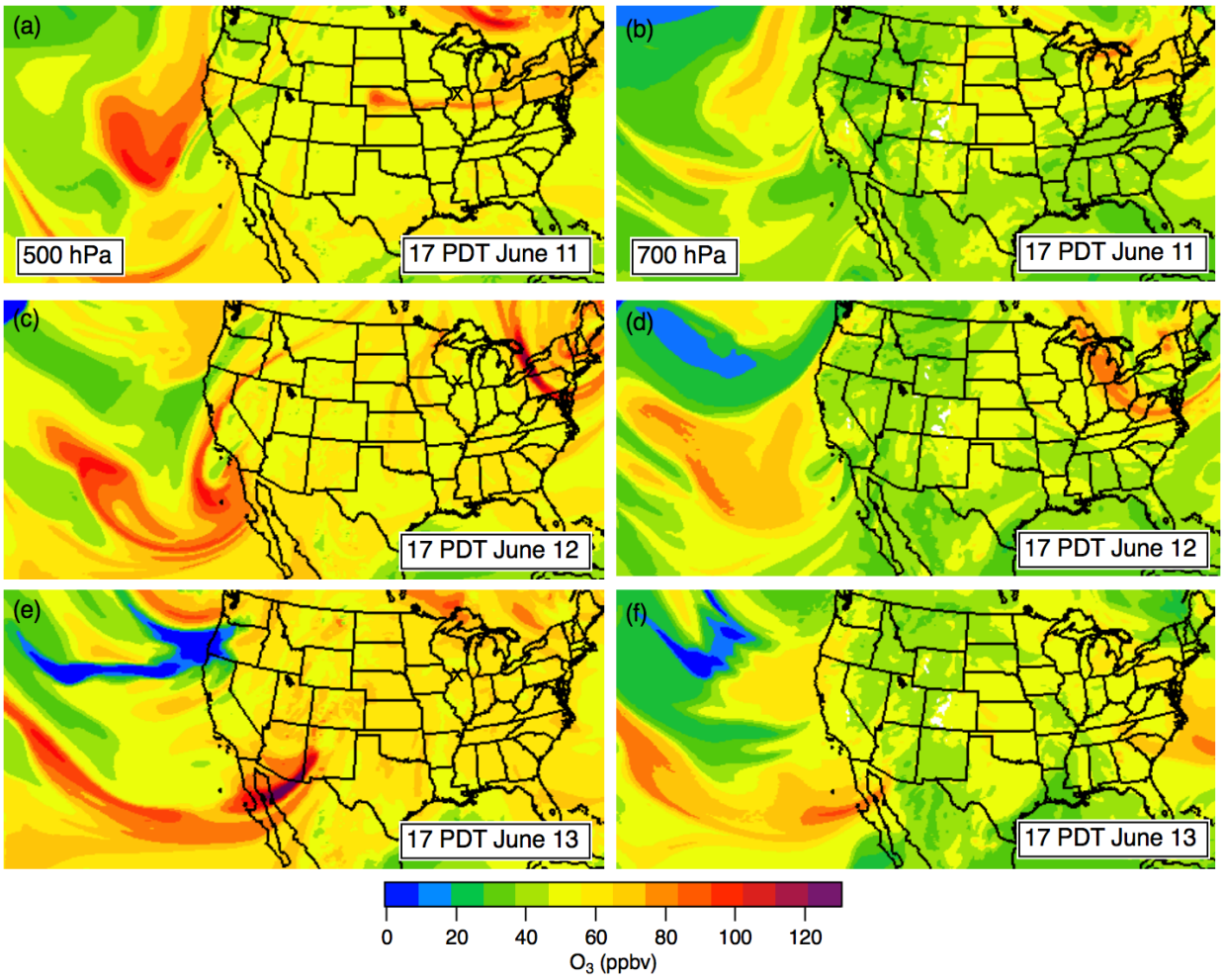

***Figure** 34: RAP-Chem model total O_3 distributions on the 500 hPa (left) and 700 hPa (right) surfaces for the afternoons of June 11-13 (00 UT on June 12-14).*

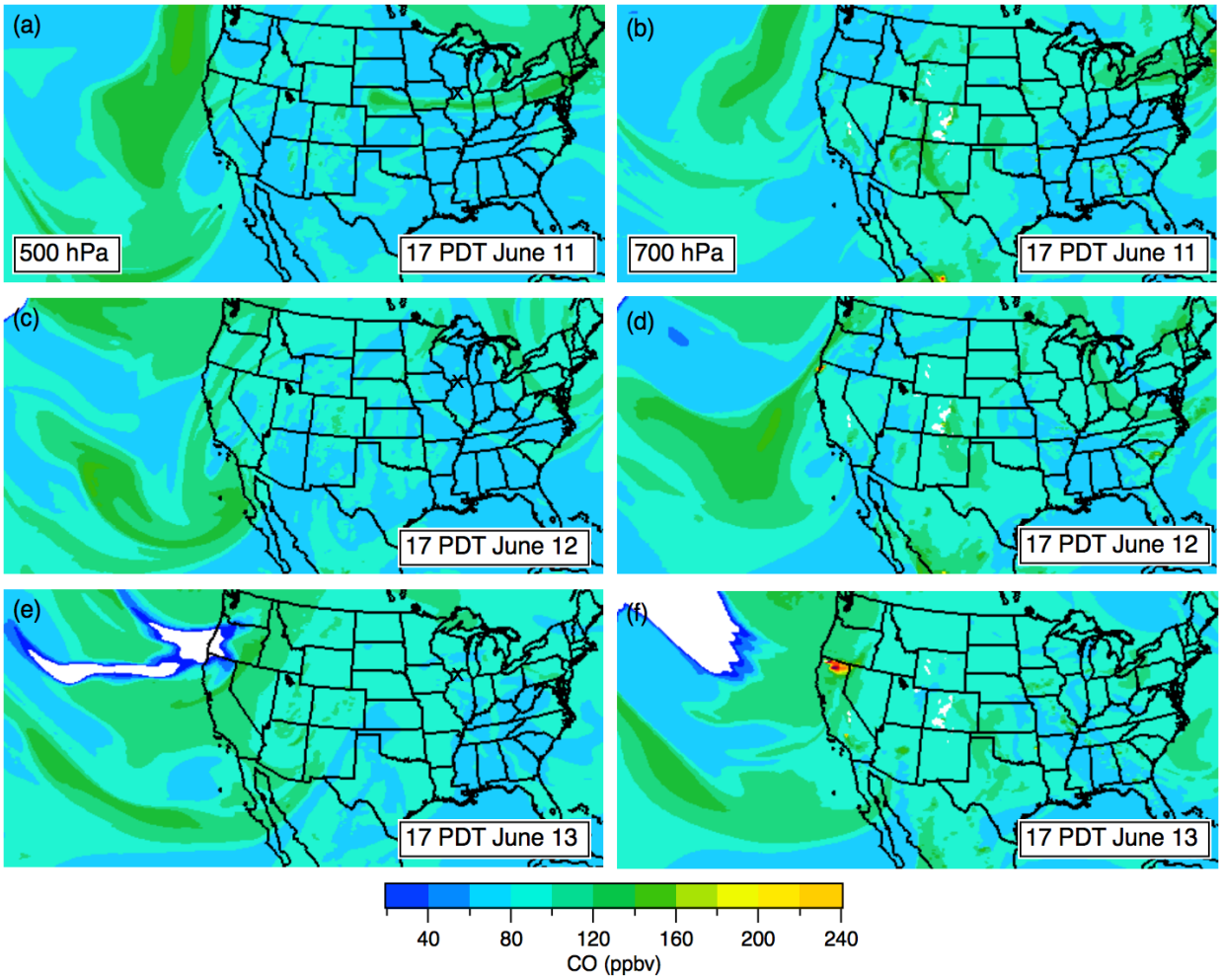

***Figure** 35: RAP-Chem model total CO distributions on the 500 hPa (left) and 700 hPa (right) surfaces for the afternoons of June 11-13 (00 UT on June 12-14). The high CO near the Oregon border on June 13 is attributed to the Pony Fire.*

The expanded FLEXPART STO3 tracer in **Figure** 36 does an excellent job of reproducing the tropopause fold seen in the TOPAZ O_3 measurements on June 12-13 (**Figure** 33). The in-situ measurements show a small enhancement in surface O_3 at the VMA when the stratospheric filament reaches the ground, but this addition is more than offset by an overall reduction in surface O_3 through the ventilation of local pollution.

FLEXPART also captures the timing but not the magnitude of the trailing Asian pollution contribution on June 14-15. The STO3 tracer shows no stratospheric contribution to the very

high (>100 ppbv) O_3 measured on June 14-15, and the AJAX flight on June 15 found CO_2 and CH_4 to also be enhanced as would be expected for a pollution source.

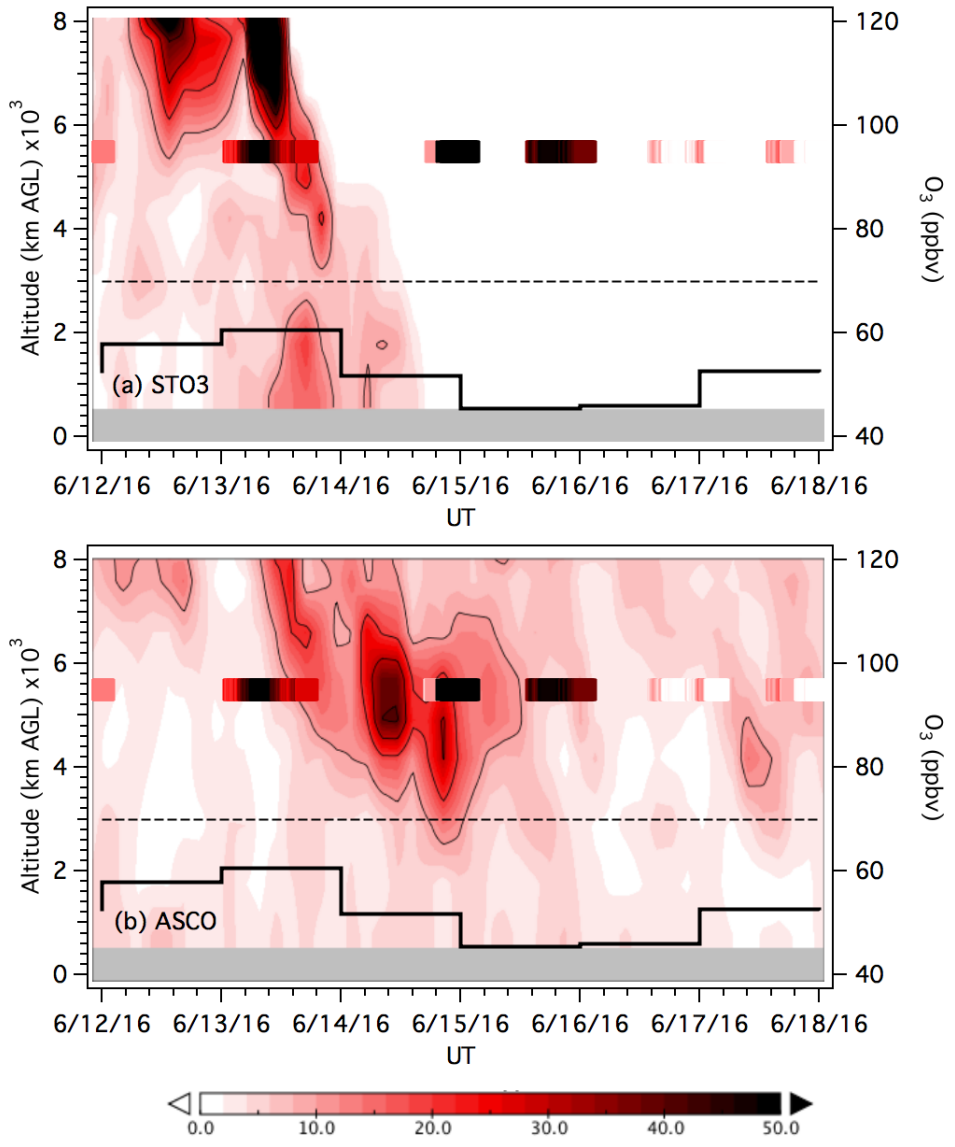

***Figure** 36: Time-height curtain plots showing the FLEXPART STO3 (top) and ASCO (bottom) tracer concentrations between June 12 and 18. The first contour line in both plots corresponds to 10 ppbv. The black staircase (right axis) shows the MDA8 O_3 measured at the VMA and the horizontal dashed line the 2015 NAAQS. The superimposed squares show the TOPAZ measurements at 5.5±0.5 km AGL using the same color scale but offset by 40 ppbv to approximate the background contribution.*

8.3 Example 3: August 2-7, 2016

One final cyclone passed through the West Coast during the last few days of the second CABOTS IOP. The NCEP/NARR daily composite 350 hPa geopotential plots in **Figure** 37 show the relatively shallow low-pressure center and more northerly path typical for this time of year. The expanded TOPAZ curtains in **Figure** 38 show high O_3 aloft on August 2 and 3 that is accompanied by, but not coincident with, high backscatter consistent with smoke from biomass burning. High backscatter near the surface is also attributed to smoke from the Soberanes Fire. A filament with 70-80 ppbv of O_3 and very low backscatter slopes downward from about 4 to 2 km AGL on August 5 and 6. The filament reaches the top of the boundary layer on the afternoon of August 6 and is followed by a sharp decrease in both O_3 and backscatter in the boundary layer.

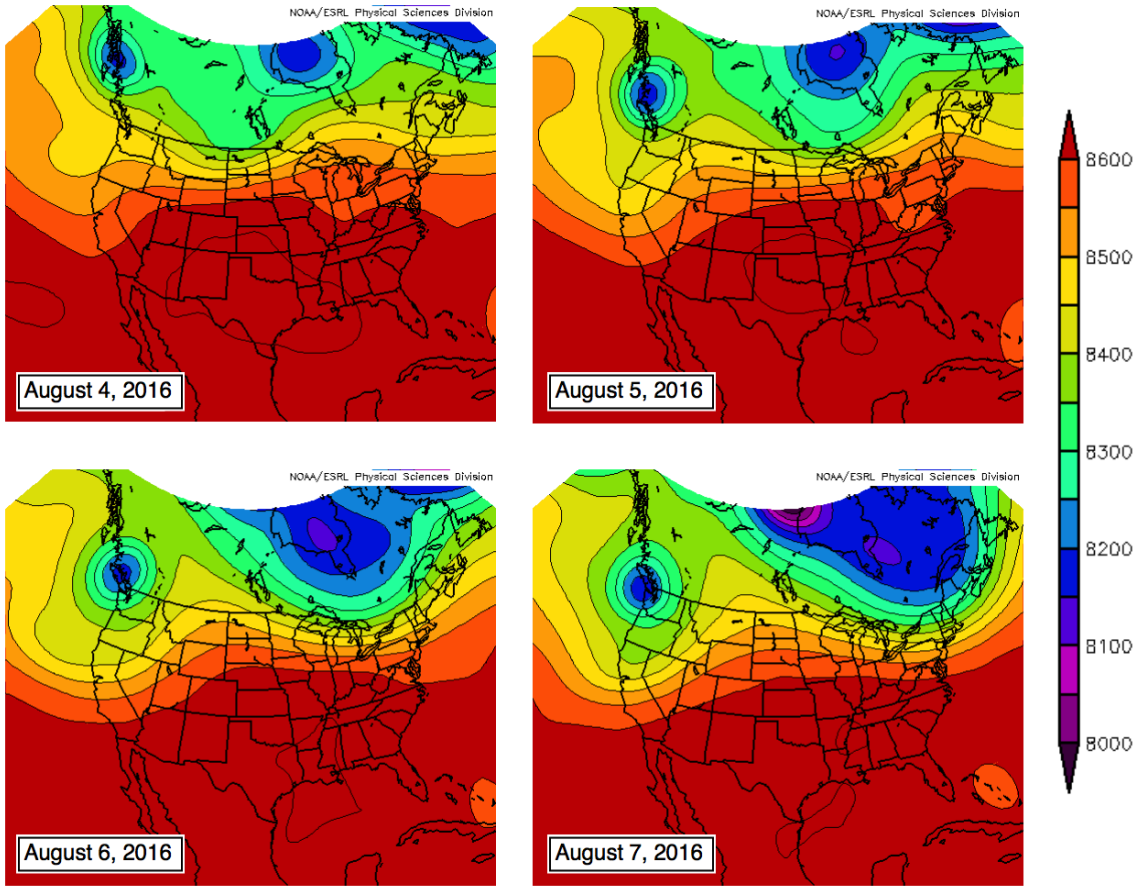

Figure 37**.** *24-hour composite North American Reanalysis (NARR) 350 hPa geopotential heights (m) for August 4-7 2016.*

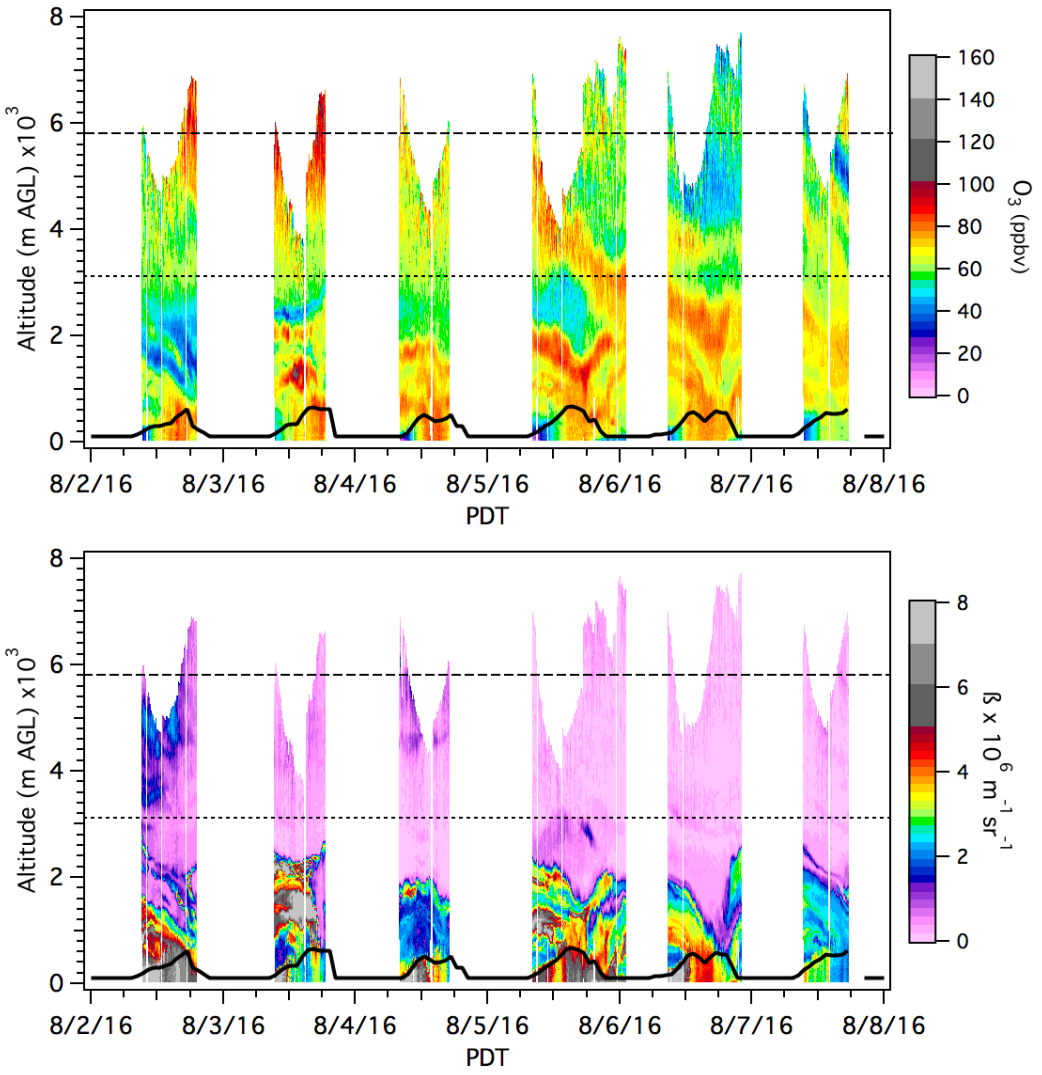

***Figure** 38: Time-height curtain plots showing the O_3 concentrations (top) and ß (bottom) measured by TOPAZ during the third STT event. The dashed and dotted horizontal lines show the approximate heights of the 500 and 700 hPa surfaces shown in the RAP-Chem analyses. The heavy solid black curves show the boundary layer heights derived from the co-located SJVAPCD RASS.*

The RAP-Chem modeled 500 hPa O_3 distribution in **Figure** 39c shows a large stratospheric intrusion off the coast of northern California on the afternoon of August 4 that appears over the SJV in the 700 hPa plot for August 5 (**Figure** 39f). This intrusion is apparently the source of the downward sloping O_3 layer in the TOPAZ measurements from August 5-6. The intrusion is accompanied by a band of elevated CO (**Figure** 40f) which does not appear to be related to the high CO emanating from widespread wildfires in the Pacific Northwest and likely represents transported pollution.

The FLEXPART tracer plots in **Figure** 41 show contributions from all three sources during the first week of August. The high O_3 aloft at the beginning of the plot appears to have both stratospheric and biomass burning contributions, which explains the proximate locations of the high O_3 and backscatter in the TOPAZ measurements. Both the STO3 and ASCO tracers show free tropospheric enhancements consistent with the descending filament in the measurements from August 5 and 6, but both tracers underestimate the measured concentrations.

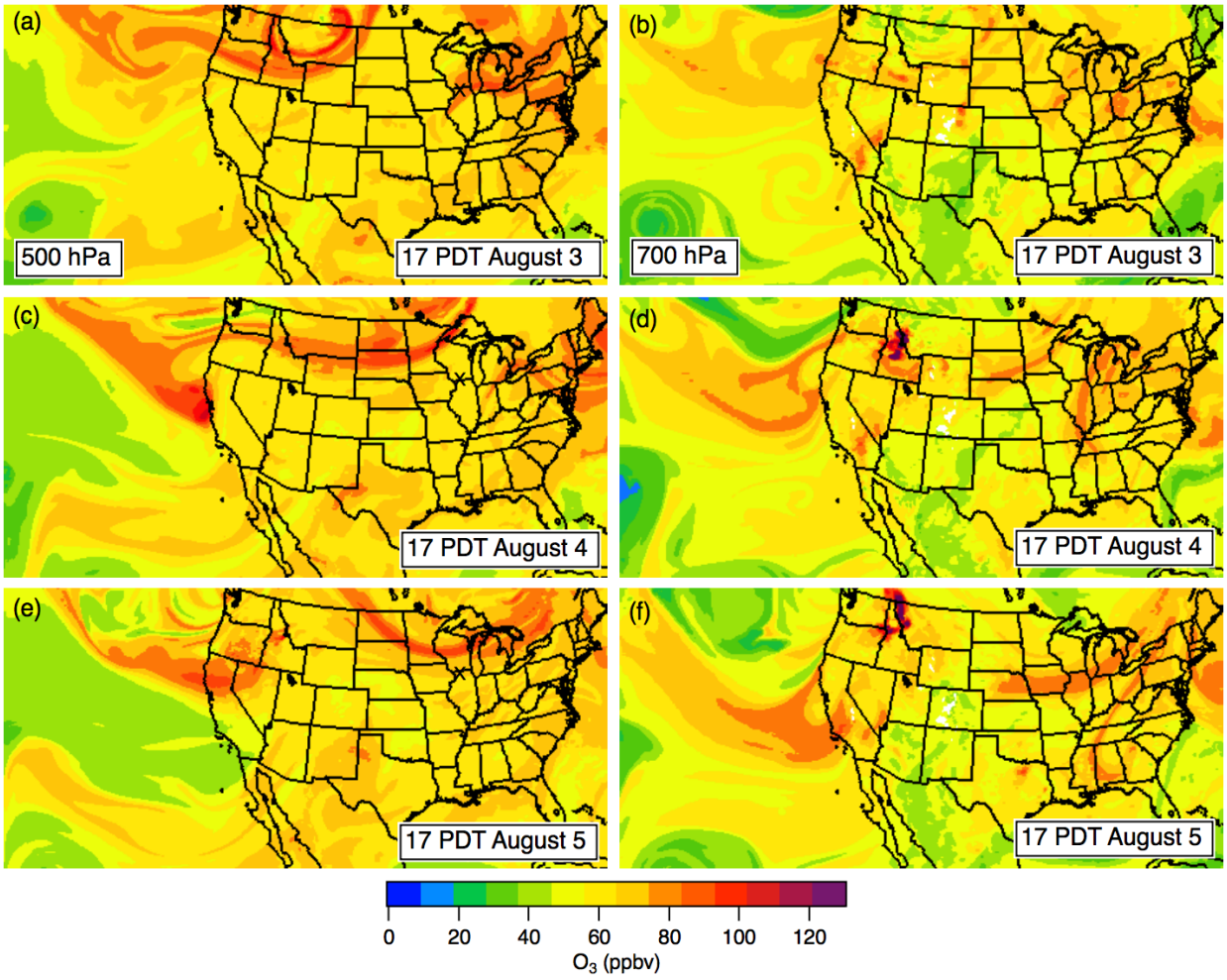

***Figure** 39: RAP-Chem model total O_3 distributions on the 500 hPa (left) and 700 hPa (right) surfaces for the afternoons of August 3-5 (00 UT on August 4-6).*

The descent of the stratospheric air and Asian pollution into the lower troposphere is more easily seen in **Figure** 42, which plots the TOPAZ measurements from August 6 with the profiler winds and RASS mixing heights. The winds shift to the north around 1600 PDT as the descending O_3 layer and an intervening layer of free tropospheric air with lower O_3 concentrations reach the top of the boundary layer. Note that there are too few turbulent

eddies in the highly laminar O_3 layer to give a radar return strong enough for wind measurements. On this day the descending air has essentially the same O_3 concentrations (≈75 ppbv) as the air in the boundary layer so is no obvious change in the O_3 curtain. The mixing is weak, but the backscatter measurements suggest that there may have been some entrainment of the cleaner air from aloft after 1700 PDT. As in the previous example, the net result is a decrease in surface O_3 and aerosol near the surface on the following day (cf. **Figure** 38). In this particular case, some of that polluted air likely had a significant biomass burning component. The impact of this potential O_3 source on surface concentrations in the SJV is explored in the next section.

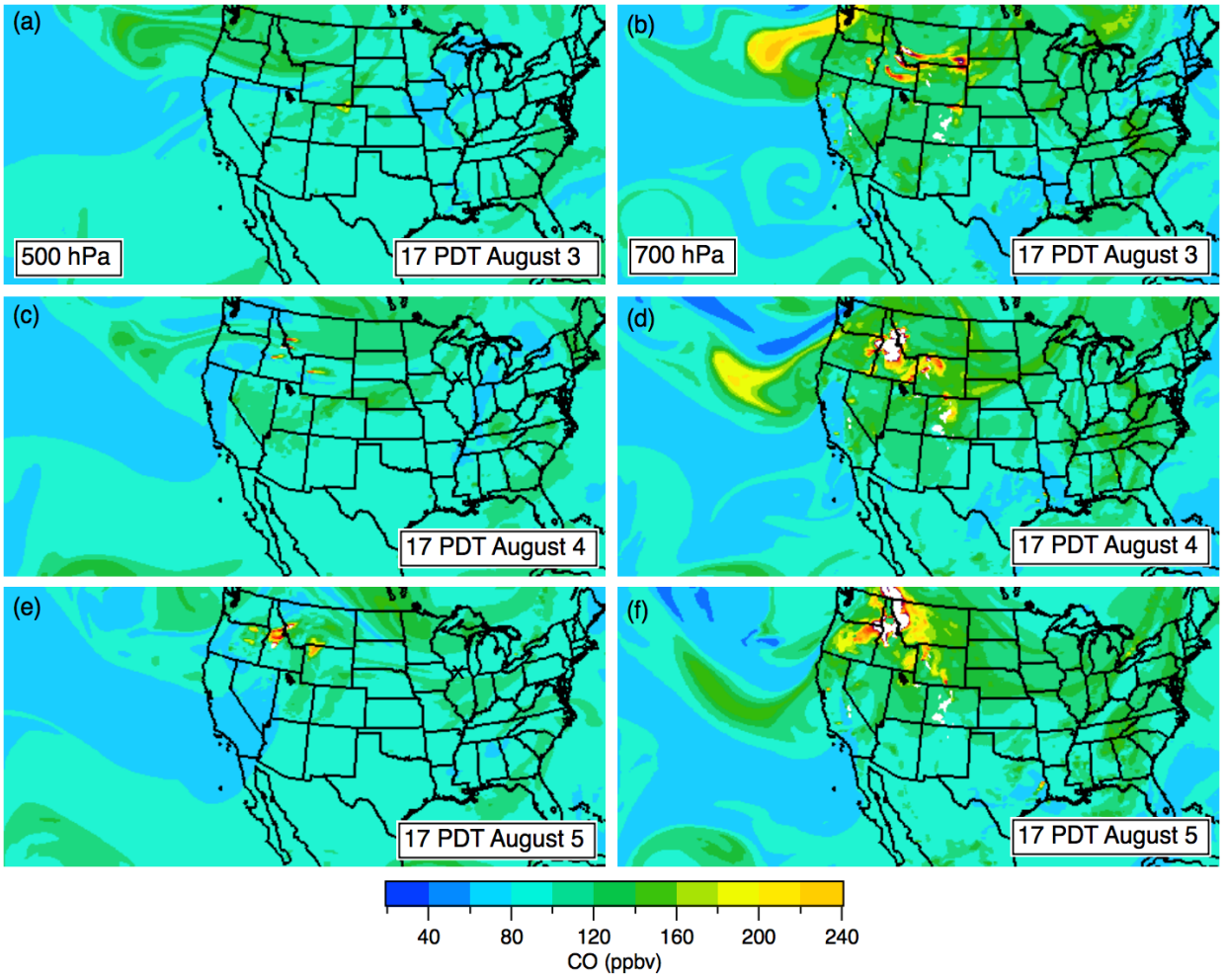

Figure 40: *RAP-Chem model total CO distributions on the 500 hPa (left) and 700 hPa (right) surfaces for the afternoons of August 3-5 (00 UT on August 4-6).*

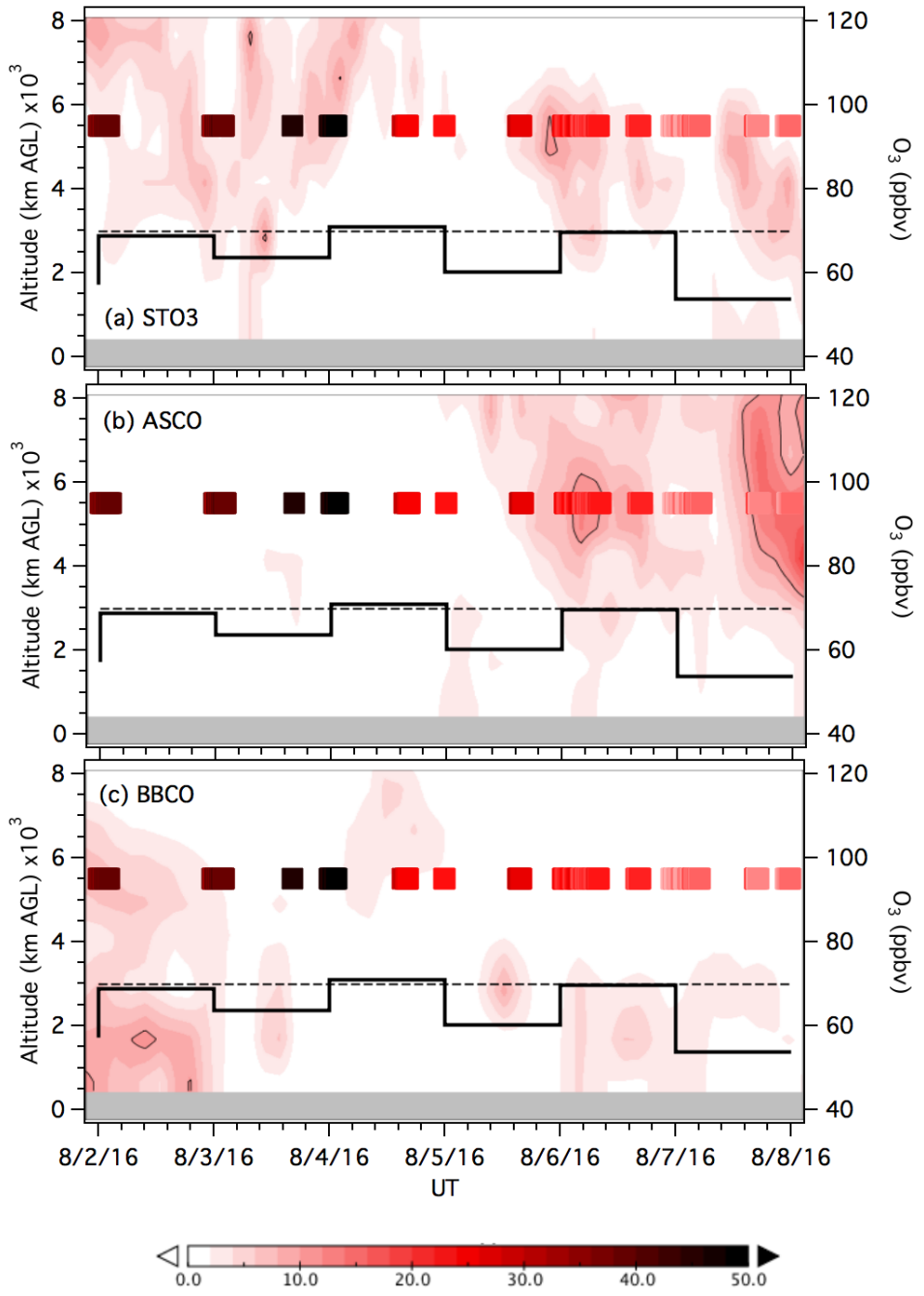

***Figure** 41: Time-height curtain plots showing the FLEXPART STO3 (top), ASCO (middle), and BBCO (bottom) tracer concentrations between August 2 and 8. The first contour line corresponds to 10 ppbv. The black staircase (right axis) shows the MDA8 O_3 measured at the VMA and the horizontal dashed line the 2015 NAAQS. The superimposed squares show the TOPAZ measurements at 5.5±0.5 km AGL using the same color scale but offset by 40 ppbv to approximate the background contribution.*

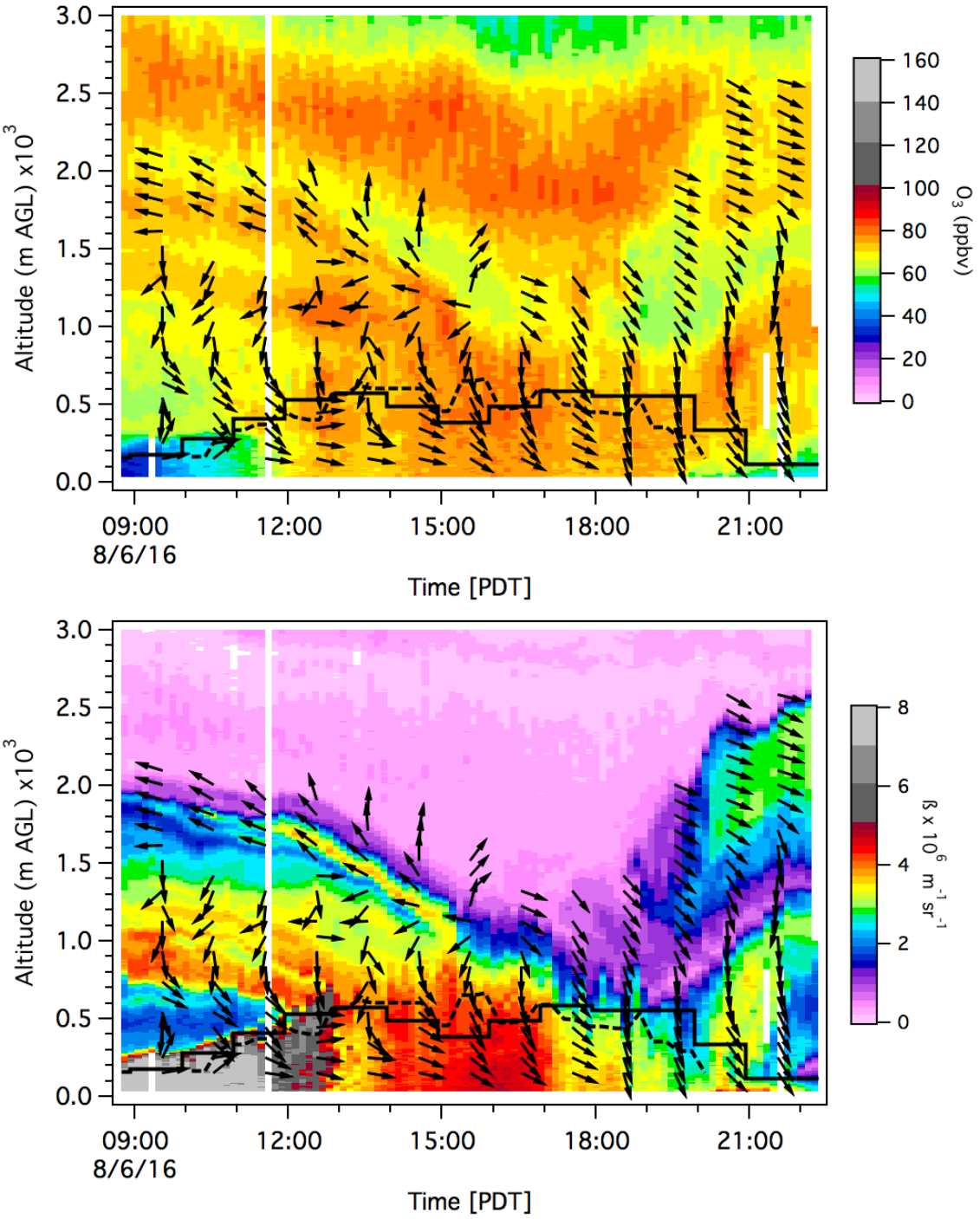

***Figure** 42: Time-height curtain plots showing the TOPAZ O_3 concentrations (top) and ß (bottom) from August 6 with the SJVAPCD profiler winds superimposed. The heavy black curves show the boundary layer heights derived from the co-located SJVAPCD RASS (solid) and NOAA ESRL Doppler lidar (dashed).*

9. Biomass burning and surface O_3 in the SJV during CABOTS

Fires generate fine particulates ($PM_{2.5}$) and a variety of gaseous compounds, including NO_x and VOCs, the photochemical precursors of O_3. The net production of O_3 by fires is highly variable, however, with many contradictory results reported in the literature [*Jaffe and Wigder*, 2012]. The NOx and VOC emission rates depend on a variety of factors including fuel type and combustion temperature, and the subsequent production of O_3 depends on the plume injection height and smoke density. The amount of O_3 produced within a given fire plume also varies with distance. Measurements made near active fires often show decreased O_3 because of titration by NO and measurements made far downwind often show little O_3 production if the NOx has been depleted or sequestered into PAN. The greatest O_3 production occurs in a kind of intermediate "Goldilocks Zone". Production can increase again much further downwind, however, if the plume descends and the PAN thermally decomposes [*Hudman et al.*, 2004], or if the plume passes over urban areas and entrains additional NOx [*Singh et al.*, 2012].

The central SJV was directly impacted by several nearby wildfires and prescribed burns that occurred during the two CABOTS IOPs (**Figure** 43 and **Table 4**). These ranged from the small but nearby Goliath Prescribed Burn in Kings Canyon National Park (759 acres about 60 km away) to the massive Soberanes Fire near Chews Ridge Observatory (132,127 acres about 200 km away). Several large fires also burned between the two IOPs (June 23-July 12) including the 48,019-acre Erskine Fire. The SJV was also impacted by smoke from wildfires in Arizona and Nevada.

Table 4. Major fires near the San Joaquin Valley during CABOTS

Name	Type	Start	Containment	Acres	County	Elevation (m)	Distance (km)
Chimney[1]	wildfire	June 1	June 5	1826	Tulare	1719	130
Coleman	wildfire	June 4	June 17	2520	Monterey	396	175
Goliath	prescribed	June 11-16	N/A	759	Tulare	1702	60
Soberanes	wildfire	July 22	Oct 12	57,800[2]	Monterey	355	200
Goose	wildfire	July 30	Aug 9	2241	Fresno	404	75

[1]Not to be confused with the Chimney Fire that burned 46,344 acres in San Luis Obispo County during August and September 2016.

[2]Acreage burned by end of the second IOP. Total burned acreage was 132,127.

The Chimney Fire burned 1826 acres of BLM land in the Chimney Peak & Owens Peak Wilderness Areas, temporarily closing the Pacific Crest Trail about 40 km NE of Lake Isabella and forcing the evacuation of the small town of Chimney Rock. The Coleman Fire started in the Los Padres National Forest in Monterey County southwest of King City on June 4 and threatened numerous structures, but burned only one. The fire was fully contained by June 17. The Goliath Prescribed Burn in the Kings Canyon National Park was initiated over several days between June

11 and 16. The massive Soberanes Fire near Big Sur and the Chews Ridge Observatory started on July 22 and scorched nearly 57,800 acres by the end of the second IOP. The Soberanes Fire destroyed 57 homes and 11 outbuildings as it burned a total of 132,127 acres of chaparral, tall grass, and timber before it was extinguished on October 12. Finally, the much smaller Goose Fire started in the foothills east of Fresno on July 30 and destroyed 4 homes and 5 outbuildings as it burned 2241 acres near the town of Prather. This fire was fought aggressively and contained on August 9. In the following discussion we contrast the impact of the Soberanes and Goose Fires on ozone in the SJV.

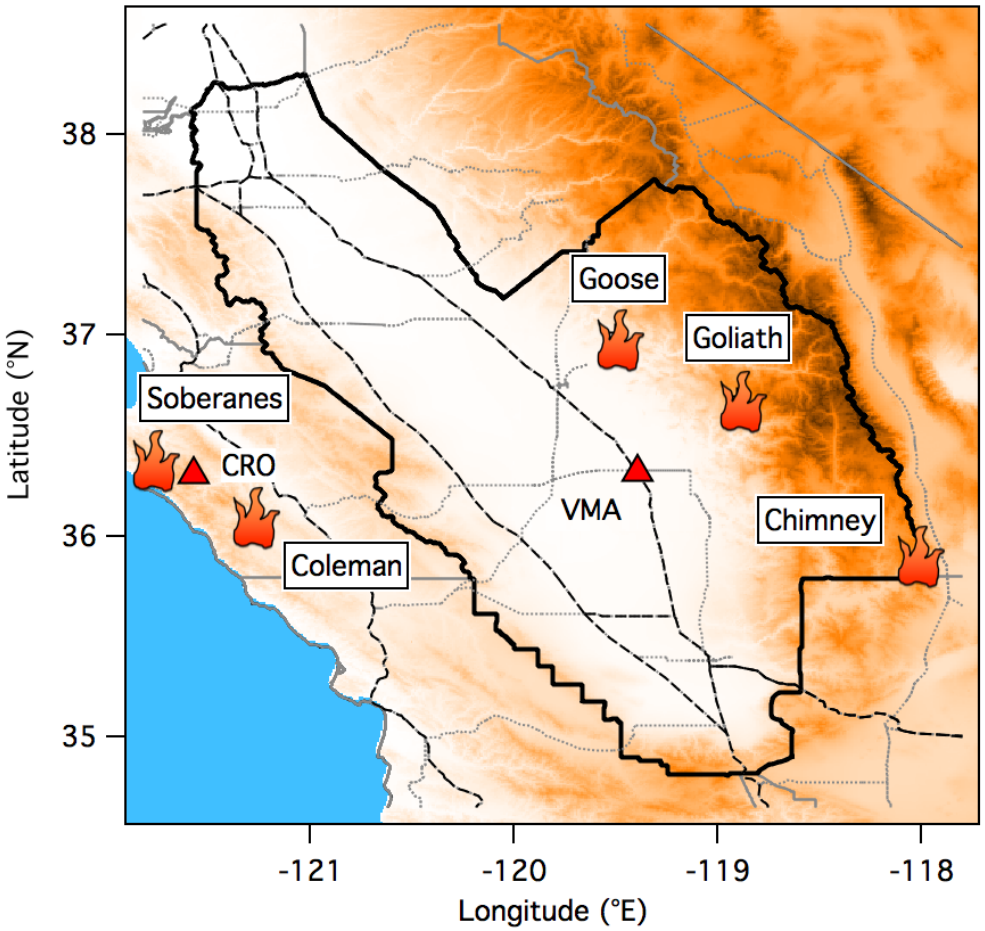

***Figure** 43. Fires larger than 1000 acres in or near the SJVAB (heavy black line) during the CABOTS IOPs.*

The smoke plume from the Soberanes Fire is clearly seen in most of the afternoon (20-22 UT) MODIS images (https://fsapps.nwcg.gov/afm/imagery.php) for July 27 to August 1 displayed in **Figure** 44**.** The much more compact plume from the Goose Fire is circled in the MODIS image from July 31.

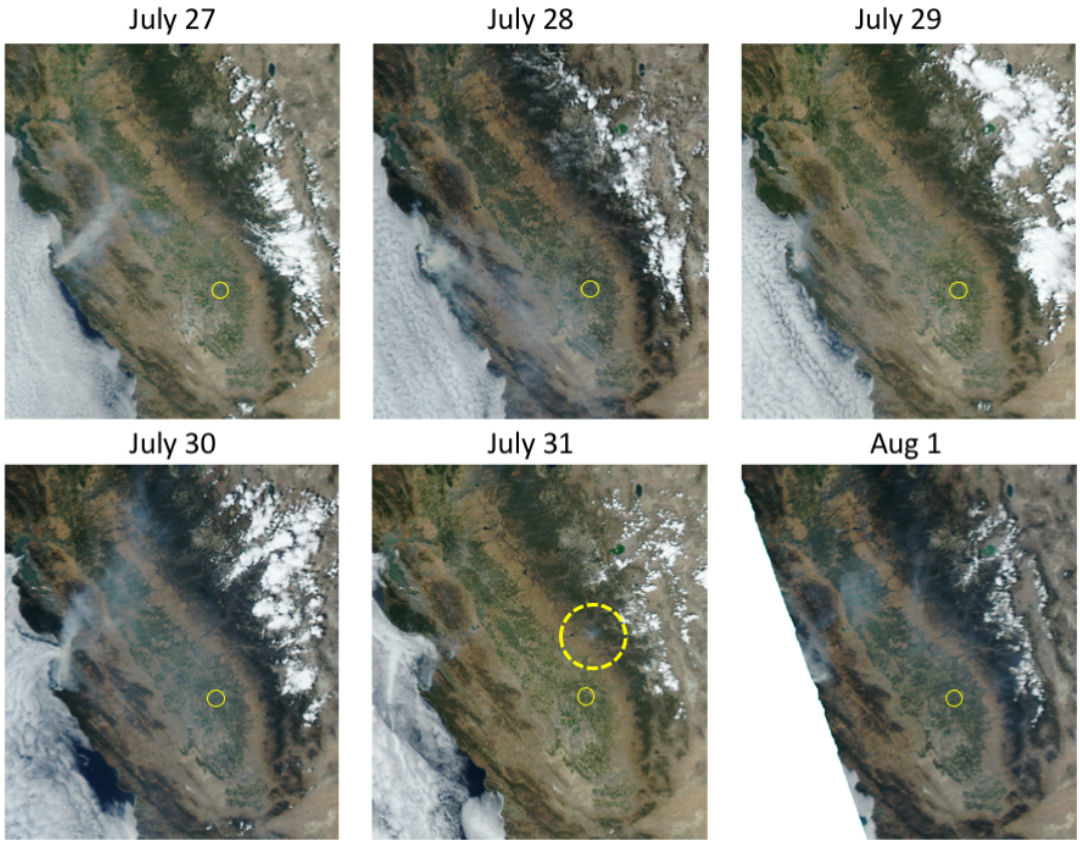

Figure *44a. MODIS images of the SJV showing smoke plumes from the Soberanes and Goose (dashed yellow circle) Fires between July 27 and August 1. The small yellow circles mark the VMA.*

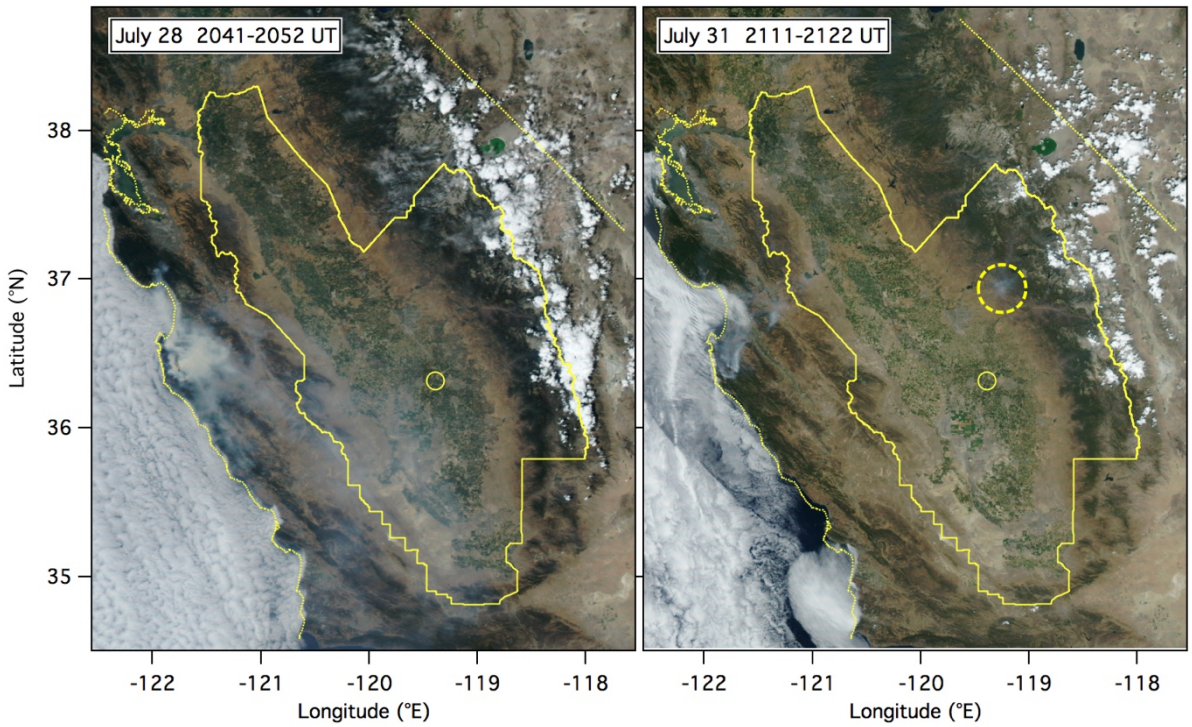

***Figure** 44b. Enlarged views of the MODIS images from July 28 and 31 showing smoke plumes from the Soberanes and Goose (dashed yellow circle) Fires. The heavy yellow line shows the SJVAB. The small yellow circles mark the VMA.*

The general appearance of the smoke seen in the MODIS images agrees quite well with the FLEXPART biomass burning CO tracer distributions at 800 hPa (≈2.0 km ASL) and 600 hPa (≈4.5 km ASL) shown in **Figure** 45. Both show the Soberanes plume advected inland across the central SJV on some days (e.g. July 27 and 30), but carried southward down the coast and into the southern SJV on others (e.g. July 28-29). Thus, the air sampled above the VMA on any given day contains smoke with a range of ages and from slightly different source regions. The FLEXPART plots suggest that most of the emissions from the Soberanes Fire were trapped by the marine inversion layer from the Pacific Ocean and remained at relatively low altitudes. This contrasts with the Goose Fire where the smoke plume remained relatively compact and much of the smoke was lofted to much higher altitudes above the Sierra foothills (**Figure** 46). The FLEXPART tracer plots also suggest that some of the smoke within the SJV during late July and early August may have originated from the five lightning-initiated fires in the Virginia Mountain Complex which burned 62,020 acres about 50 km northeast of Reno between July 28 and August 5.

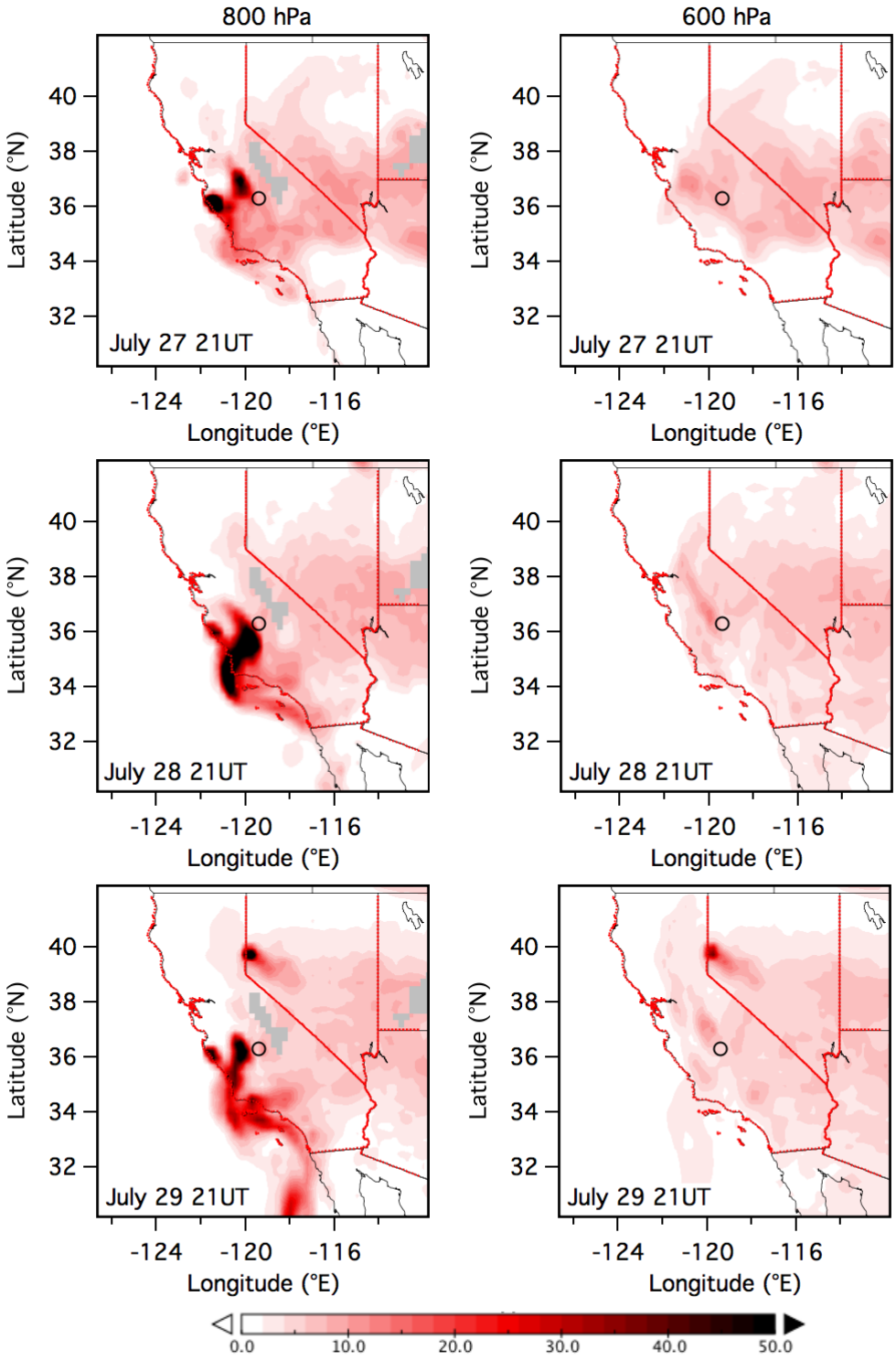

***Figure** 45. FLEXPART BBCO tracer (ppbv) distributions at 800 (left) and 600 (right) hPa. The open circle marks the VMA and the gray regions represent terrain above the 800 hPa pressure level.*

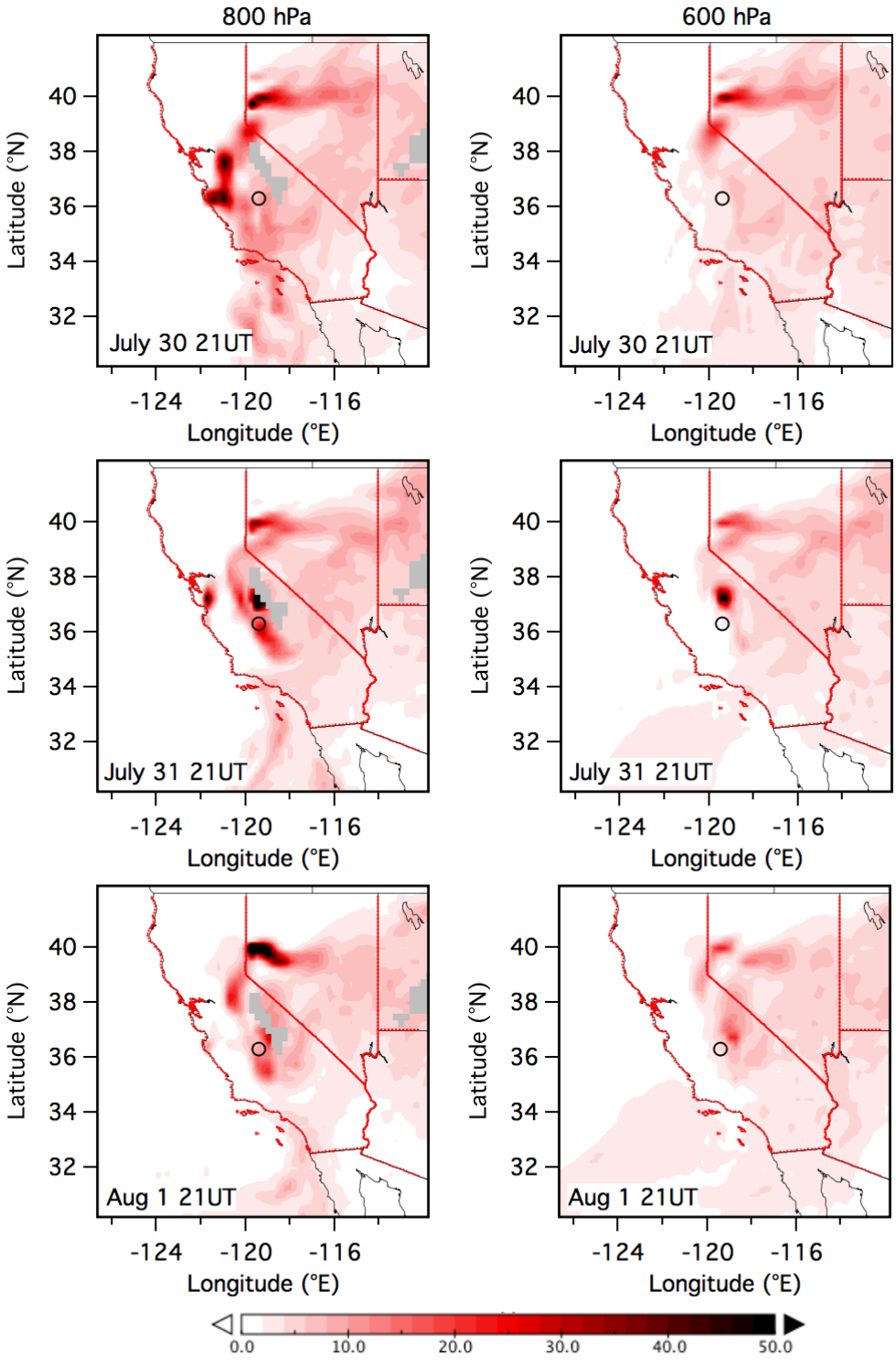

***Figure** 45 (continued). FLEXPART BBCO tracer (ppbv) distributions at 800 (left) and 600 (right) hPa. The open circle marks the VMA and the gray regions represent terrain above the 800 hPa pressure level.*

***Figure** 46. Smoke plumes from the Soberanes Fire on July 22 (left) and the Goose Fire on July 30 (right). Photographs from CalFire.*

Smoke from the Soberanes Fire was also visible from the VMA in late July and early August (**Figure** 47) and the TOPAZ lidar measured large backscatter enhancements in the lowest 3 km above the VMA. This is seen in **Figure** 48, which contrasts the lidar backscatter measurements from the end of July with those from the end of May. In May, the highest backscatter was found in the shallow boundary layers with weaker backscatter caused by thin aerosol layers in the buffer layer between about 1 and 2 km. In July, the backscatter in the buffer zone increased dramatically after July 24 when smoke from the Soberanes Fire appeared above the VMA with more modest increases in the boundary layer. Both curtain plots show sporadic backscatter layers between 4 and 5 km in the free troposphere. The FLEXPART tracer distributions in **Figure** 45 indicate that the July enhancement was caused by the nearby Goose Fire (July 30-31). The corresponding FLEXPART distributions for late May (not shown) suggest that the free tropospheric layers in the upper panel of **Figure** 48 were caused by smoke from a cluster of lightning-caused wildfires within the Coconino National Forest in Arizona (May 28-29).

Figure 49 is similar to **Figure** 48, but shows the corresponding O_3 measurements. High concentrations were measured both in and above the boundary layer, with the high O_3 concentrations in the buffer zone coinciding with the regions of increased backscatter. Smaller O_3 increases are also seen above 4 km in both plots, but these are displaced from the regions of highest backscatter. The scatter plots in **Figures** 50-52 show the relationships between O_3 and backscatter measured in all three altitude layers. Only afternoon-evening measurements (13-21 PDT) are shown to eliminate the confounding effects of surface deposition and titration in the boundary layer measurements. The gray points show all of the measurements from each IOP and the colored points highlight those from the indicated days.

***Figure** 47. Smoke from the Soberanes Fire as seen from the Visalia Municipal Airport on July 29, 2016. Top, looking north in the mid-afternoon, and bottom, looking west at sunset. Photographs by A. Langford.*

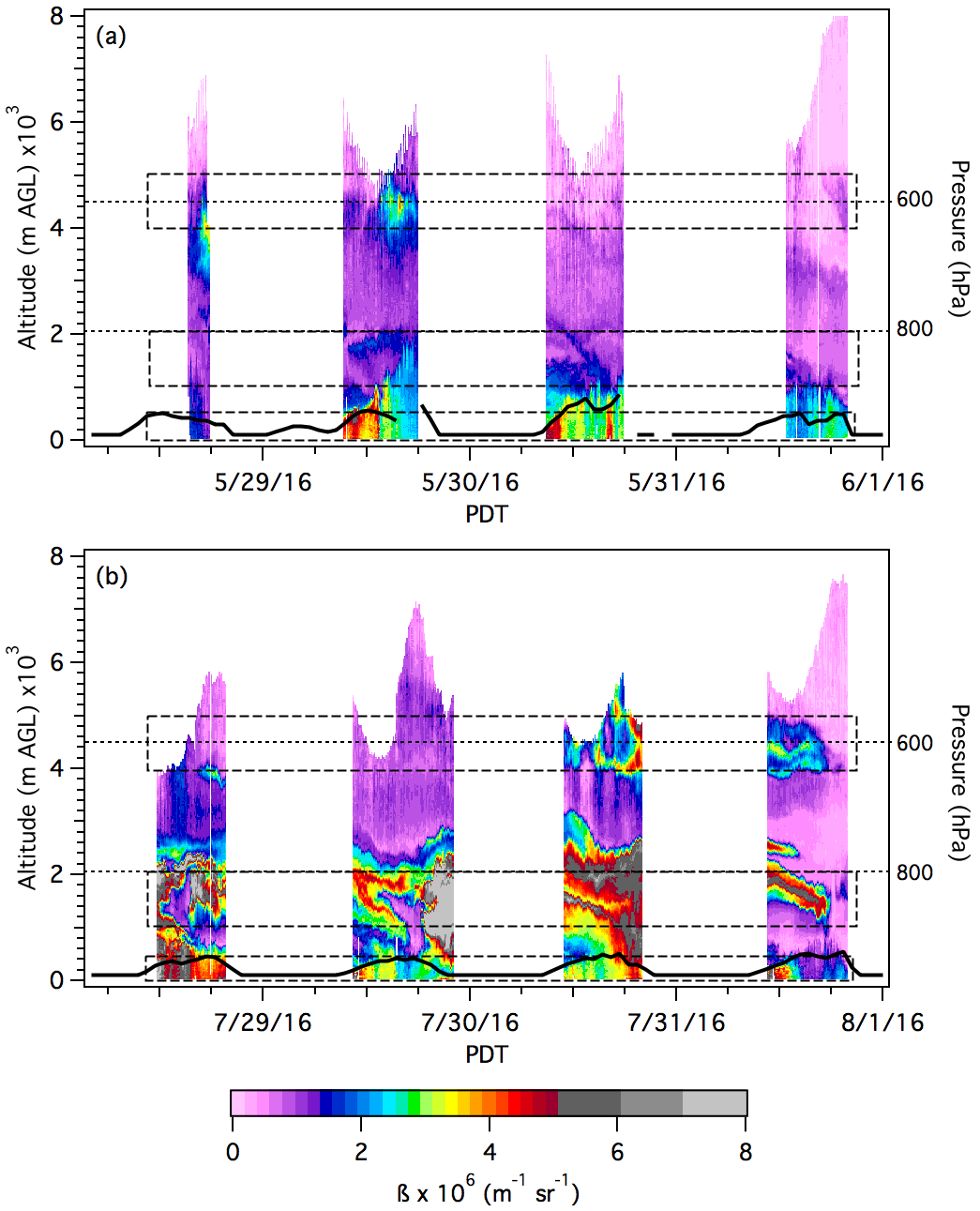

***Figure** 48. Backscatter measurements from (a) May 28-31 and (b) July 28-31. The short-dash lines mark the approximate 800 and 600 hPa levels and the heavy solid black curve shows the boundary layer height inferred from the co-located RASS. The dashed boxes show the boundary layer, buffer zone, and free tropospheric layers used in **Figures** 50-53.*

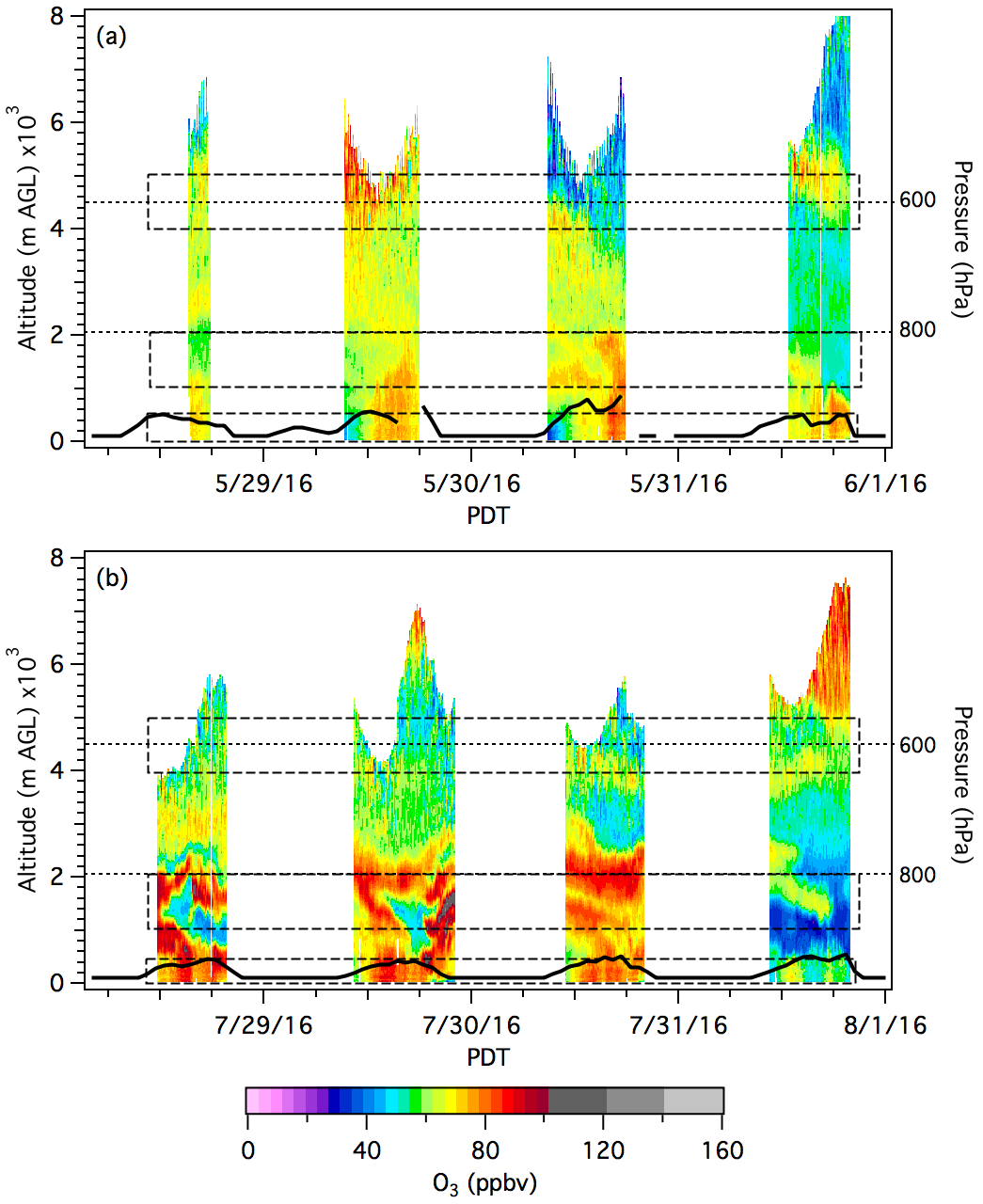

***Figure** 49. Ozone measurements from (a) May 28-31 and (b) July 28-31. The short-dash lines mark the approximate 800 and 600 hPa levels and the heavy solid black curve shows the boundary layer height inferred from the co-located RASS. The dashed boxes show the boundary layer, buffer zone, and free tropospheric layers used in **Figures** 50-53.*

The boundary layer measurements from the first IOP (left panel of **Figure** 50) show a lot of scatter, but the ozone and backscatter measurements were positively correlated on most days. The correlation was very strong on some days (e.g. May 28), consistent with a common source.

The correlations were more robust during the second IOP, when the peak backscatter coefficients were about a factor of two higher.

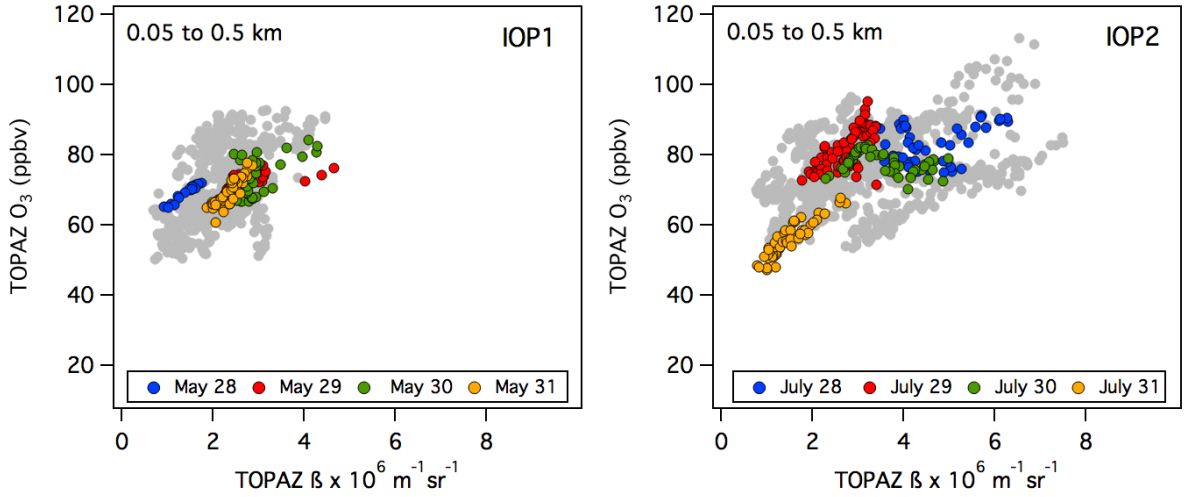

***Figure** 50. Ozone-backscatter relationship in the boundary layer (0.05 to 0.5 km) during the first (left) and second (right) IOP. The gray points show the measurements from the entire IOP and the colored points highlight the measurements from the days shown in **Figures** 48 and 49.*

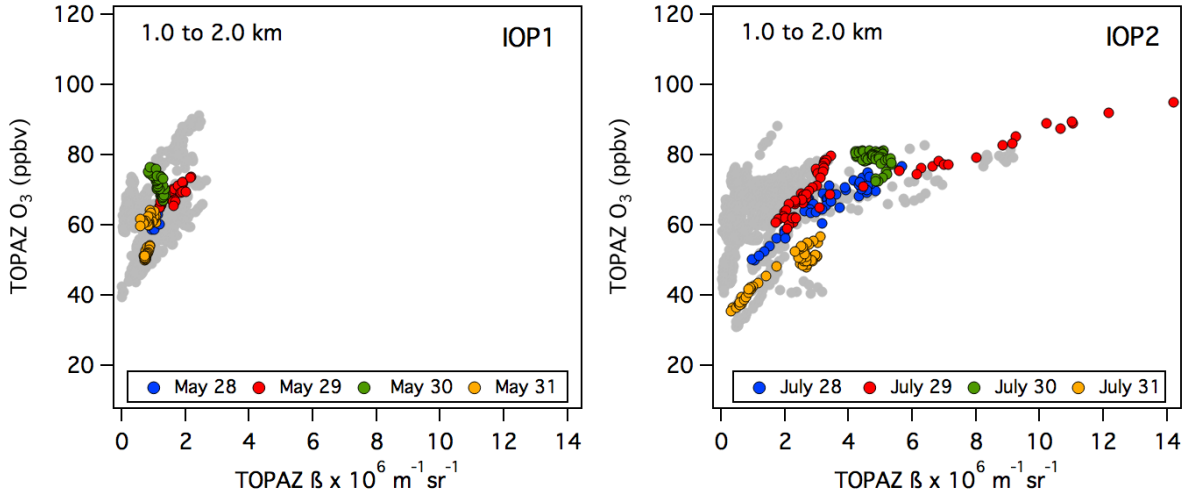

***Figure** 51. Same as **Figure** 50, but for the buffer zone layer (1.0 to 2.0 km).*

Figure 51 shows that the post-Soberanes backscatter enhancement was much larger in the buffer zone (1-2 km) and more strongly correlated with ozone.

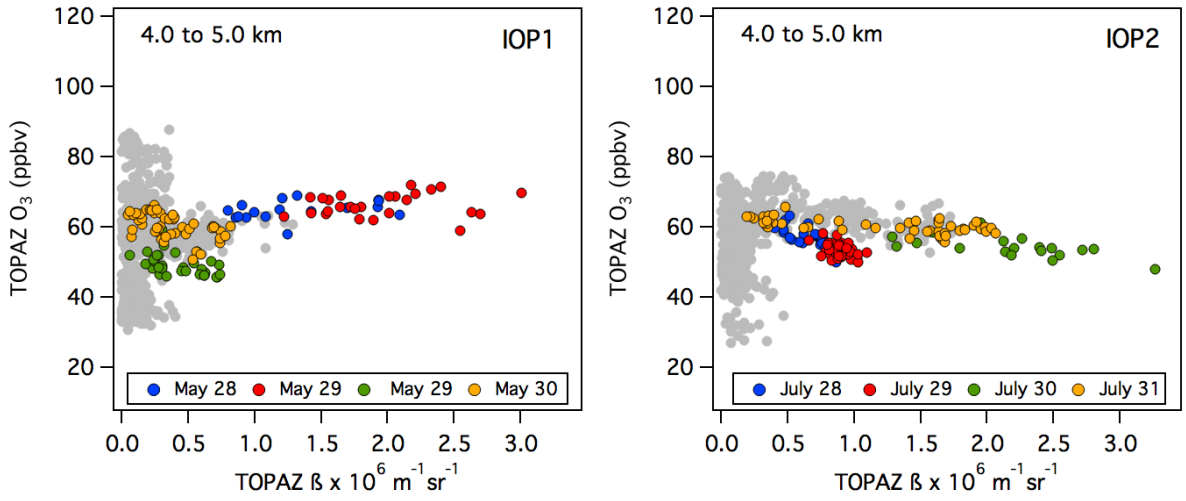

***Figure** 52. Same as **Figure** 51, but for the free tropospheric layer (4.0 to 5.0 km).*

The free tropospheric (4-5 km AGL) measurements in **Figure** 52 appear qualitatively different with little or no ozone production in the plume from the Arizona (May 28-29) fires, and a weakly negative correlation consistent with O_3 destruction in the Goose (July 30-31) Fire plume. A close examination of the curtain plots shows that there was, in fact, some O_3 production in both cases, but the enhancements are displaced to the edges of the smoke plumes.

The buffer layer measurements show that there was substantial production of ozone in the Soberanes Fire plume, and that much of this ozone remained available for entrainment into the boundary layer. The O_3-ß relationship changed from day to day and sometimes over the course of a single day, presumably because of differences in the age and composition of the sampled plume. This is shown more clearly in **Figure** 53 which plots the buffer zone (upper panel) and boundary layer (lower panel) measurements from July 29. Two distinct O_3-ß relationships are seen in each plot, consistent with the advection of two different air masses over the VMA. The enlarged curtain plots with co-located profiler horizontal wind measurements in **Figure** 54 show that both plumes were advected to the VMA from a westerly to northerly direction with the transition between the two plumes occurring between ≈1500 and 1800 PDT. A region of much cleaner air with ≈50-60 ppbv of O_3 appeared in the buffer zone between the two plumes.

Although the O_3/ß slopes cannot be converted to absolute production rates since the ozone and smoke particles are formed by different physical and chemical processes, they can be used to identify changes in airmass and to estimate the O_3 enhancement in the fire plumes. Linear regression of the colored points in **Figure** 53 show very strong correlations (R^2>0.85) between O_3 and ß in both plumes, and the net increase in O_3 provides a rough estimate of the total O_3 enhancement. The first airmass sampled in the buffer zone (upper panel, plume A) shows an ozone enhancement of ≈20 ppbv and the second, smokier airmass (plume B) an enhancement of ≈25 ppbv. The corresponding enhancements in the boundary layer were ≈15 and 20 ppbv.

Similar contributions are estimated for the entire period from July 27 to 30, the highest ozone days in the SJV during CABOTS (cf. **Figure** 10).

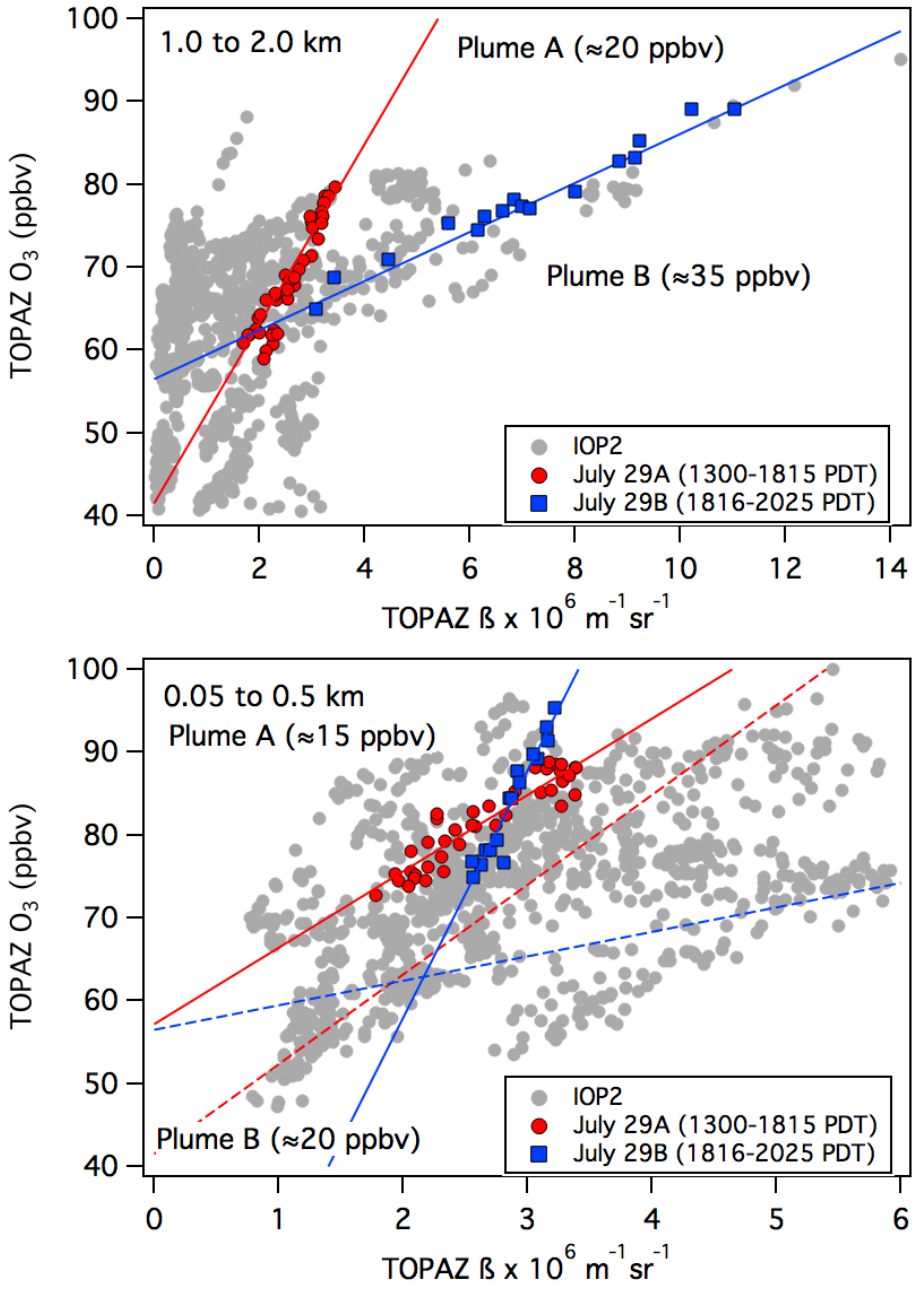

***Figure** 53. Ozone-backscatter relationships in the buffer zone (1-2 km, upper panel) and in the boundary layer (0.05 – 0.5 km, lower panel) on July 29 (red: plume A, blue: plume B). The gray points show all the daytime measurements from the second IOP. The dashed lines in the lower panel show the buffer zone regression fits from the upper panel.*

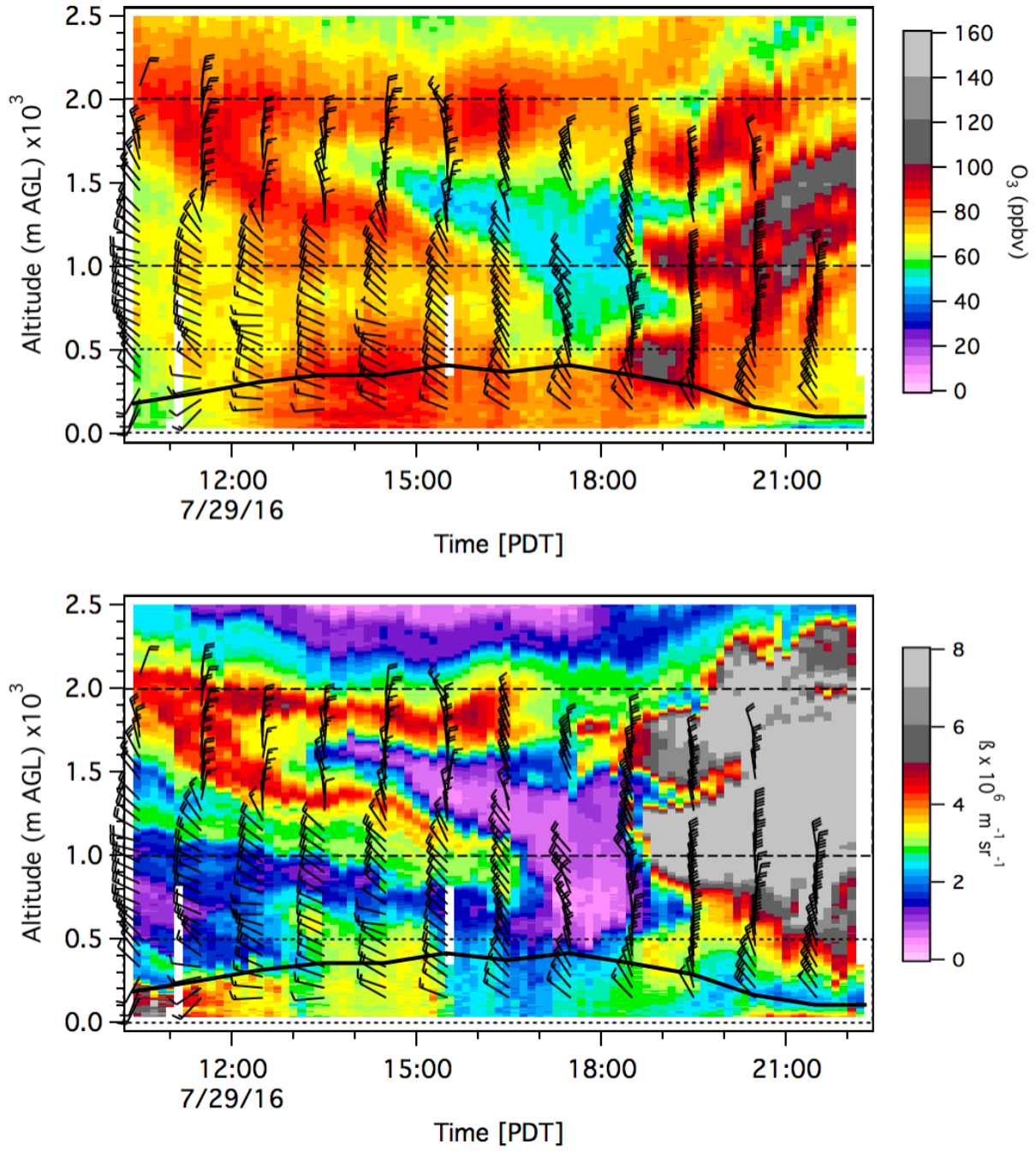

***Figure** 54. Ozone (top) and backscatter (bottom) curtain plots from July 29 with the co-located SJVAPCD profiler wind measurements and RASS boundary layer height superimposed (heavy black curve). The dotted and dashed lines bracket the boundary layer (0.05 to 0.5 km AGL) and buffer layer (1-2 km AGL) bins used to isolate the data in **Figure** 53.*

10. Summary and Conclusions

The 440 hours of lidar profiles acquired during the CABOTS field experiment greatly expand our knowledge of the vertical distribution of O_3 above the central San Joaquin Valley, and provide new insights into the processes contributing to the high surface O_3 found there. The lidar measurements confirmed the unusually shallow convective mixed layers of the SJV and the formation of a persistent buffer layer above the boundary layer between about 1 and 2 km.

The lidar retrievals are in excellent agreement with measurements made by the UC Davis/Scientific Aviation Mooney and NASA AJAX Alpha Jet aircraft during spiral profiles and low approaches at VMA, and the ozone mixing ratios measured by the lidar along a low elevation slant path at a height of 27.5±5 m and a distance of 800 m also agreed with measurements from the nearest regulatory monitors at Visalia (10 km) and Hanford (22 km). The lidar retrievals matched the *in-situ* measurements at VMA when the latter were filtered to exclude local influences.

The TOPAZ lidar also frequently detected elevated O_3 layers between 4 and 6 km above the valley floor consistent with biomass burning, transport from Asia, or descent from the lower stratosphere. Most of these layers passed over the Sierra Nevada into the Intermountain West where they may have been entrained by the much deeper convective mixed layers that form in this hot, dry higher elevation region [Langford et al., 2015, 2018a]. The boundary layers in the valley were too shallow to capture this transported ozone, but a few of these layers descended into the SJV behind cold fronts. These events *decreased* surface O_3 since the diluted lower stratospheric air and Asian pollution displaced even more polluted surface air. Similar behavior was previously observed in the South Coast Air Basin during CalNex [*Langford et al.,* 2012].

This somewhat paradoxical result does not imply that stratospheric intrusions and Asian pollution do not contribute to surface O_3 in the Central Valley. These very same events might have *increased* surface O_3 had they occurred in April or early May when there is less local photochemical production of O_3. Furthermore, Asian pollution transported just above the marine boundary layer [*Holzer and Hall*, 2007] and stratospheric intrusions that develop much further west over the Pacific Ocean [*Cooper et al.*, 2005] mix with free tropospheric air to become part of the background air flowing through the Carquinez Strait and over the relatively low Coastal Ranges [*Parrish et al.*, 2009; *Parrish et al.*, 2010].

The TOPAZ measurements during the second IOP showed that the SJV was severely impacted by smoke and O_3 created by the Soberanes Fire near Big Sur. The measurements suggest that surface O_3 in the central SJV was increased by 10-20 ppbv or more each day during the first two weeks after the fire started, including the highest O_3 days of 2016. The emissions from this fire may be responsible for the 10% increase in the number of exceedance days in the SJVAB in 2016 compared to other recent years.

References

Ahmadov, R., et al. (2012), A volatility basis set model for summertime secondary organic aerosols over the eastern United States in 2006, *J. Geophys. Res.-Atmos.*, *117*, doi:Artn D06301 10.1029/2011jd016831.

Alvarez, R. J., II, et al. (2011), Development and Application of a Compact, Tunable, Solid-State Airborne Ozone Lidar System for Boundary Layer Profiling, *J. Atmos. Ocean Tech.*, *28*(10), 1258-1272, doi:10.1175/Jtech-D-10-05044.1.

Avnery, S., D. L. Mauzerall, J. F. Liu, and L. W. Horowitz (2011a), Global crop yield reductions due to surface ozone exposure: 1. Year 2000 crop production losses and economic damage, *Atmos. Environ.*, *45*(13), 2284-2296, doi:10.1016/j.atmosenv.2010.11.045.

Avnery, S., D. L. Mauzerall, J. F. Liu, and L. W. Horowitz (2011b), Global crop yield reductions due to surface ozone exposure: 2. Year 2030 potential crop production losses and economic damage under two scenarios of O-3 pollution, *Atmos. Environ.*, *45*(13), 2297-2309, doi:10.1016/j.atmosenv.2011.01.002.

Bao, J. W., S. A. Michelson, P. O. G. Persson, I. V. Djalalova, and J. M. Wilczak (2008), Observed and WRF-simulated low-level winds in a high-ozone episode during the Central California Ozone Study, *J. Appl. Meteorol. Clim.*, *47*(9), 2372-2394, doi:10.1175/2008jamc1822.1.

Beaver, S., and A. Palazoglu (2009), Influence of synoptic and mesoscale meteorology on ozone pollution potential for San Joaquin Valley of California, *Atmos. Environ.*, *43*(10), 1779-1788, doi:10.1016/j.atmosenv.2008.12.034.

Bianco, L., I. V. Djalalova, C. W. King, and J. M. Wilczak (2011), Diurnal Evolution and Annual Variability of Boundary-Layer Height and Its Correlation to Other Meteorological Variables in California's Central Valley, *Boundary-Layer Meteorology*, *140*(3), 491-511, doi:10.1007/s10546-011-9622-4.

Bonin, T. A., A. Choukulkar, W. A. Brewer, S. P. Sandberg, A. M. Weickmann, Y. L. Pichugina, R. M. Banta, S. P. Oncley, and D. E. Wolfe (2017), Evaluation of turbulence measurement techniques from a single Doppler lidar, Atmos Meas Tech, 10(8), 3021-3039, doi:10.5194/amt-10-3021-2017.

Brioude, J., et al. (2007), Mixing between a stratospheric intrusion and a biomass burning plume, *Atmos. Chem. Phys.*, *7*(16), 4229-4235.

Brock, C. A., et al. (2004), Particle characteristics following cloud-modified transport from Asia to North America, *J. Geophys. Res.-Atmos.*, *109*(D23), doi:10.1029/2003jd004198.

Brown-Steiner, B., and P. Hess (2011), Asian influence on surface ozone in the United States: A comparison of chemistry, seasonality, and transport mechanisms, *J. Geophys. Res.*, *116*, doi:10.1029/2011JD015846.

Brune, W. H., et al. (2016), Ozone production chemistry in the presence of urban plumes, *Faraday Discussions*, *189*, 169-189, doi:10.1039/c5fd00204d.

Caputi, D. J., I. Faloona, J. Trousdell, J. Smoot, N. Falk, and S. Conley (2018), Residual Layer Ozone, Mixing, and the Nocturnal Jet in California's San Joaquin Valley, *Atmos. Chem. Phys. Discuss.*, *2018*, 1-33, doi:10.5194/acp-2018-854.

Cooper, O. R., et al. (2004a), On the life cycle of a stratospheric intrusion and its dispersion into polluted warm conveyor belts, *J. Geophys. Res.*, *109*(D23).

Cooper, O. R., et al. (2004b), A case study of trans-Pacific warm conveyor belt transport: The influence of merging airstreams on trace gas import to North America, *J. Geophys. Res.*, *108*(D23S08), doi:10.1029/2003JD003624.

Cooper, O. R., et al. (2011), Measurement of western U.S. baseline ozone from the surface to the tropopause and assessment of downwind impact regions, *J. Geophys. Res.*, *116*, doi:10.1029/2011JD016095.

Cooper, O. R., et al. (2010), Increasing springtime ozone mixing ratios in the free troposphere over western North America, *Nature*, *463*(7279), 344-348.

Cooper, O. R., et al. (2005), Direct transport of midlatitude stratospheric ozone into the lower troposphere and marine boundary layer of the tropical Pacific Ocean, *J. Geophys. Res.-Atmos.*, *110*(D23), doi:Artn D23310
Doi 10.1029/2005jd005783.

Dabdub, D., L. L. DeHaan, and J. H. Seinfeld (1999), Analysis of ozone in the San Joaquin Valley of California, *Atmospheric Environment*, *33*(16), 2501-2514, doi:Doi 10.1016/S1352-2310(98)00256-8.

De Young, R. J., V. B. Grant, and K. Severance (2005), Aerosol transport in the California Central Valley observed by airborne lidar, *Environ. Sci. Technol.*, *39*(21), 8351-8357, doi:10.1021/es0487401.

Emanuel, K. A., and M. Zivkovic-Rothman (1999), Development and evaluation of a convective scheme for use in climate models, *J. Atmos. Sci.*, *56*, 1766-1782.

Faloona, I. (2018), Ozone in the Lower Atmosphere and its Contribution to High Ozone Concentrations at Ground-Level in the Southern San Joaquin Valley.*Rep. Contract No. 14-308*, University of California, Davis, California Air Resources Board and the California Environmental Protection Agency.

Fast, J. D., et al. (2012), Transport and mixing patterns over Central California during the carbonaceous aerosol and radiative effects study (CARES), *Atmos. Chem. Phys.*, *12*(4), 1759-1783, doi:10.5194/Acp-12-1759-2012.

Francesca Di, G., S. Remy, P. Florian, and W. Fredrik (2016), Improving GFAS and CAMS biomass burning estimations by means of the Global ECMWF Fire Forecast system (GEFF), edited, ECMWF.

Gaudel, A., et al. (2018), Tropospheric Ozone Assessment Report: Present-day distribution and trends of tropospheric ozone relevant to climate and global atmospheric chemistry model evaluation, *Elementa-Sci Anthrop*, *6*, doi:ARTN 39
10.1525/elementa.291.

Gohm, A., F. Harnisch, J. Vergeiner, F. Obleitner, R. Schnitzhofer, A. Hansel, A. Fix, B. Neininger, S. Emeis, and K. Schaafer (2009), Air Pollution Transport in an Alpine Valley: Results From Airborne and Ground-Based Observations, *Boundary-Layer Meteorology*, *131*(3), 441-463, doi:10.1007/s10546-009-9371-9.

Goldstein, A. H., D. B. Millet, M. McKay, L. Jaeglé, L. Horowitz, O. Cooper, R. Hudman, D. J. Jacob, S. Oltmans, and A. Clarke (2004), Impact of Asian emissions on observations at Trinidad Head, California, during ITCT 2k2, *J. Geophys. Res.*, *109*(D23S17).

Goliff, W. S., W. R. Stockwell, and C. V. Lawson (2013), The regional atmospheric chemistry mechanism, version 2, *Atmospheric Environment*, *68*, 174-185, doi:10.1016/j.atmosenv.2012.11.038.

Grell, G. A., S. E. Peckham, R. Schmitz, S. A. McKeen, G. J. Frost, W. C. Skamarock, and B. Eder (2005), Fully coupled 'online' chemistry in the WRF model, *Atmospheric Environment*, *39*, 6957-6976.

Guenther, A., T. Karl, P. Harley, C. Wiedinmyer, P. I. Palmer, and C. Geron (2006), Estimates of global terrestrial isoprene emissions using MEGAN (Model of Emissions of Gases and Aerosols from Nature), *Atmospheric Chemistry & Physics*, *6*, 29.

Hamill, P., L. T. Iraci, E. L. Yates, W. Gore, T. P. Bui, T. Tanaka, and M. Loewenstein (2016), A New Instrumented Airborne Platform for Atmospheric Research, *Bull. Am. Meteorol. Soc.*, *97*(3), 397-404, doi:10.1175/Bams-D-14-00241.1.

Hanna, S. R. (1982), Applications in air pollution modeling, in *Atmospheric Turbulence and Air Pollution Modelling*, edited by F. T. M. Nieuwstadt and H. van Dop, D. Reidel Publishing Company, Dordrecht, Holland.

Holzer, M., and T. M. Hall (2007), Low-level transpacific transport, *J. Geophys. Res.*, *112*, D09103.

Hudman, R. C., et al. (2004), Ozone production in transpacific Asian pollution plumes and implications for ozone air quality in California, *J. Geophys. Res.*, *109*(D23), doi:10.1029/2004jd004974.

Jacob, D. J., J. A. Logan, and P. P. Murti (1999), Effect of rising Asian emissions on surface ozone in the United States, *Geophys. Res. Lett.*, *26*(14), 2175-2178, doi:10.1029/1999gl900450.

Jaffe, D., H. Price, D. Parrish, A. Goldstein, and J. Harris (2003a), Increasing background ozone during spring on the west coast of North America, *Geophys. Res. Lett.*, *30*(12), doi:10.1029/2003gl017024.

Jaffe, D. A., et al. (1999), Transport of Asian air pollution to North America, *Geophys. Res. Lett.*, *26*(6), 711-714.

Jaffe, D. A., O. R. Cooper, A. M. Fiore, B. H. Henderson, G. S. Tonneson, A. G. Russell, D. K. Henze, A. O. Langford, M. Lin, and T. Moore (2018), Scientific assessment of background ozone over the U.S.: Implications for air quality management., *Elem Sci Anth.*, *6*(1), doi:http://doi.org/10.1525/elementa.309.

Jaffe, D. A., I. McKendry, T. Anderson, and H. Price (2003b), Six 'new' episodes of trans-Pacific transport of air pollutants, *Atmospheric Environment*, *37*(3), 14.

Jaffe, D. A., and N. L. Wigder (2012), Ozone production from wildfires: A critical review, *Atmospheric Environment*, *51*, 1-10, doi:Doi 10.1016/J.Atmosenv.2011.11.063.

Johnson, B. J., S. J. Oltmans, H. Vomel, H. G. J. Smit, T. Deshler, and C. Kroger (2002), Electrochemical concentration cell (ECC) ozonesonde pump efficiency measurements and tests on the sensitivity to ozone of buffered and unbuffered ECC sensor cathode solutions, *J. Geophys. Res.*, *107*(D19), doi:10.1029/2001jd000557.

Lagarias, J. S., and W. W. Sylte (1991), Designing and Managing the San Joaquin Valley Air-Quality Study, *J. Air Waste Manage. Assoc.*, *41*(9), 1176-1179, doi:10.1080/10473289.1991.10466912.

Langford, A. O., J. Brioude, O. R. Cooper, C. J. Senff, R. J. Alvarez, R. M. Hardesty, B. J. Johnson, and S. J. Oltmans (2012), Stratospheric influence on surface ozone in the Los Angeles area during late spring and early summer of 2010, *J. Geophys. Res.*, *117*, D00V06, doi:10.1029/2011JD016766.

Langford, A. O., R. B. Pierce, and P. J. Schultz (2015a), Stratospheric intrusions, the Santa Ana winds, and wildland fires in Southern California, *Geophys. Res. Lett.*, *42*(14), 6091-6097, doi:10.1002/2015gl064964.

Langford, A. O., C. J. Senff, R. J. Alvarez, R. M. Banta, and R. M. Hardesty (2010), Long-range transport of ozone from the Los Angeles Basin: A case study, *Geophys. Res. Lett.*, *37*, L06807, doi:10.1029/2010gl042507.

Langford, A. O., C. J. Senff, R. J. Alvarez, R. M. Banta, R. M. Hardesty, D. D. Parrish, and T. B. Ryerson (2011), Comparison between the TOPAZ Airborne Ozone Lidar and In Situ Measurements during TexAQS 2006, *J. Atmos. Ocean. Tech.*, *28*(10), 1243-1257, doi:10.1175/Jtech-D-10-05043.1.

Langford, A. O., et al. (2015b), An overview of the 2013 Las Vegas Ozone Study (LVOS): Impact of stratospheric intrusions and long-range transport on surface air quality, *Atmos. Environ.*, *109*, 305-322, doi:10.1016/J.Atmosenv.2014.08.040.

Leblanc, T., et al. (2018), Validation of the TOLNet lidars: the Southern California Ozone Observation Project (SCOOP), *Atmos. Meas. Tech.*, *11*(11), 6137-6162, doi:10.5194/amt-11-6137-2018.

Li, J., A. Mahalov, and P. Hyde (2016), Impacts of agricultural irrigation on ozone concentrations in the Central Valley of California and in the contiguous United States based on WRF-Chem simulations, *Agricultural and Forest Meteorology*, *221*, 34-49, doi:10.1016/j.agrformet.2016.02.004.

Lin, M. Y., A. M. Fiore, O. R. Cooper, L. W. Horowitz, A. O. Langford, H. Levy, B. J. Johnson, V. Naik, S. J. Oltmans, and C. J. Senff (2012a), Springtime high surface ozone events over the western United States: Quantifying the role of stratospheric intrusions, *J. Geophys. Res.*, *117*, D00v22, doi:10.1029/2012jd018151.

Lin, M. Y., et al. (2012b), Transport of Asian ozone pollution into surface air over the western United States in spring, *J. Geophys. Res.*, *117*, D00v07, doi:10.1029/2011JD016961.

Lin, Y. L., and I. C. Jao (1995), A Numerical Study of Flow Circulations in the Central Valley of California and Formation Mechanisms of the Fresno Eddy, *Mon. Wea. Rev.*, *123*(11), 3227-3239, doi:10.1175/1520-0493(1995)123<3227:Ansofc>2.0.Co;2.

Malicet, J., D. Daumont, J. Charbonnier, C. Parisse, A. Chakir, and J. Brion (1995), Ozone UV Spectroscopy .2. Absorption Cross-Sections and Temperature-Dependence, *J. Atmos. Chem.*, *21*(3), 263-273, doi:10.1007/Bf00696758.

Nowak, J., et al. (2004), Gas-phase chemical characteristics of Asian emission plumes observed during ITCT 2K2 over the eastern North Pacific Ocean, *J. Geophys. Res.*, *109*(D23S19), doi:10.1029/2003JD004488.

Olivier, J. G. J., J. A. Van Aardenne, F. Dentener, L. Ganzeveld, and J. A. H. W. Peters (2005), Recent trends in global greenhouse gas emissions: regional trends and spatial distribution of key sources, in *Non-CO_2 Greenhouse Gases (NCGG-4)* edited by A. v. Amstel, pp. 325-330, Millpress, Rotterdam.

Pagowski, M., G. A. Grell, S. A. McKeen, S. E. Peckham, and D. Devenyi (2010), Three-dimensional variational data assimilation of ozone and fine particulate matter observations: some results using the Weather Research and Forecasting - Chemistry model and Grid-point Statistical Interpolation, *Quarterly Journal of the Royal Meteorological Society*, *136*(653), 2013-2024, doi:10.1002/qj.700.

Panek, J., D. Saah, A. Esperanza, A. Bytnerowicz, W. Fraczek, and R. Cisneros (2013), Ozone distribution in remote ecologically vulnerable terrain of the southern Sierra Nevada, CA, *Environmental Pollution*, *182*, 343-356, doi:10.1016/j.envpol.2013.07.028.

Parrish, D. D., K. C. Aikin, S. J. Oltmans, B. J. Johnson, M. Ives, and C. Sweeny (2010), Impact of transported background ozone inflow on summertime air quality in a California ozone exceedance area, *Atmospheric Chemistry and Physics*, *10*(20), 10093-10109, doi:Doi 10.5194/Acp-10-10093-2010.

Parrish, D. D., D. B. Millet, and A. H. Goldstein (2009), Increasing ozone in marine boundary layer inflow at the west coasts of North America and Europe, *Atmos. Chem. Phys.*, *9*(4), 1303-1323.

Pierce, R. B., et al. (2003), Regional Air Quality Modeling System (RAQMS) predictions of the tropospheric ozone budget over east Asia, *J. Geophys. Res*, *108*(D21), 8825, doi:10.1029/2002jd003176.

Pierce, R. B., et al. (2007), Chemical data assimilation estimates of continental US ozone and nitrogen budgets during the Intercontinental Chemical Transport Experiment-North America, *J. Geophys. Res*, *112*(D12), doi:10.1029/2006jd007722.

Price, H. U., D. A. Jaffe, O. R. Cooper, and P. V. Doskey (2004), Photochemistry, ozone production, and dilution during long-range transport episodes from Eurasia to the northwest United States, *J. Geophys. Res.*, *109*(D23S13), doi:10.1029/2003JD004400, doi:10.1029/2003jd004400.

Proffitt, M. H., and A. O. Langford (1997), Ground-based differential absorption lidar system for day or night measurements of ozone throughout the free troposphere, *Appl Optics*, *36*(12), 2568-2585.

Pusede, S. E., and R. C. Cohen (2012), On the observed response of ozone to NOx and VOC reactivity reductions in San Joaquin Valley California 1995-present, *Atmos. Chem. Phys.*, *12*(18), 8323-8339, doi:10.5194/acp-12-8323-2012.

Pusede, S. E., et al. (2014), On the temperature dependence of organic reactivity, nitrogen oxides, ozone production, and the impact of emission controls in San Joaquin Valley, California, *Atmos. Chem. Phys.*, *14*(7), 3373-3395, doi:10.5194/acp-14-3373-2014.

Rampanelli, G., D. Zardi, and R. Rotunno (2004), Mechanisms of up-valley winds, *J. Atmos. Sci.*, *61*(24), 3097-3111, doi:10.1175/Jas-3354.1.

Reid, J. S., R. Koppmann, T. F. Eck, and D. P. Eleuterio (2005), A review of biomass burning emissions part II: intensive physical properties of biomass burning particles, *Atmos. Chem. Phys.*, *5*, 799-825, doi:10.5194/acp-5-799-2005.

Reynolds, S., C. Bohnenkamp, A. Kaduwela, B. Katayama, E. Shipp, J. Sweet, S. Tanrikulu, and S. Ziman (2010), Central California Ozone Study: Synthesis of Results, *Nato Sci Peace Sec B*, 571-574.

Ryerson, T. B., et al. (2013), The 2010 California Research at the Nexus of Air Quality and Climate Change (CalNex) field study, *J. Geophys. Res.*, *118*(11), 5830-5866, doi:10.1002/Jgrd.50331.

Ryoo, J. M., M. S. Johnson, L. T. Iraci, E. L. Yates, and W. Gore (2017), Investigating sources of ozone over California using AJAX airborne measurements and models.: Assessing the contribution from longrange transport, *Atmos. Environ.*, *155*, 53-67, doi:10.1016/j.atmosenv.2017.02.008.

Schaack, T. K., T. H. Zapotocny, A. J. Lenzen, and D. R. Johnson (2004), Global climate simulation with the university of Wisconsin global hybrid isentropic coordinate model, *J. Climate*, *17*(15), 2998-3016, doi:10.1175/1520-0442(2004)017<2998:Gcswtu>2.0.Co;2.

Senff, C. J., R. J. Alvarez, R. M. Hardesty, R. M. Banta, and A. O. Langford (2010), Airborne lidar measurements of ozone flux downwind of Houston and Dallas, *J. Geophys. Res.*, *115*, doi:10.1029/2009jd013689.

Singh, H. B., C. Cai, A. Kaduwela, A. Weinheimer, and A. Wisthaler (2012), Interactions of fire emissions and urban pollution over California: Ozone formation and air quality simulations, *Atmospheric Environment*, *56*, 45-51, doi:Doi 10.1016/J.Atmosenv.2012.03.046.

St. Clair, J. M., A. K. Swanson, S. A. Bailey, G. M. Wolfe, J. E. Marrero, L. T. Iraci, J. G. Hagopian, and T. F. Hanisco (2017), A new non-resonant laser-induced fluorescence instrument for the airborne in situ measurement of formaldehyde, *Atmos Meas Tech*, *10*(12), 4833-4844, doi:10.5194/amt-10-4833-2017.

Stohl, A., C. Forster, A. Frank, P. Seibert, and G. Wotawa (2005), Technical note: The Lagrangian particle dispersion model FLEXPART version 6.2, *Atmos. Chem. Phys.*, *5*, 2461-2474.

Tanaka, T., et al. (2016), Two-Year Comparison of Airborne Measurements of CO2 and CH4 With GOSAT at Railroad Valley, Nevada, *Geoscience and Remote Sensing, IEEE Transactions on*, *54*(8), 4367-4375, doi:10.1109/Tgrs.2016.2539973.

Trousdell, J. F., S. A. Conley, A. Post, and I. C. Faloona (2016), Observing entrainment mixing, photochemical ozone production, and regional methane emissions by aircraft using a simple mixed-layer framework, *Atmos. Chem. Phys.*, *16*(24), 15433-15450, doi:10.5194/acp-16-15433-2016.

U.S. Environmental Protection Agency (2014), Policy Assessment for the Review of the Ozone National Ambient Air Quality Standards,*Rep. EPA-452/R-14-006*, Research Triangle Park, North Carolina.

U.S. Environmental Protection Agency (2015), National Ambient Air Quality Standards for Ozone: Final Rule, in *EPA–HQ–OAR–2008–0699; FRL–9933–18– OAR*, edited by U. S. Environmental Protection Agency, Federal Register.

Verstraeten, W. W., J. L. Neu, J. E. Williams, K. W. Bowman, J. R. Worden, and K. F. Boersma (2015), Rapid increases in tropospheric ozone production and export from China, *Nat. Geosci.*, *8*(9), 690-+, doi:10.1038/Ngeo2493.

Völger, P., J. Bösenberg, and I. Shult (1996), Scattering properties of selected model aerosols calculated at UV-wavelengths: Implications for DIAL measurements of tropospheric ozone., *Contributions to Atmospheric Physics*, *69*, 177-187.

Wang, L. H., et al. (2017), Quantifying TOLNet ozone lidar accuracy during the 2014 DISCOVER-AQ and FRAPPE campaigns, *Atmos Meas Tech*, *10*(10), 3865-3876, doi:10.5194/amt-10-3865-2017.

Yates, E. L., L. T. Iraci, D. Austerberry, R. B. Pierce, M. C. Roby, J. M. Tadic, M. Loewenstein, and W. Gore (2015), Characterizing the impacts of vertical transport and photochemical ozone production on an exceedance area, *Atmos. Environ.*, *109*, 342-350, doi:10.1016/j.atmosenv.2014.09.002.

Yates, E. L., L. T. Iraci, M. C. Roby, R. B. Pierce, M. S. Johnson, P. J. Reddy, J. M. Tadic, M. Loewenstein, and W. Gore (2013), Airborne observations and modeling of springtime

stratosphere-to-troposphere transport over California, *Atmos. Chem. Phys.*, *13*(24), 12481-12494, doi:10.5194/Acp-13-12481-2013.

Zardi, D., and C. D. Whiteman (2013), Diurnal Mountain Wind Systems, in *Mountain Weather Research and Forecasting: Recent Progress and Current Challenges*, edited by F. K. Chow, S. F. J. De Wekker and B. J. Snyder, pp. 35-119, Springer Netherlands, Dordrecht, doi:10.1007/978-94-007-4098-3_2.

Zaveri, R. A., et al. (2012), Overview of the 2010 Carbonaceous Aerosols and Radiative Effects Study (CARES), *Atmospheric Chemistry and Physics*, *12*(16), 7647-7687, doi:Doi 10.5194/Acp-12-7647-2012.

Zhang, L., et al. (2008), Transpacific transport of ozone pollution and the effect of recent Asian emission increases on air quality in North America: an integrated analysis using satellite, aircraft, ozonesonde, and surface observations, *Atmos. Chem. Phys.*, *8*(20), 6117-6136, doi:10.5194/acp-8-6117-2008.

Zhang, L., D. J. Jacob, M. Kopacz, D. K. Henze, K. Singh, and D. A. Jaffe (2009), Intercontinental source attribution of ozone pollution at western US sites using an adjoint method, *Geophys. Res. Lett.*, *36*, doi:10.1029/2009gl037950.

Zhong, S. Y., C. D. Whiteman, and X. D. Bian (2004), Diurnal evolution of three-dimensional wind and temperature structure in California's Central Valley, *J. Appl. Meteorol.*, *43*(11), 1679-1699, doi:10.1175/Jam2154.1.